Politecnico di Torino

Master's Degree in Aerospace Engineering
A.Y. 2025/2026

Master's Degree Thesis

Preliminary Design and Analysis of a VTOL Vehicle for Martian Exploration

Supervisors:

Prof. Domenic D'Ambrosio

Prof. Manuel Carreno Ruiz

Candidate:

Christian Tamasi S331701

July 2026

Abstract

The successful operation of Ingenuity demonstrated the feasibility of powered flight in the Martian atmosphere and opened new possibilities for aerial mobility in planetary exploration. Future aerial vehicles could support surface missions by reaching areas that are difficult or slow to access with rovers, providing local reconnaissance, target assessment and short-range scientific observations.

However, flight on Mars remains highly challenging due to the very low atmospheric density, low Reynolds number regime, reduced speed of sound and limited onboard energy availability. These conditions strongly affect rotor sizing, hover power and mission endurance, making the design of a Martian VTOL vehicle a coupled mass–energy problem.

This thesis presents a preliminary sizing and feasibility analysis of an electric multicopter VTOL vehicle for local Martian exploration. A reference mission is considered, including vertical take-off, climb, cruise to a target area, hovering and science operations, vertical descent to the surface and a subsequent sleep and recharge phase. A simplified mass–energy model is developed to estimate rotor size, power demand, mission energy and battery mass.

The analysis focuses on a hexacopter configuration and investigates the effect of key design parameters, including gross mass, payload mass, disk loading, battery specific energy and night-survival thermal loads. The results highlight the main trade-offs governing the feasibility of a Martian multicopter, showing the strong coupling between rotor area, power requirements, energy storage and operational capability.

The study does not aim to define a fully optimized vehicle design; rather, it uses the developed sizing framework to identify a physically plausible preliminary reference configuration, while highlighting the key trade-offs among rotor sizing, energy storage, payload capability and operational constraints that should guide future Martian VTOL platform development.

Keywords: Mars Exploration, VTOL, Multicopter, Mass–Energy Sizing, Rotorcraft, Preliminary Design.

Contents

1. Introduction

1.1 Context of Martian Exploration

For decades, Mars has represented one of the primary targets of planetary exploration, both because of its intrinsic scientific interest and because of the role it plays in the future prospects of space research. The study of Mars makes it possible to investigate the geological and climatic evolution of a terrestrial body different from Earth, while also providing valuable insights into the possible existence of past environments favourable to liquid water and, potentially, to conditions compatible with habitability.
Figure 1.1.1 summarises some of the main milestones in the robotic exploration of Mars, highlighting the gradual transition from flyby and orbital missions to increasingly sophisticated surface platforms, up to the introduction of aerial mobility with Ingenuity [29].

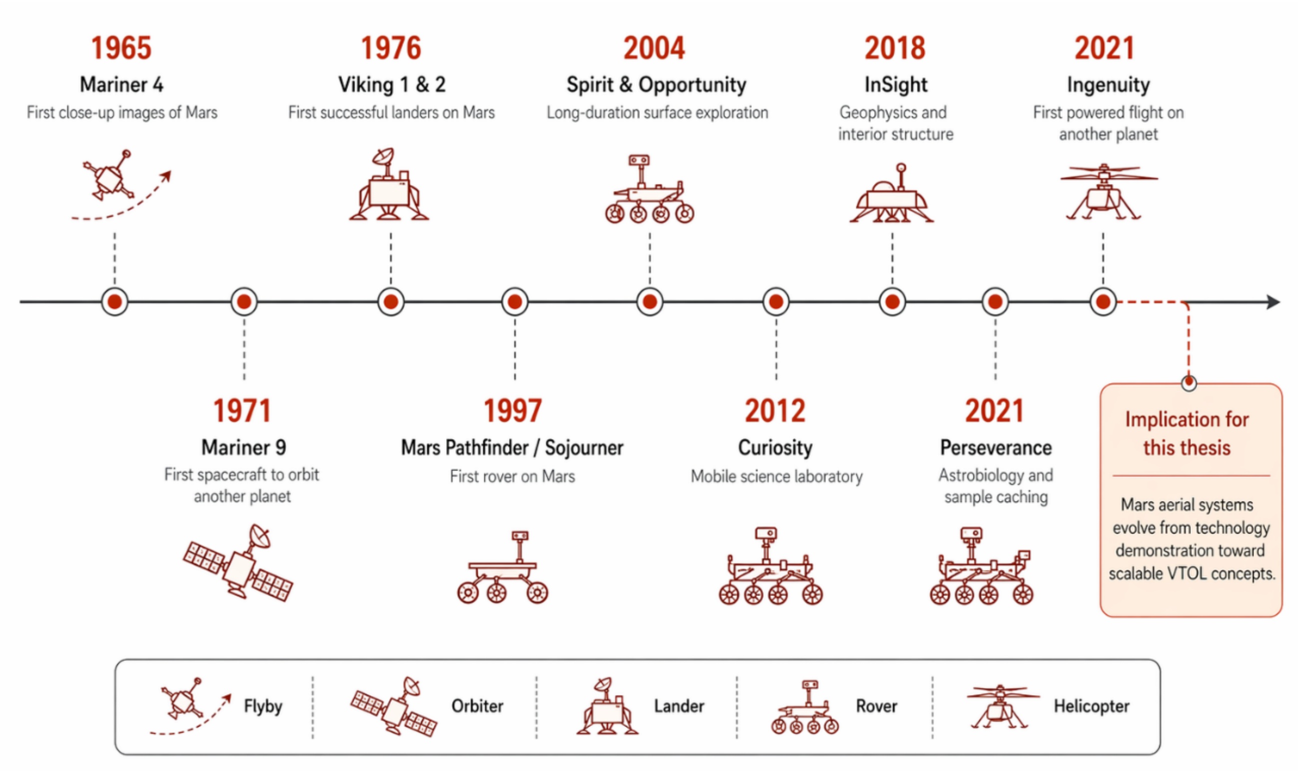

Figure 1.1.1 — Mars exploration milestones toward aerial mobility

This evolution shows how Martian exploration has progressively moved towards systems that are increasingly autonomous, mobile, and capable of operating close to the surface, thereby paving the way for more ambitious future VTOL concepts.

Over the last decades, robotic missions have significantly expanded our knowledge of the Martian environment, providing fundamental data on soil composition, atmospheric structure, surface morphology, and the planet's hydrological history. Within this framework, rovers have played a central role, owing to their ability to operate directly on the surface and to conduct highly detailed in situ scientific analyses [37], [38], [39]. However, the effectiveness of these systems is accompanied by clear operational limitations. Surface mobility enables accurate exploration, but it is necessarily slow and spatially constrained, especially in the presence of rough terrain, natural obstacles, or regions that are difficult to access. As a result, although rovers provide a high local scientific return, they cannot, on their own, ensure rapid and extensive coverage of the surrounding terrain [5], [11].

In this context, interest has progressively grown in complementary platforms capable of extending the operational capabilities of planetary missions. Among these, aerial systems represent a particularly promising solution, as they can overcome the constraints imposed by ground locomotion and provide faster access to scientifically relevant areas. The introduction of aerial mobility into Martian exploration can therefore be regarded as a natural evolution of traditional robotic architectures, opening new perspectives for missions that are more flexible, responsive, and spatially extended [5], [11].

1.2 Motivation for Aerial Systems

Against this background, the motivation for introducing aerial systems into Martian exploration lies in the need to overcome the intrinsic limitations of surface mobility and to provide faster access to scientifically relevant areas. While rovers remain essential assets for detailed in situ investigation, their operational range is constrained by terrain roughness, natural obstacles, slope limitations, and the inherently slow pace of ground locomotion. A flying platform, by contrast, can cover larger distances in shorter time intervals, overfly hazardous or inaccessible terrain, and provide a broader local perspective on the surrounding environment [5], [11].

Figure 1.2 — Ingenuity Mars Helicopter deployed on the Martian surface. Source: [40]

For this reason, aerial systems should not be regarded as replacements for rovers, but rather as complementary assets within a more flexible exploration architecture: their role is particularly relevant for local reconnaissance, close-range terrain observation, preliminary identification of scientific targets, and support to the path-planning activities of surface vehicles. In this sense, aerial mobility introduces an intermediate operational layer between orbital remote sensing and ground-based exploration, enabling data acquisition at local scale to be performed more rapidly, selectively, and responsively [19], [29].

Among the possible aerial configurations, vertical take-off and landing vehicles (VTOL) offer a decisive operational advantage: the ability to operate without dedicated take-off or landing infrastructure, and such capability is especially relevant on Mars, where the surface is irregular, unprepared, and often uncertain from an operational standpoint [5], [6]. The interest in VTOL platforms therefore does not derive solely from the possibility of achieving flight in the Martian atmosphere, but from the possibility of doing so in a manner consistent with the actual constraints of robotic surface missions.

However, the operational benefits offered by aerial mobility are accompanied by several design challenges, since Martian VTOL vehicle must provide flexibility, controlled flight and hovering capability in an environment where thrust generation is strongly penalised by the low atmospheric density, while the available energy is highly constrained. This tension between operational usefulness and the physical sustainability of flight constitutes the central motivation for the analysis developed in this thesis.

1.3 Challenges of Flight on Mars

Atmospheric flight on Mars presents challenges that are substantially different from those encountered on Earth, as it must take place in an environment characterised by a rarefied atmosphere, low temperatures, and limited energy availability. Among these factors, the dominant constraint is the extremely low atmospheric density, which drastically reduces the ability of the fluid to generate lift and thrust and therefore makes vehicle support particularly demanding [2].

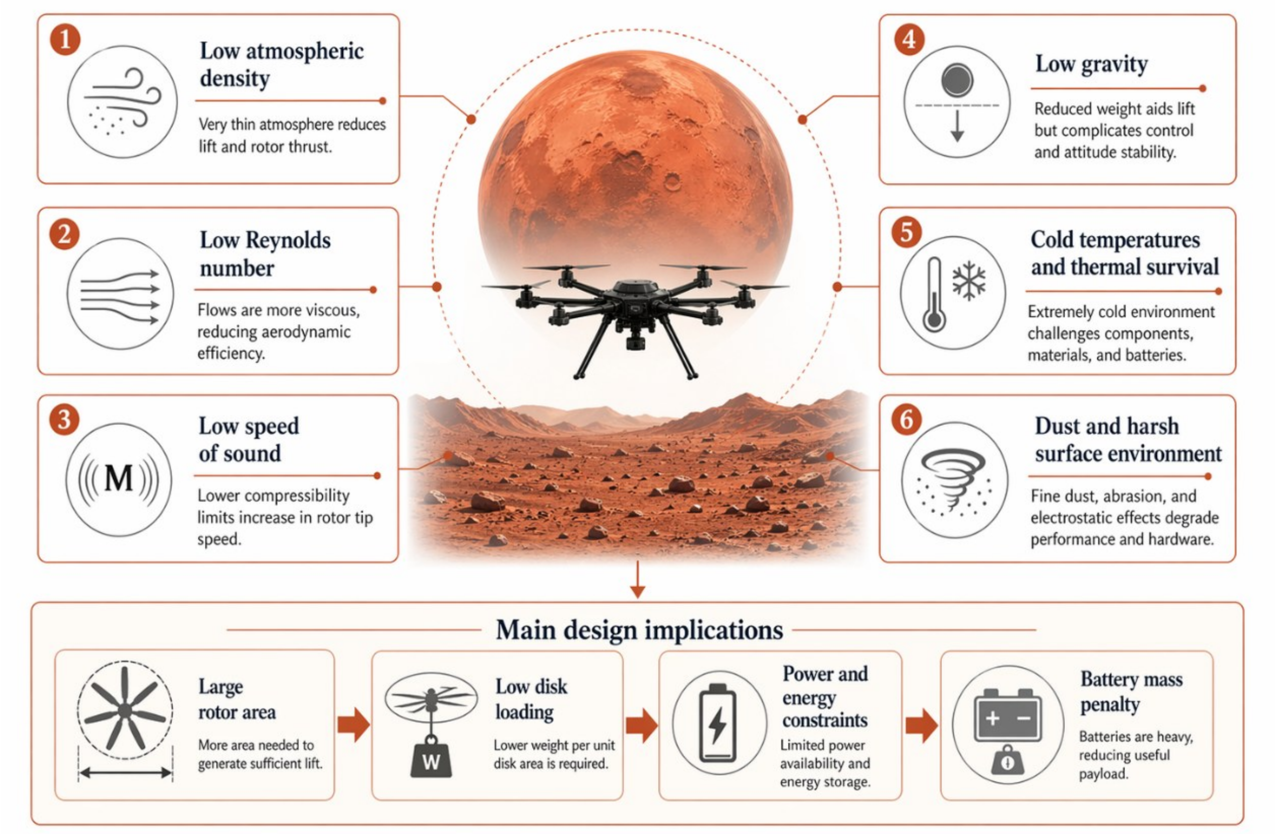

Figure 1.3 — Main environmental challenges affecting flight on Mars

In the case of a VTOL system, and especially for a multicopter configuration, this condition requires the vehicle to accelerate large volumes of fluid in order to generate the required thrust. This has direct consequences for rotor sizing, hover power requirements, and, more generally, the overall energy balance of the system. At the same time, the energy available on board is necessarily limited, meaning that flight on Mars is not only an aerodynamic problem, but also one that is strongly coupled with the mass and sizing of the energy system [2].

As a result, the design of a Martian aerial vehicle cannot be approached as a simple adaptation of terrestrial configurations, since it requires an integrated framework in which the environment, mission requirements, power demand, and available energy are treated consistently. This coupling between aerodynamic constraints and energy limitations forms one of the central technical foundations of the present work [4].

1.4 Objectives of the thesis

This thesis aims to assess the preliminary feasibility of a VTOL vehicle intended to operate in the Martian atmosphere, with particular focus on a multicopter configuration: the interest in this architecture derives from its relative simplicity, its ability to perform pure vertical take-off and landing, and its adaptability to unstructured operational scenarios, which are consistent with robotic surface missions.
The main purpose of the work is to develop a preliminary mass–energy model capable of linking environmental conditions, mission requirements, and the main design variables of the system. In particular, the model is intended to estimate the power required during the most relevant phases of the operational profile, the overall mission energy, and the mass of the energy storage system needed to sustain flight.
On this basis, the thesis investigates the influence of key parameters such as the number of rotors, rotor diameter, total vehicle mass, payload mass, and available energy capacity, in order to highlight the main trade-offs between configuration, power demand, endurance, and the overall plausibility of the system.
The aim is therefore not to define a final design, but rather to identify physically consistent preliminary configurations and to construct a design space that can support and guide future developments.

1.5 Methodology

The present work follows an analytical–numerical methodology aimed at the preliminary sizing of a multicopter vehicle for the Martian environment.
The first step consists in defining the reference environmental conditions and the operational mission framework, in order to identify the main physical and performance constraints governing the design problem. A simplified rotor-system model is then developed to estimate the thrust requirement, power demand, and energy consumption associated with the main flight phases.
Based on this formulation, the model is implemented in MATLAB and used to solve the mass–energy balance iteratively. This allows the consistency between total vehicle mass, propulsion requirements, battery mass, and available onboard energy to be assessed.
Finally, the developed framework is used to investigate the influence of the main design variables through parametric analyse: the purpose is not to obtain a fully optimized configuration, but to highlight the principal trade-offs affecting the proposed vehicle and to identify physically plausible regions of the design space.

2. Martian Environment and Design Constraints

2.1 Martian Environment

2.1.1 Atmospheric properties

The Martian atmosphere represents the primary physical constraint for atmospheric flight on the planet, as it directly affects the generation of lift and thrust, the aerodynamic regime of the vehicle, and the propulsion requirements associated with the mission.
Unlike Earth's atmosphere, the Martian atmosphere is characterised by a much lower density and an extremely reduced surface pressure, so the fluid available for the generation of aerodynamic forces is far more rarefied, with direct consequences for the feasibility of flight [25].

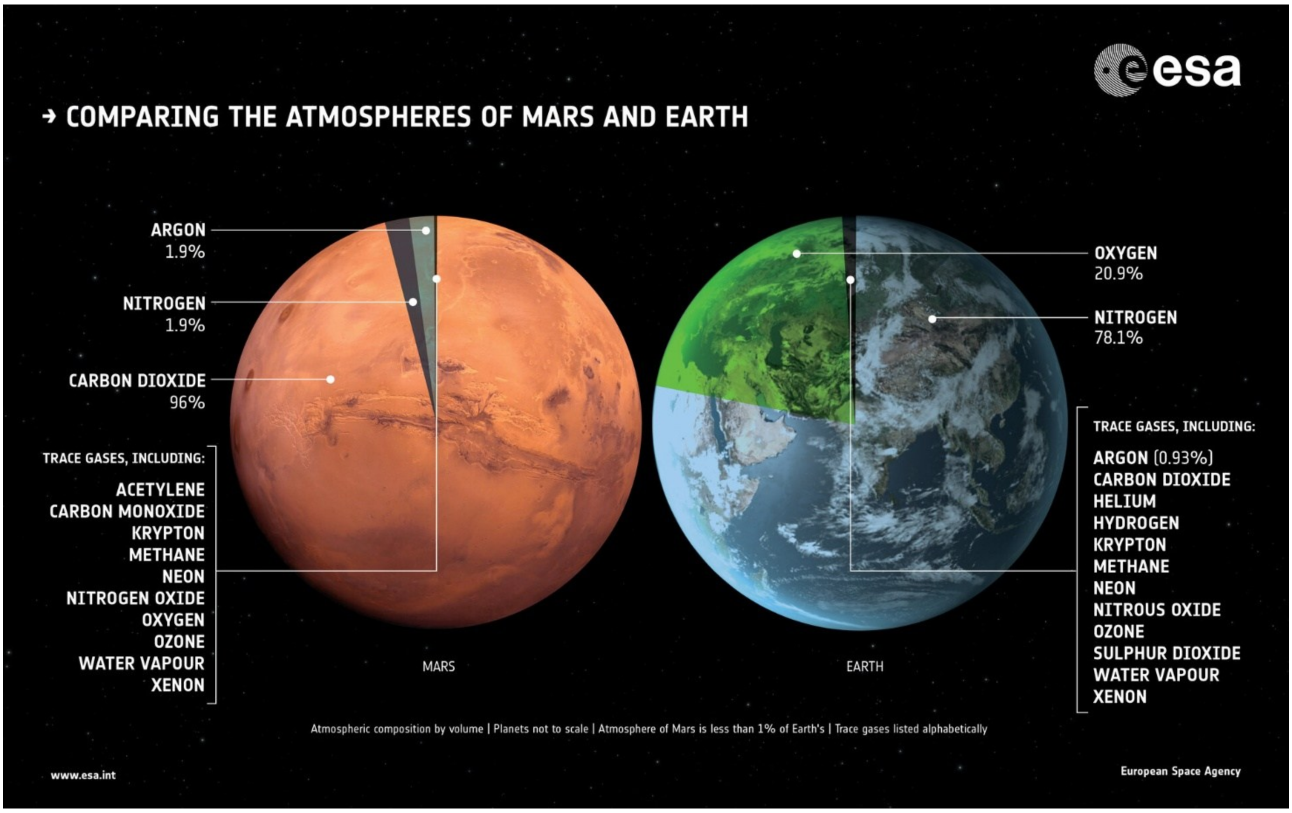

Figure 2.1.1 — Comparison between the atmospheric compositions of Mars and Earth. Source: ESA [26]

As shown in Figure 2.1.1, the atmosphere of Mars is dominated by carbon dioxide, which accounts for approximately 95% of the mixture, with smaller contributions from nitrogen and argon [26]. This composition, combined with the low temperatures typical of the Martian environment, leads to thermodynamic properties that differ from those of terrestrial air and affects, in particular, the speed of sound and the behaviour of the gas under the operating conditions considered. In situ measurements and simplified atmospheric models show that the speed of sound on Mars is significantly lower than on Earth, typically lying in the range of 200–250 m/s [2], and that makes Mach-number-related constraints more restrictive, especially for rotor-based systems.

A further relevant aspect is the Reynolds number, which, for a given geometric scale and operating velocity, is much lower than on Earth due to the rarefied atmosphere. This leads to a degradation of airfoil aerodynamic performance and to increased sensitivity to viscous effects, with particularly critical implications for the design of rotors intended to operate under low-density conditions [7].

In the context of this thesis, these properties are not treated merely as an environmental description, but rather as the physical framework within which the preliminary sizing of the vehicle must be developed. In particular, the combination of low density, low pressure, and reduced speed of sound requires the adoption of configurations characterised by large rotor disk areas, low disk loading values, and careful control of operating velocities. In this way, the atmospheric properties of Mars constitute the starting point for the evaluations of thrust, power, and energy.

2.1.2 Gravity and its effects

Martian gravity, approximately equal to 3.71 m/s^2, corresponds to slightly less than 40% of Earth's gravity [25]: for a given vehicle mass, this results in a lower weight and, in principle, reduces the thrust required for vehicle support, and that could be considered a favourable condition for flight.

However, in the Martian case this advantage is only partial, since the lower gravitational acceleration does not compensate for the effects of the extremely low atmospheric density, which remains the dominant constraint for the generation of lift and thrust. For a VTOL system, and especially for a multicopter configuration, the reduced weight decreases the total thrust requirement, but it does not remove the need to impart momentum to an extremely rarefied fluid.

2.1.3 Temperature conditions

The thermal conditions on Mars represent an additional relevant constraint for vehicle design, particularly with regard to the energy system: near the surface, temperatures can vary significantly between day and night, typically ranging from approximately 150 K to 250 K [25]. This large thermal excursion is related to the rarefied atmosphere, which limits convective heat transfer and makes the environment particularly sensitive to radiative exchanges.

In the present study, the most relevant aspect of the thermal environment is its impact on energy availability. Low temperatures can reduce battery performance by decreasing effective capacity and efficiency, thereby imposing a direct constraint on vehicle endurance [16]. In addition, possible auxiliary thermal loads required for vehicle survival during non-operational phases must be considered, an aspect that becomes relevant in the energy modelling.

From an aerodynamic standpoint, temperature also affects the speed of sound and, consequently, the operational limits associated with the Mach number, particularly with respect to rotor tip speed.

2.1.4 Solar irradiance and energy availability

Due to the greater distance of Mars from the Sun, the solar irradiance outside the atmosphere is approximately 590 W/m^2, less than half the terrestrial value [34], while at surface level this availability is further reduced by atmospheric absorption, radiative scattering, and the presence of suspended dust.

In the context of the present work, this aspect is relevant because the limited overall energy availability makes the sizing of the energy storage system particularly stringent; a further critical element is the temporal variability of irradiance, which depends on latitude, season, and local atmospheric conditions, and can be significantly reduced during dust storms.

Before defining the specific reference site and operating conditions adopted for the sizing model, it is useful to introduce an indicative comparison between Earth and Mars. The parameters reported in Table 2.1 are not intended as fixed design inputs, since density, pressure, and temperature vary significantly with altitude, latitude, season, local time, and dust conditions. They can rather be considered as order-of-magnitude references that frame the main environmental differences relevant to atmospheric flight.

Parameter	Earth	Mars
Gravity	9.81 m/s^2	3.71 m/s^2
Surface pressure	~101 kPa	~0.6–1 kPa
Atmospheric density	~1.2 kg/m^3	~0.010–0.020 kg/m^3
Main atmospheric composition	N_2/O_2-dominated	CO_2-dominated
Near-surface temperature	~288 K	~150–250 K
Solar irradiance outside the atmosphere	~1361 W/m^2	~590 W/m^2
Speed of sound	~340 m/s	~200–250 m/s
Day length	23 h 56 min	24 h 37 min

Table 2.1.1 — Indicative comparison between Earth and Mars environmental conditions.

2.2 Reference Site and Operating Conditions

2.2.1 Selection of the reference site

In order to develop a coherent preliminary analysis, the model must be anchored to a specific operational case rather than relying on overly generic average Martian conditions. In the present work, Jezero Crater under springtime conditions is therefore adopted as the reference site, consistently with the framework used in NASA studies on the Mars Science Helicopter (MSH) [2]. This choice allows the sizing process to be based on a mission context already discussed in the reference literature on Martian rotorcraft, while maintaining a clear connection with a realistic operational scenario.

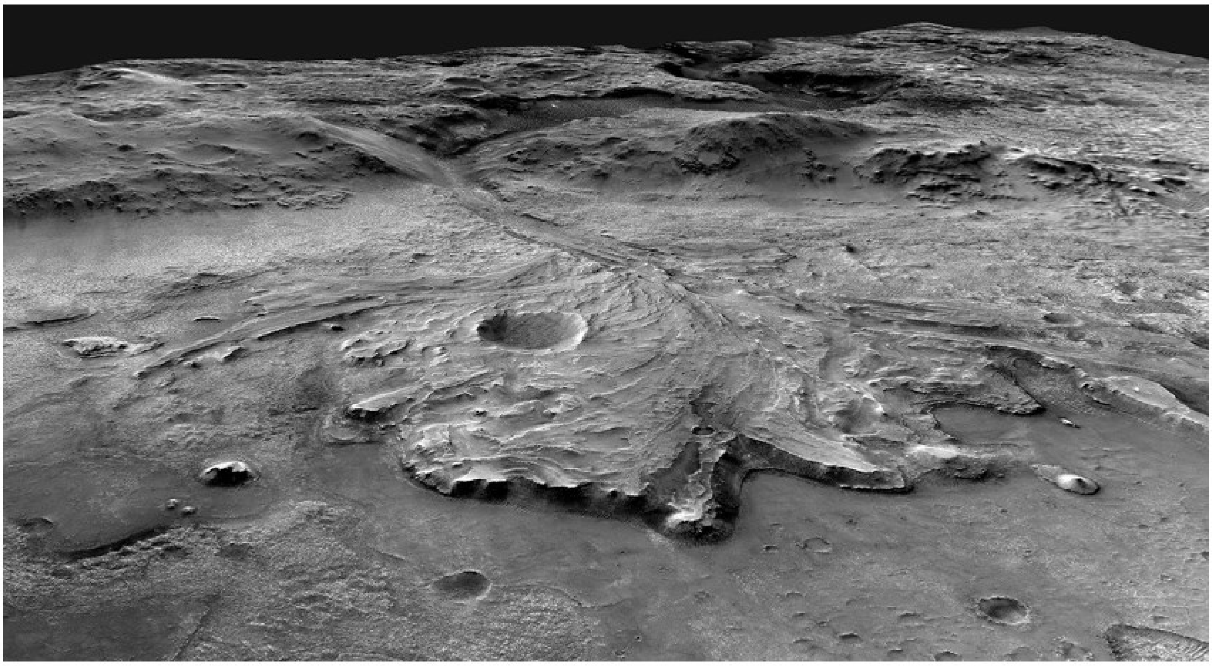

Figure 2.2.1 — Jezero Crater delta, reference site for the present study. Source: [41]

The adoption of Jezero Crater is appropriate not only from an engineering standpoint, but also from a scientific one, since it is regarded as an ancient lacustrine environment, characterised by inlet channels and well-preserved deltaic deposits, and since it was selected as the operating site of the Perseverance rover precisely because of its high geological and astrobiological interest [28]. In this sense, Jezero represents a particularly credible reference case for a local aerial mission supporting surface exploration, in which mobility, close-range observation, and rapid access to scientifically relevant targets play a central role.

2.2.2 Reference atmospheric and operating conditions

Based on the reference case defined above, the present study adopts a set of nominal atmospheric and operating conditions representative of near-surface springtime conditions at Jezero Crater, shown in table 2.2.1

Parameter	**Adopted value**	**Notes**
Reference site	Jezero Crater	Selected as representative operational scenario
Season	Springtime conditions	Consistent with the MSH reference framework
Atmospheric density	0.015 kg/m^3	Near-surface nominal value
Temperature	−50 °C / 223 K	Used for gas-property estimation
Gravity	3.71 m/s^2	Assumed constant over the operating envelope
Atmospheric composition	CO_2-dominated	Representative of the Martian lower atmosphere
Speed of sound	~233 m/s	Derived from the reference temperature and Martian gas properties

Table 2.2.1 — Nominal reference conditions adopted for the sizing model.

Starting from these reference quantities, the additional environmental parameters used in the model are derived, in particular the reference speed of sound and the operational constraints associated with the local Mach number; these values provide the environmental baseline for the valuation of thrust, power demand, and mission energy.

2.2.3 Assumptions and simplifications

Consistently with the preliminary design phase, the springtime conditions at Jezero Crater are treated in the present work as a nominal, steady, and spatially uniform case, so local and temporal variations of the atmosphere are therefore not explicitly modeled, nor are the effects of wind, turbulence, or diurnal variations in environmental conditions.

This simplification is not intended to neglect the actual variability of the Martian environment, but rather to provide an analytical model that is sufficiently simple and interpretable for the preliminary exploration of the design space. The adopted environmental case should therefore be interpreted as a reference condition for first-order sizing, while more detailed analyses would require the inclusion of atmospheric variability, wind disturbances, thermal cycles, and site-dependent operational margins.

2.3 VTOL Configuration Selection

2.3.1 VTOL configurations overview

The main VTOL architectures potentially applicable to Martian exploration can be grouped into three broad categories: multirotor configurations, hybrid configurations with lifting wings, and convertible configurations, such as tilt-rotor or tilt-wing vehicles.
The fundamental difference among these architectures lies in the way the vehicle generates lift during the different phases of flight and in the level of mechanical and control complexity required to transition from vertical take-off to forward flight [11].

Multirotor configurations, such as the one shown in Figure 2.3.1, generate both lift and thrust through their rotors throughout all operational phases: this architecture is inherently suited to pure vertical take-off and landing, does not require transition mechanisms, and is particularly consistent with short-range local missions. Its main drawback is the strong dependence on the rotor system even during forward flight, which results in relatively high power requirements [2].

Figure 2.3.1 — Representative unmanned multirotor VTOL configuration. Source: [43].

Hybrid fixed-wing VTOL configurations, such as the one shown in Figure 2.3.2, combine a vertical lift system with lifting surfaces designed to generate aerodynamic lift during cruise. This solution can improve the efficiency of forward flight, since the wing reduces the load required from the rotors or vertical propulsion units. Several concepts of this type have been proposed in the literature, including winged vehicles assisted by vertical propulsion systems, tailsitter configurations, and mixed solutions [6], [46].

Figure 2.3.2 — Representative hybrid fixed-wing VTOL configuration. Source: [44]

A third category is represented by convertible architectures, including tilt-rotor and tilt-wing concepts, such as the configuration shown in Figure 2.3.3, in which either the rotors or the entire wing rotate in order to transition from vertical to horizontal flight. In principle, such solutions offer an interesting compromise between VTOL capability and cruise efficiency, but they require transition mechanisms, control strategies, and structural integration that are significantly more complex than those of a pure rotorcraft configuration. This aspect is frequently addressed in the literature on future Martian aerial platforms, particularly for long-range missions [11].

Figure 2.3.3 — Representative convertible tilt-rotor VTOL UAV configuration. Source: [45]

2.3.2 Performance implications in Martian environment

When these architectures are transferred to the Martian environment, the differences among them become more pronounced.

In the case of multirotor vehicles, the main penalty is energetic: vehicle support remains entirely dependent on the rotors, even during forward flight. However, this direct dependence on the rotor system also eliminates the need for complex transition phases and makes the configuration particularly consistent with pure vertical operations in unstructured environments. Studies on the Mars Science Helicopter [2], together with more recent parametric analyses of Martian multirotors, show that this architecture remains particularly competitive for local and regional missions, where operational robustness and architectural simplicity are as important as pure aerodynamic efficiency.

Hybrid and fixed-wing VTOL configurations can offer a significant advantage during cruise, since the wing reduces the load required from the rotor or propulsion system, but this advantage becomes fully relevant only when the mission range is sufficiently large to compensate for the associated increase in mass, lifting surface area, and system complexity. In the Martian case, wing-generated lift remains strongly penalised by the low atmospheric density, which requires relatively high flight speeds, large lifting surfaces, or both. These requirements are further constrained by packaging within the aeroshell, as well as by possible deployment or geometric reconfiguration needs [46].

Convertible architectures, such as tilt-rotor and tilt-wing vehicles, also introduce the specific challenge of transition, since in an environment characterised by low density, low Reynolds numbers, local Mach-number constraints, and strong onboard autonomy requirements, managing the conversion between vertical and horizontal flight adds a further level of design risk. The literature shows that such solutions remain theoretically attractive for longer-range missions, but they are more difficult to stow, deploy, and control than a pure rotorcraft configuration [11].

A further element to consider is the ground operational context, since take-off and landing on Mars occur in the presence of uneven terrain, natural obstacles, local slopes, and dust lifted by rotors or jets.

This reduces the attractiveness of solutions that require favourable surface conditions, transition trajectories close to the ground, or geometries that are particularly sensitive to environmental interactions. In this sense, the operational simplicity of a multicopter represents a concrete advantage, rather than merely a conceptual simplification.

Although it does not represent a high-fidelity performance comparison, the matrix in Figure 2.3.4 provides a qualitative assessment of the main VTOL architectures considered in the present study. The multicopter achieves the highest scores in the criteria related to vertical take-off and landing capability, mechanical simplicity, and compatibility with operations from unprepared surfaces. These aspects are particularly relevant in the Martian context, where onboard autonomy, system reliability, and the reduction of architectural complexity are critical factors for a local robotic mission.

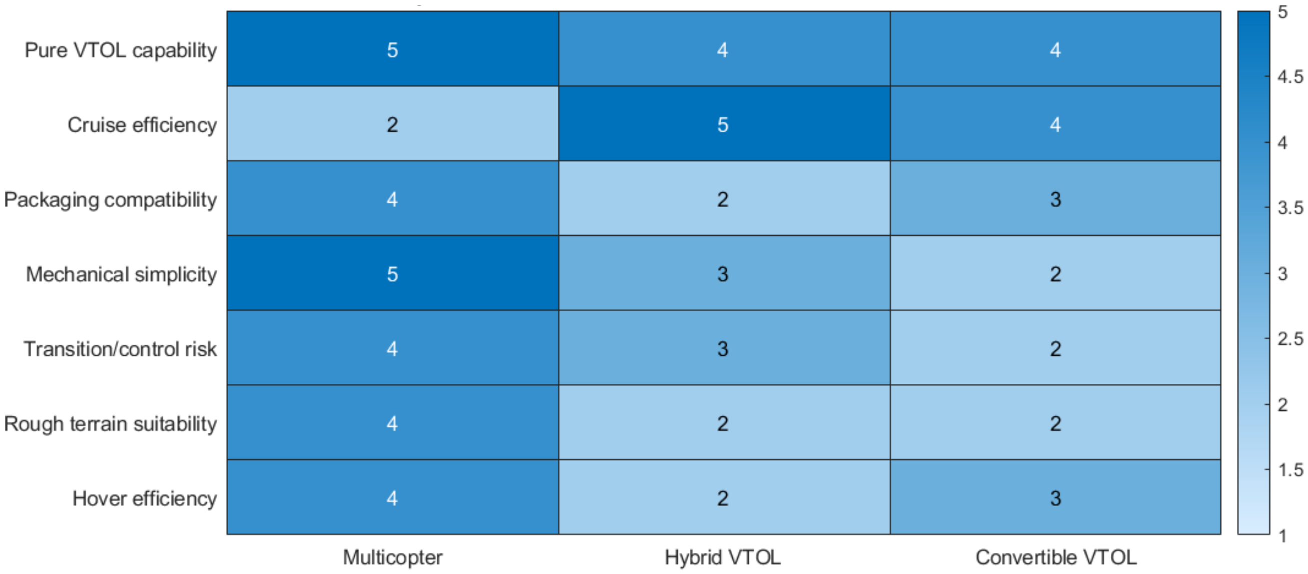

Figure 2.3.4 — Comparative assessment of candidate VTOL architectures for Mars

The multicopter configuration, however, presents an evident penalty in terms of cruise efficiency, since vehicle support is entirely provided by the rotors even during forward flight, and since this architecture cannot exploit dedicated lifting surfaces to reduce energy consumption during the transfer phase. For this reason, although it is favourable for vertical operations and control simplicity, the multicopter does not represent the most efficient solution for long-range missions.

Hybrid fixed-wing configurations, by contrast, show their greatest advantage during cruise, owing to the presence of a main lifting surface that reduces the load required from the propulsion system during forward flight. This benefit, however, is accompanied by significant penalties in terms of packaging, compatibility with rough terrain, and hovering efficiency. The wing and the subsystems dedicated to vertical flight increase the overall complexity of the vehicle and introduce mass and volume penalties that are not always favourable for local operations in the Martian environment.

Convertible configurations, such as tilt-rotor or tilt-wing vehicles, represent an intermediate compromise: they can provide good cruise performance together with full VTOL capability, but require more complex transition mechanisms and control logic. Their main limitation is therefore not their theoretical performance, but the architectural risk associated with the reconfiguration between vertical and horizontal flight, which is particularly critical in an unstructured environment and under limited operational autonomy.

2.3.3 Selected configuration rationale

On the basis of the previous considerations, the multicopter configuration is selected as the reference architecture for the present study: this choice doesn't imply that the multicopter is the most efficient solution in absolute terms, but rather that it represents the architecture most consistent with the objectives of the thesis and with the preliminary level of the analysis. In particular, a multicopter allows the study to focus on the central problem of Martian flight: the generation of thrust in a rarefied atmosphere under severe mass and energy constraints, without introducing at this stage the additional complexity associated with lifting wings, conversion mechanisms, or transition flight logic.

From an operational point of view, the multicopter provides direct VTOL capability, without requiring runways, prepared surfaces, or transitions between different flight modes, and at the same time this architecture makes it possible to investigate in a clear and direct manner the effect of design variables such as rotor number, rotor disk area, and disk loading on the mass–energy balance of the system.
The selected configuration is also consistent with recent literature on Martian rotorcraft, since in NASA studies on the MSH [2], alongside the coaxial configuration, multirotor and hexacopter architectures are considered credible options for larger scientific platforms carrying more significant payloads than Ingenuity.
Naturally, the absence of dedicated lifting surfaces means that vehicle support remains entirely provided by the rotors even during cruise, potentially resulting in higher power requirements than those of hybrid or fixed-wing configurations. However, this penalty is accepted as a trade-off in favour of greater architectural simplicity, reduced transition risk, and improved tractability of the preliminary model.
On this basis, the multicopter configuration is adopted as the reference architecture for the following chapters, where the mass–energy model is developed and the design space associated with the selected system is explored.

2.4 Effects on Aerodynamics

2.4.1 Low Reynolds Number Regime

One of the most relevant aerodynamic effects of flight on Mars is operation in a low-Reynolds-number regime: due to the extremely rarefied atmosphere, the Reynolds number is much lower than in terrestrial conditions, even for the same geometric scale and characteristic velocity. For a representative case at comparable altitude, with the same characteristic length and velocity, the Reynolds number on Mars can be approximately two orders of magnitude lower than on Earth, decreasing from values of the order of $10^6$to values of the order of $10^4 - 10^5$[7], [46].

This change substantially modifies the behaviour of the boundary layer, since as the Reynolds number decreases, viscous effects become relatively more important than inertial effects, transition to turbulence is delayed, and the laminar boundary layer becomes more vulnerable to adverse pressure gradients. As a consequence, the flow exhibits a greater tendency to separate, with an associated increase in drag and a degradation of the aerodynamic performance of conventional airfoils [46]. Furthermore, performance degradation may already begin below a critical Reynolds number of the order of 5×10^5[32], whereas the flight of small vehicles on Mars often occurs well below this threshold.

A particularly important phenomenon in this regime is the formation of a laminar separation bubble [42], [46], namely a localised separation of the boundary layer followed, in some cases, by reattachment after transition. This phenomenon is schematically shown in Figure 2.4.1, where the separation of the laminar boundary layer, the separated-flow region, and the reattachment after transition can be observed.

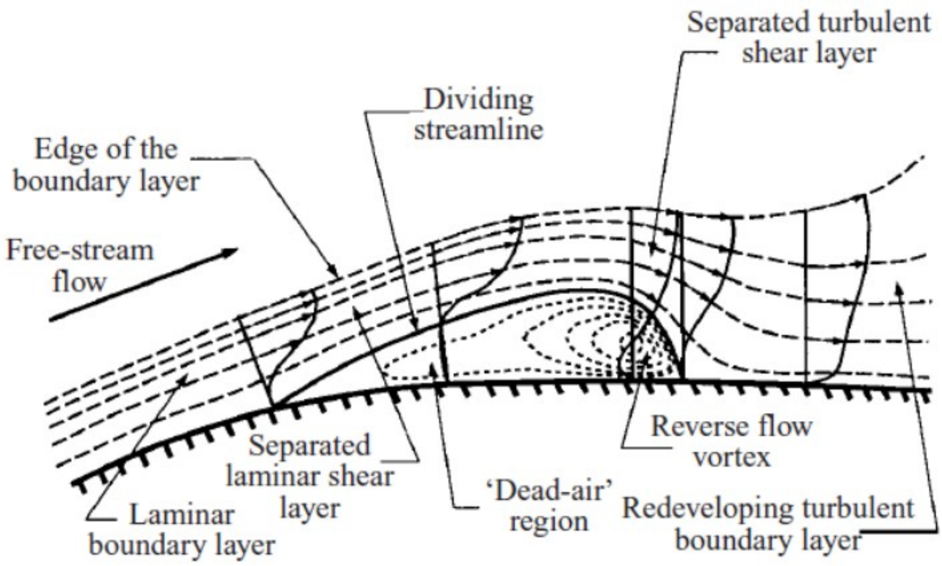

Figure 2.4.1 — Schematic representation of a laminar separation bubble over an airfoil. Source: [42]

The presence of a laminar separation bubble introduces a strong sensitivity of aerodynamic performance to airfoil geometry and operating conditions, contributing to the non-linearity of aerodynamic curves and to the reduction of the lift-to-drag ratio. For this reason, the low-Reynolds-number problem should not be regarded as a secondary consequence of low atmospheric density, but rather as one of the main aerodynamic constraints of Martian flight.

2.4.2 Effects of Low Atmospheric Density

Since aerodynamic forces scale with ρV^2 [23], the rarefaction of the atmosphere substantially reduces the ability of the fluid to generate lift and thrust for a given velocity and geometric scale. As a result, configurations designed for the terrestrial environment cannot be directly transferred to the Martian context without a significant revision of the design criteria.
This condition imposes a direct trade-off between operating velocity, the size of the aerodynamically active surfaces, and vehicle architecture: maintaining the same aerodynamic force in a rarefied atmosphere requires either an increase in velocity or an increase in reference area.

These two effects can be visualised in simplified form: the Figure 2.4.2 shows that, for a fixed area and aerodynamic coefficient, the required velocity increases as atmospheric density decreases. Figure 2.4.3, instead, shows that, if velocity is kept constant, the required surface area increases much more markedly.
This observation has an immediate design implication: increasing velocity can only partially mitigate the penalty associated with atmospheric rarefaction, while introducing additional constraints in terms of compressibility, propulsion requirements, and vehicle control. Increasing the aerodynamic surface

area, on the other hand, reduces the severity of these constraints, but it introduces penalties in terms of mass, volume, and structural integration.

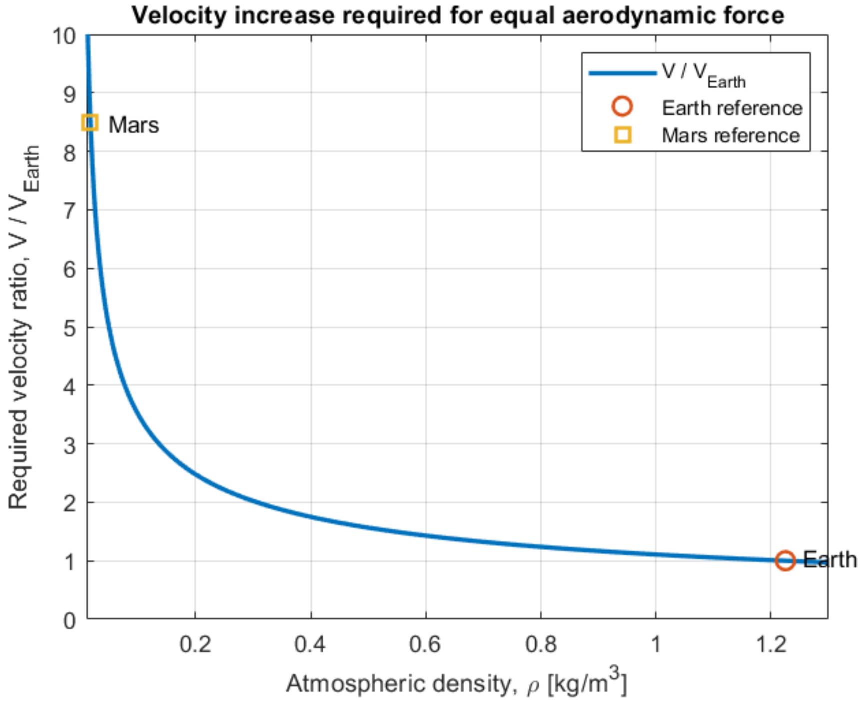

Figure 2.4.2 — Effect of atmospheric density on the velocity required to generate the same aerodynamic force

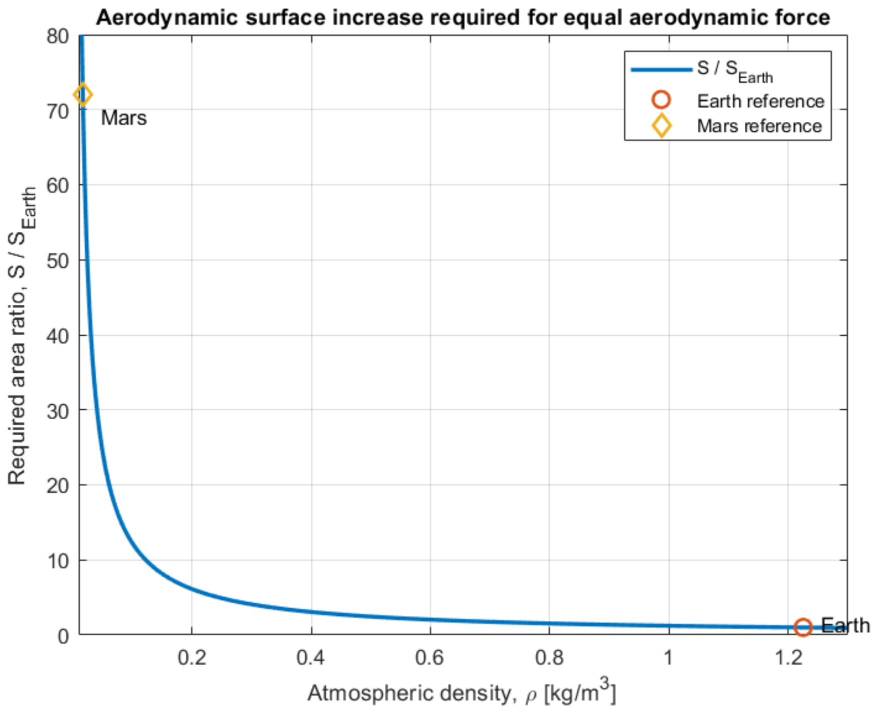

Figure 2.4.3 — Aerodynamic surface increase required at lower atmospheric density to generate the same aerodynamic force

2.4.3 Compressibility Effects

Although the operating speeds considered in this study are not high in absolute terms, compressibility effects become relevant in the Martian context because the speed of sound is lower than on Earth. For the same characteristic velocity, the Mach number is therefore higher on Mars, reducing the available operating margin before compressibility effects begin to affect aerodynamic performance in a non-negligible way [2].

Figure 2.4.4 illustrates this effect in general terms by comparing the Mach number associated with a given characteristic velocity in the terrestrial and Martian atmospheres: the plot shows that, for the same velocity, the Mach number is systematically higher in the Martian atmosphere because of the lower speed of sound, limiting the possibility of compensating for the low atmospheric density simply by increasing the operating speeds.

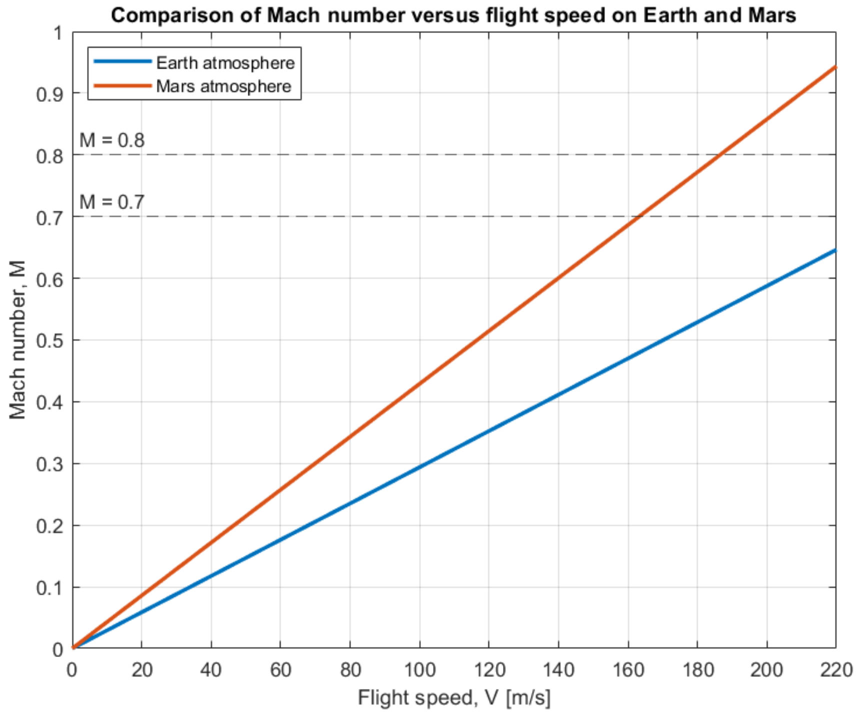

Figure 2.4.4 —Mach number comparison between Earth and Mars

In the case of a rotorcraft, however, the issue is not limited to the forward speed of the vehicle, since even if the cruise speed of the multicopter remains moderate, the local velocities along the blades can be much higher, especially near the blade tip. For this reason, the most representative parameter is the tip Mach number:

$$M_{\mathrm{tip}} = \frac{V_{\mathrm{tip}}}{a}$$

where V_{tip} is the blade tip speed and a is the speed of sound in the Martian atmosphere. Since the latter is lower than on Earth, the rotor can approach compressible-flow conditions even when the translational speed of the vehicle is relatively low. Studies on the MSH [2] show that blade tip Mach number, particularly on the advancing blade, is a critical parameter for rotor efficiency, since it is associated with airfoil drag-divergence limits.

This aspect is further complicated by the fact that Martian rotors operate simultaneously at low Reynolds numbers and at non-negligible local Mach numbers. The compressibility constraint can also be interpreted in terms of the maximum allowable rotational speed for a given rotor radius. The blade tip speed can be written as:

$$V_{\mathrm{tip}} = \Omega R$$

or, in terms of rotational speed expressed in rpm:

$$V_{\mathrm{tip}} = \frac{2\pi R \cdot RPM}{60}$$

Substituting this relation into the definition of tip Mach gives the maximum rotational speed compatible with an assigned M_{tip} limit:

$$RPM_{\max} = \frac{60 M_{\mathrm{tip,max}} a}{2\pi R}$$

Figure 2.4.5 was obtained by applying this relation for different limiting values of $M_{\mathrm{tip,max}}$, assuming a Martian speed of sound of approximately 233 $\mathrm{m/s}$.

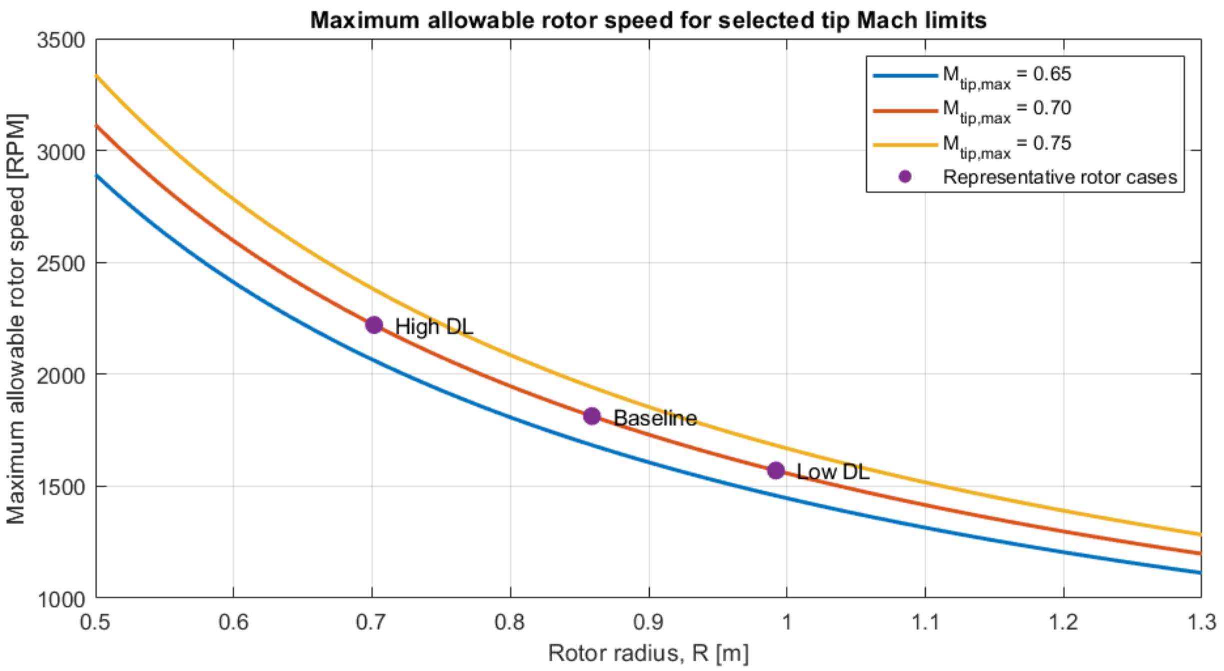

Figure 2.4.5 — Maximum allowable rotor speed as a function of rotor radius for selected tip Mach limits in Martian atmosphere

The plot shows that, as rotor radius increases, the maximum allowable rotational speed decreases: such a behaviour highlights an important compromise in Martian rotor sizing, namely that larger rotors help reduce disk loading and induced power, but they also reduce the available rotational-speed margin before critical tip Mach values are reached.

In this work, compressibility is therefore not treated as the dominant phenomenon governing the overall flight condition, but as a plausibility constraint on rotor sizing, so the mass–energy model does not include a detailed blade design or an explicit estimate of the required rotational speed, but tip Mach number is considered as a consistency parameter with respect to the rotor diameters obtained from the sizing process. In this way, the compressibility constraint is retained within the design process without introducing a level of aerodynamic detail that would not be consistent with the preliminary nature of the study.

2.4.4 Summary of Aerodynamic Implications

The aerodynamic effects discussed in the previous sections are strongly coupled and should not be interpreted as independent constraints:

- low atmospheric density reduces the aerodynamic forces available for a given velocity and reference area;
- the resulting low-Reynolds-number regime increases the relevance of viscous effects and separation phenomena;
- the reduced speed of sound makes local Mach-number constraints more restrictive, especially near the rotor tips.

The main implications of these effects are summarised in Table 2.4.1, where each aerodynamic phenomenon is linked to its primary consequence for the preliminary design of a Martian multicopter. Overall, the table shows that Martian multicopter design is governed by a coupled aerodynamic constraint: low density drives the need for large rotor areas, low Reynolds numbers penalise blade efficiency, and the reduced speed of sound limits the admissible rotor tip speed.

Aerodynamic effect	Main consequence	Design implication
Low Reynolds number regime	Increased viscous effects, delayed transition, higher risk of separation and airfoil performance degradation	Rotor aerodynamic efficiency cannot be assumed equivalent to terrestrial conditions
Laminar separation bubble	Non-linear airfoil behaviour, increased drag and lower lift-to-drag ratio	Airfoil performance becomes highly sensitive to geometry and operating conditions
Low atmospheric density	Reduced aerodynamic force generation for a given velocity and reference area	The vehicle must rely on either larger reference areas or higher operating velocities
Velocity increase as compensation	Higher speed can recover part of the aerodynamic force but increases propulsive and Mach-related constraints	Increasing operating speed alone is not a sufficient solution
Larger aerodynamic surface as compensation	Required disk or lifting area increases significantly as density decreases	Aerodynamic benefits must be balanced against mass, packaging and structural penalties
Compressibility effects	Mach number is higher for the same velocity because of the lower Martian speed of sound	Local Mach-number limits become more restrictive
Rotor tip Mach constraint	Blade-tip regions may approach compressibility-related penalties even at moderate vehicle speeds	Tip Mach must be checked as a rotor aerodynamic consistency parameter

Table 2.4.1 — Summary of the main aerodynamic effects relevant to Martian multicopter design.

2.5 Effects on Rotorcraft Design

2.5.1 Thrust generation requirements

The first design requirement is the ability to generate enough thrust to support the vehicle weight in an extremely rarefied atmosphere. In hover, the total thrust must balance the system weight,

$$T = mg_M$$

while, as a first approximation, momentum theory [30] gives the following relation for an ideal actuator disk in hover:

$$T = 2\rho A v_i^2$$

where ρ is the atmospheric density, A is the rotor disk area, and v_i is the induced velocity. This expression shows that, for a given thrust requirement, the low Martian density requires either an increase in induced velocity or an increase in the available rotor disk area. The literature on Martian rotorcraft clearly indicates that the most favorable solution is generally to increase the disk area, in order to limit the energetic cost of thrust generation.

The advantage of large rotor disk areas follows from the fact that induced power increases rapidly as disk loading increases [30], so Martian rotorcrafts tend to be designed with low disk-loading values, large rotor diameters, and carefully limited operating speeds. In a multicopter configuration, the total thrust is distributed among multiple rotors,

$$T_{\text{tot}} = \sum_{i=1}^{N_r} T_i$$

Assuming identical rotors and a uniform load distribution, each rotor provides a thrust contribution equal to T_{tot}/N_r where N_r is the number of rotors; such an approach makes it possible to increase the total disk area without relying on a single large rotor, improving modularity and integration, while at the same time introducing implications in terms of structural mass, control, and system complexity.

2.5.2 Rotor sizing implications

The Martian environmental conditions make rotor sizing one of the most delicate steps of the design process. The central parameter is disk loading, defined as the ratio between the required thrust and the available rotor disk area [30]:

$$DL = \frac{T}{A}$$

In this thesis, disk loading is therefore expressed as a force-to-area ratio, in $\mathrm{N/m^2}$. Any literature values reported as mass per unit area must consequently be converted using Martian gravity. For a given vehicle weight, reducing disk loading decreases the induced velocity and therefore the power required for lift generation, so in an atmosphere such as that of Mars, maintaining high DL values is particularly penalizing from an energy point of view. For a multicopter the total disk area can be expressed as:

$$A_{\text{tot}} = N_r A_{\text{rotor}}$$

This relation makes one of the main design trade-offs explicit: increasing the number of rotors or their diameter helps reducing disk loading, but also introduces penalties in terms of size, mass, and integration complexity. Figure 2.5.1 clarifies this aspects by showing the rotor radius required as the target disk loading varies, for different numbers of rotors and for a fixed representative vehicle mass.

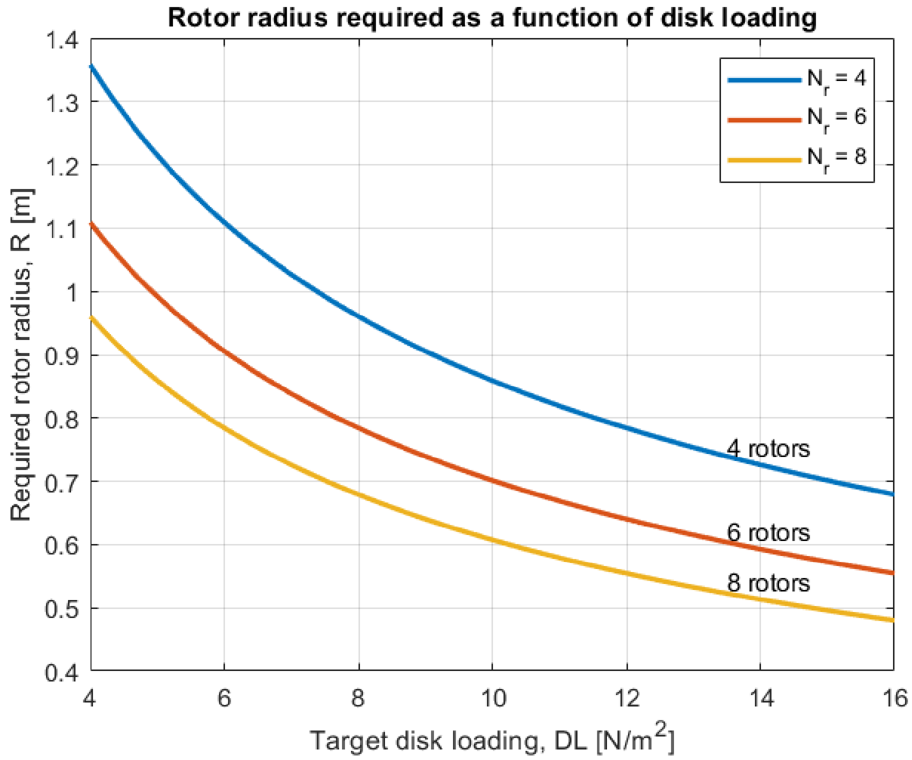

Figure 2.5.1 — Required rotor radius as a function of target disk loading for different rotor configurations

The figure shows that reducing disk loading requires a significant increase in rotor scale, whereas increasing the number of rotors makes it possible to achieve the same target with smaller rotor radius. The plot therefore highlights that rotor sizing does not depend on a single parameter, but on the compromise between total disk area, number of rotors, and geometric constraints of the configuration. This trade-off will be revisited in the parametric analyses of Chapter 6, where disk loading is varied to assess its effect on rotor diameter, hover power, and mission energy.

2.5.3 Power requirements for hover

Hovering represents the main performance constraint for a Martian multicopter, since in this phase the entire vehicle weight must be supported by the rotors alone. According to momentum theory [30], the ideal induced power can be written as

$$P_i = T v_i$$

and, by combining this expression with the thrust relation, one obtains

$$P_i = \frac{T^{3/2}}{\sqrt{2\rho A}}$$

where T is the total required thrust, ρ is the atmospheric density, and A is the total rotor disk area. This formulation shows that the energetic cost of lift generation increases rapidly as atmospheric density decreases and disk loading increases. For this reason, the estimation of hover power is a central element in the preliminary sizing of rotorcraft intended to operate in the Martian environment.

In addition to induced power, profile power must also be considered, since it accounts for the aerodynamic drag of the blades during rotation: as in the MSH study [2], the rotor power in hover is decomposed into an induced contribution and a profile contribution, the latter being associated with the aerodynamic resistance of the rotating blades [2]. A simplified expression for profile power can be written as

$$P_0 = \frac{1}{8}\rho A_b V_{\text{tip}}^3 C_{d,\text{mean}}$$

where A_b is the total blade area, V_{tip} is the blade tip speed, and $C_{d,\text{mean}}$ is the mean section drag coefficient. This relation shows that, for a given geometry, profile power scales with the cube of blade tip speed and with the average drag of the blade sections. The profile term is therefore particularly important in the Martian case, because the low Reynolds numbers tend to increase airfoil drag, while compressibility constraints require careful control of blade tip speed [7], [8].

To account for losses relative to the ideal induced-power estimate, a correction factor k, or induced power factor, is introduced, which represents the increase in actual induced power relative to the value predicted by momentum theory. Following this approach, rotor power can be expressed as the sum of the corrected induced contribution and the profile contribution [46]:

$$P_{\text{rotor}} = kT\sqrt{\frac{T}{2\rho A}} + \frac{1}{8}\rho A_b V_{\text{tip}}^3 C_{d,\text{mean}}$$

The first term represents the power required to generate thrust, while the second represents the power dissipated to overcome the aerodynamic drag of the blades. In this thesis, this formulation is used as the physical basis for interpreting the role of rotor disk area, disk loading, and blade tip speed in the power requirement of the multicopter. In the mass–energy model developed in Chapter 4, rotor power is then converted into the power required from the battery through the efficiencies of the propulsive chain. In general form,

$$P_{\text{hover,elec}} = \frac{P_{\text{rotor}}}{\eta_{\text{prop}}}$$

where η_{prop} represents the overall efficiency of the propulsive chain, including motor, power electronics, and possible mechanical losses. This distinction makes it possible to separate the aerodynamic problem, associated with thrust generation, from the energy problem, associated with the power actually required from the onboard system.

Preliminary studies on Martian rotorcraft adopt a similar logic, highlighting the need to balance the reduction of induced power through low disk-loading values with the control of profile losses and local Mach limits through an appropriate choice of blade tip speed, solidity, and rotor loading [4]. The resulting design problem is therefore strongly coupled: increasing rotor disk area reduces induced power, but may penalize mass, overall size, and packaging; increasing rotational speed facilitates thrust generation, but increases profile losses and brings the rotor closer to compressibility limits.

2.5.4 Energy and endurance limitations

The power constraint translates directly into an energy constraint: the energy required by a mission can be expressed in general form as

$$E = \int P(t)\,dt$$

and therefore it depends on the full operational profile of the vehicle. In a VTOL mission, phases such as take-off, climb, operational hovering, transfer flight, and landing contribute differently to the overall energy balance: hovering tends to be the most demanding phase in terms of instantaneous power, whereas the transfer segment may have a significant impact on the total mission energy.
The onboard available energy depends on the battery pack mass and on its specific energy and, as a first approximation, can be written as

$$E_{\text{avail}} = m_{\text{bat}}\epsilon_{\text{spec}}$$

where m_{bat} is the battery mass and ϵ_{spec} is the pack-level specific energy. Consequently, endurance can be estimated in simplified form as

$$t_{\text{max}} = \frac{E_{\text{avail}}}{\bar{P}}$$

where $\bar{P}$ is an equivalent average power over the mission profile. This relation highlights the direct connection between energy capacity, required power, and operating time, but it should not be interpreted as a complete estimate of the actual endurance, since it does not yet include margins, auxiliary loads, depth-of-discharge limits, or thermal conditions.
The critical point in the Martian case is that mass, power, and energy are strongly coupled, so increasing battery mass increases the available energy, but it also increases the vehicle weight, which requires greater thrust and therefore higher power during the flight phases [4].

Another key aspect is that in the Martian context a significant fraction of the energy capacity may be absorbed by auxiliary loads, thermal management, onboard electronics, and survival during non-operational phases. The experience of Ingenuity [16] has shown that night survival can represent a relevant contribution to the energy budget, mainly because of the low ambient temperatures on Mars.

As a result, vehicle endurance cannot be interpreted as a simple ratio between battery capacity and flight power, but as the outcome of a broader balance involving mission profile, propulsion, energy-system mass, and auxiliary loads. This interdependence is precisely what makes an iterative mass–energy approach necessary for the preliminary sizing developed in the following chapters.

2.5.5 Summary of Rotorcraft Design Implications

The design implications discussed in this section are summarised in Table 2.5.1. The table links the main rotorcraft-level constraints to the corresponding design response and highlights the variables that will be explicitly treated in the mass–energy model developed in the following chapters. Overall, these considerations show that the preliminary design of a Martian multicopter cannot be reduced to rotor sizing alone, since rotor disk area, disk loading, hover power, battery mass and endurance are strongly coupled:

- increasing rotor area can reduce induced power, but may penalise mass and integration
- increasing battery mass can improve available energy, but also increases the thrust and power required for flight

This coupling motivates the mass–energy modelling approach developed in the following chapter.

Design aspect	Main constraint	Design implication
Thrust generation	The vehicle must balance its weight in a rarefied atmosphere	Sufficient total rotor disk area is required to generate thrust without excessive induced velocity
Rotor sizing	High disk loading is energetically penalising in low-density conditions	Low disk loading and large rotor diameters are favoured
Multirotor architecture	Total thrust is distributed among several rotors	Disk area can be split across multiple rotors, improving modularity but increasing integration complexity
Hover power	Induced power increases as atmospheric density decreases and disk loading increases	Hover becomes a sizing-critical condition for the propulsion system
Profile power	Blade drag and tip speed contribute significantly to rotor losses	Tip speed, solidity and mean airfoil drag must be controlled to avoid excessive profile losses
Energy storage	Mission energy depends on both power level and phase duration	Battery mass must be sized from the complete mission profile, not from hover power alone
Endurance	Available energy is limited and coupled with vehicle mass	Increasing battery mass improves energy capacity but also increases thrust and power demand
Auxiliary and survival loads	Energy is also required for thermal survival and onboard systems	Battery sizing must include non-propulsive loads and energy margins

Table 2.5.1 — Summary of the main rotorcraft design implications for a Martian multicopter

3. Mission Definition and Requirements

3.1 Mission Objectives and Scenario

3.1.1 Mission objectives

The present work investigates the preliminary feasibility of an electric VTOL vehicle intended to operate in the Martian atmosphere, with particular attention to a multicopter configuration.
The aim of the work is not to define a final vehicle design, nor to optimize a single configuration, but rather to develop a physically grounded preliminary model capable of linking the operating environment, mission requirements, and the main design variables of the system. On this basis, the analysis is intended to identify plausible configurations and to clarify the key trade-offs between rotor disk area, power demand, endurance, energy-system mass, and the overall scale of the vehicle.

The contribution of the work is therefore twofold: it provides a quantitative basis for assessing the preliminary feasibility of a Martian multicopter concept and, at the same time, it offers a structured analysis of the main design drivers. This makes it possible to identify the parameters that most strongly affect system feasibility and to evaluate how far the configuration can be scaled toward more demanding mission requirements.

3.1.2 Operational scenario

The operational scenario considered in the present study is that of a lightweight robotic aerial platform used in support of a broader Martian exploration architecture, and it is assumed to operate close to the surface and to perform short-range local missions from a fixed reference point, which may be represented, for example, by a lander, a rover, or a surface station.

Within this context, the vehicle is intended to carry out repeated sorties of limited duration rather than fully autonomous long-range missions, so its main functions include:

- reconnaissance of nearby areas;
- observation of scientific targets;
- support for route planning of surface assets;
- exploration of rough or high-risk terrain

The scenario considered is therefore consistent with local aerial mobility missions, in which the vehicle acts as a capability multiplier for a wider surface exploration mission.
The reference architecture is that of a supported system, in which the aerial platform represents a local operational asset rather than an exploration vehicle entirely separated from the rest of the mission: this assumption makes it possible to focus the analysis on the central problem addressed in this work, namely the physical and energetic sustainability of flight on Mars, without extending the study to a broader system-level assessment that would also require full mission self-sufficiency to be considered.

3.1.3 Reference mission profile

It is necessary to define a reference mission profile that is realistic enough to represent a plausible operational sortie, while remaining sufficiently simple to be used as the basis for the mass–energy model developed in the following chapters.

The reference case is defined as a local one-way mission composed of the following phases: vertical take-off, climb to the operating altitude, transfer toward a target area, hovering or station-keeping for observation and sensing activities, followed by descent and vertical landing. Having successfully completed the sortie, the case study investigates a ground phase with a thermal-survival requirement before the next recharge cycle.

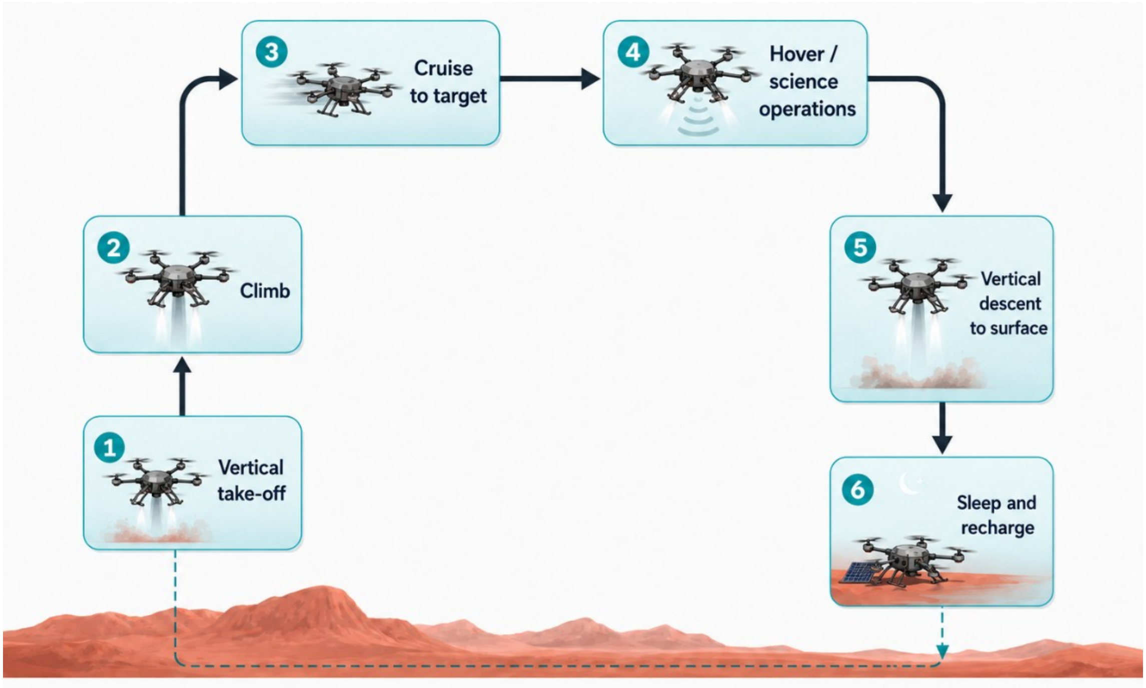

Figure 3.1.1 — Reference mission profile

The reference mission is not introduced as the definitive description of a single, rigidly prescribed operation, but rather as a functional structure intended to identify the flight phases that most strongly affect system sizing. In the case of a multicopter configuration, the mission profile covers segments in which lift is provided entirely by the rotors under nearly quasi-steady conditions, such as take-off, initial climb, and hovering, and segments in which the vehicle operates in forward flight at moderate speed. This distinction is particularly important because the different phases do not contribute equally either to peak power demand or to the overall mission energy.

In particular, take-off, initial climb and hovering represent the most severe conditions in terms of required thrust and instantaneous power, whereas the transfer phase, although generally less demanding in terms of peak power, may contribute significantly to the overall energy budget when the operating distance is not negligible. Descent and landing, by contrast, are not considered sizing-critical for the first-order design of the vehicle and are therefore treated in a more simplified manner in the following analysis.

The mission profile therefore serves a dual purpose: on the one hand, it defines the reference case on which the baseline sizing is built, while on the other it provides the logical structure for the following parametric analysis of endurance, range, and energy loads; in this way it represents the direct link between the operational scenario, the mission requirements and the sizing model.

3.2 Mission Requirements and Sizing Logic

3.2.1 Mission requirements and design drivers

In the present study, mission requirements define the operational functions that the multicopter must be able to perform within the Martian exploration scenario considered, so they describe the expected mission behavior, the operating context, and the main functional capabilities required of the platform.

ID	Mission requirement	Rationale
MR-01	The mission shall employ an aerial VTOL platform to support local Martian surface exploration.	Establishes the mission as an aerial-support capability rather than a standalone long-range aircraft mission.
MR-02	The mission shall be performed within the Martian near-surface atmospheric environment.	Defines the operational environment that drives the aerodynamic and energy constraints of the vehicle.
MR-03	The mission shall operate in support of a surface exploration architecture, such as a lander, rover, or fixed surface station.	Clarifies that the VTOL vehicle acts as a complementary asset within a broader robotic mission.
MR-04	The mission shall enable vertical take-off from an unprepared Martian surface.	Captures the need to operate without runways or prepared launch infrastructure.
MR-05	The mission shall include a climb phase to reach a local operating altitude suitable for terrain reconnaissance and target access.	Connects the mission profile to the need for safe clearance and local mobility.
MR-06	The mission shall include a cruise segment from the initial surface asset toward a selected target area.	Defines the aerial mobility function of the mission.
MR-07	The mission shall allow hover or station-keeping over the target area for local science or reconnaissance operations.	Represents the key operational advantage of a VTOL multicopter compared with purely surface assets.
MR-08	The mission shall perform a vertical descent to the Martian surface near the target area.	Makes clear that the post-hover phase is a descent to the target surface, not a return to the initial site.
MR-09	The mission shall be considered a one-way local sortie, with no mandatory return to the initial take-off location.	Removes ambiguity from the mission architecture and distinguishes the reference case from an out-and-back profile.
MR-10	The mission shall include a post-landing surface phase for sleep, survival, and recharge.	Accounts for the operational cycle after landing and links the mission to non-propulsive energy needs.
MR-11	The mission shall carry a scientific or reconnaissance payload compatible with local terrain observation and target assessment.	Defines the functional purpose of the payload without imposing a detailed instrument design at mission level.

MR-12	The mission shall support repeated sorties, subject to recharge and survival constraints.	Frames the vehicle as a reusable local exploration asset rather than a single-use probe.
DR-01	The mission shall minimize dependence on complex deployment or transition mechanisms.	Supports the selection of a multicopter architecture and limits unnecessary architectural complexity.
DR-02	The mission shall be compatible with preliminary mass–energy sizing based on mission phases, environmental conditions, and vehicle-scale variables.	Links the mission definition to the modeling strategy used in the thesis.

Table 3.2.1 — Preliminary mission requirements for the Mars VTOL reference mission

Since this work is carried out at a preliminary feasibility level, these requirements are formulated at mission level and are intended to guide both the development of the model and the parametric analysis. The requirements reported in Table 3.2.1 therefore define the functional framework of the mission: the preliminary mass–energy model developed in the following chapters is used to translate the operational profile into physical design quantities. Parameters such as payload mass, cruise distance, hovering duration, battery mass, power demand, endurance, and range are therefore not introduced at this stage as independent mission-level requirements, but rather as baseline assumptions, design variables, or outputs of the sizing process.

3.2.2 Preliminary sizing logic

The sizing logic adopted in this work is built upon the mission requirements and the main design drivers identified in the previous section: as summarized in Figure 3.2.1, the problem is organized according to an input–model–output sequence in which the inputs define the operational and physical context of the mission, the mass–energy model converts this information into design-relevant quantities, and the outputs are then used to assess the preliminary plausibility of the configuration.

The first block collects the main sizing inputs and drivers, which represent the starting point for evaluating how the vehicle configuration must adapt to the constraints imposed by the mission and by the operating environment. Throrugh the central block, which represents the preliminary mass–energy model, the operational profile is translated into directly comparable physical quantities, such as power demand, required energy, and energy-storage mass.

The model outputs make it possible to assess whether a given combination of mission profile, payload mass, and gross mass leads to a physically plausible configuration. The lower block of the figure then represents the feasibility-assessment stage, in which the model results are interpreted in terms of mass–energy closure, scaling effects, and comparison between alternative configurations.

The dashed connections indicate that the process is not purely linear, since the outputs obtained from the model may require a revision of the initial inputs or design assumptions, especially when battery mass, power demand, or rotor dimensions become incompatible with a realistic configuration. In this way, Figure 3.2.1 represents the methodological approach adopted in the thesis: starting from mission requirements and design drivers, estimating the main physical quantities through a preliminary model, and using the results to identify the most promising regions of the design space.

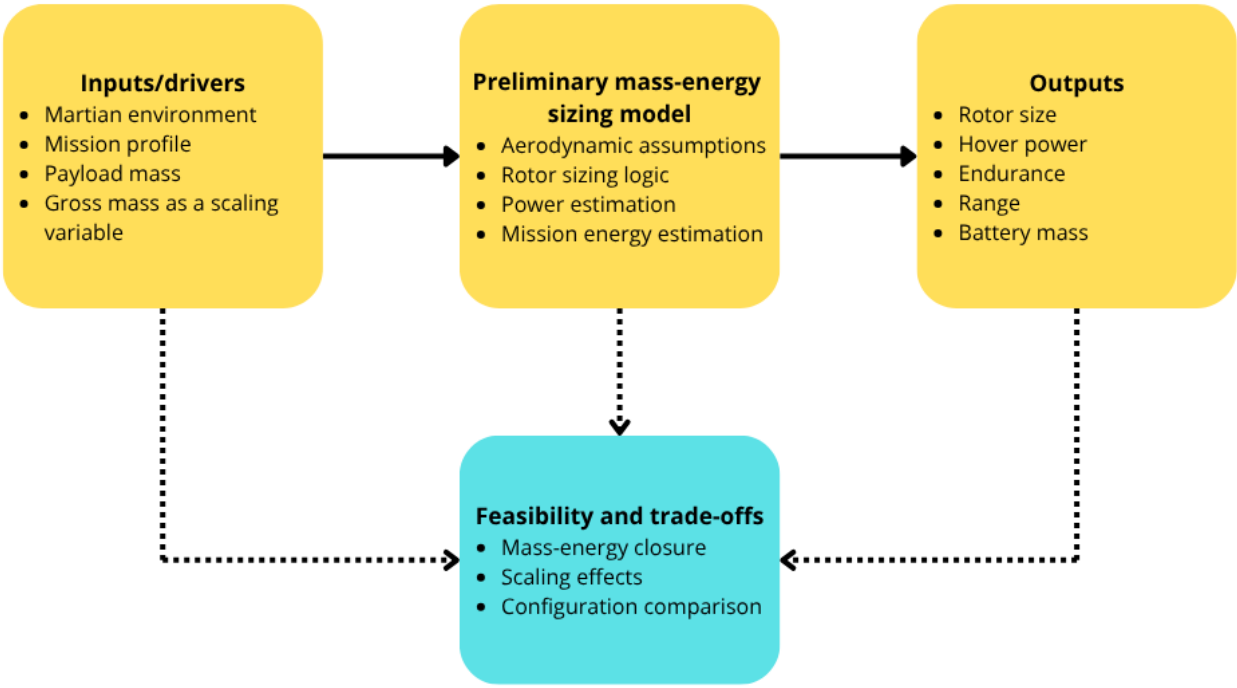

Figure 3.2.1 — Preliminary mass–energy sizing logic and feasibility assessment workflow

3.3 Design Assumptions

3.3.1 Aerodynamic assumptions

The aerodynamic behavior of the vehicle is described through a preliminary model aimed at evaluating the main design trade-offs rather than at reproducing the flow field around the system with high fidelity, so the multicopter is assumed to operate under nominal conditions representative of the case study defined in the previous sections, with particular attention to hovering and low-speed forward flight.

The rotor system is modeled through a global performance representation based on the distinction between induced power and profile power [30], the rotors are assumed to be identical and the total thrust is considered to be uniformly distributed among them. As a consequence, the model does not resolve in detail the radial load distribution along the blades, the specific geometry of the rotor sections, the aerodynamic interactions between rotors, or wake effects.
Blade performance is not derived from dedicated experimental data or from a detailed blade-element analysis, but is instead represented through global coefficients consistent with the preliminary level of the study. This choice allows the model to remain physically interpretable and suitable for parametric analysis, while acknowledging that the resulting values should be interpreted as feasibility estimates rather than high-fidelity aerodynamic predictions.
Ground effect, wind, atmospheric turbulence, and local gusts are also excluded from the model, in order to isolate the influence of the dominant parameters, especially atmospheric density, rotor disk area, disk loading, and vehicle mass, while leaving more detailed aerodynamic analyses to future developments.

3.3.2 Mission and energy modeling assumptions

The mission profile is also represented in simplified form, with the aim of building an operational framework that is coherent and analytically manageable, so the reference mission is not described as a detailed sequence of events with a complete trajectory, but rather as a set of functional phases representative of a typical local sortie.

In the following development of the model, not all phases are treated with the same level of detail: greater attention is given to the conditions that most strongly affect sizing, particularly hovering, initial climb, and forward flight [2]. Descent and landing, by contrast, are treated in a more compact manner, since they are less critical for the definition of the preliminary configuration.

Consistently with the preliminary nature of the study, the mission profile is therefore not used to represent a high-fidelity mission simulation, but as a functional framework on which the performance model and the following baseline sizing are built. In this way, the different phases become operational categories to which representative power levels and energy contributions can be assigned, while keeping the design process sufficiently general to support the later parametric exploration.

The main operational quantities, such as mission duration, useful range, and hovering time, are not introduced in this chapter as final and immutable specifications, but as reference parameters that will be quantified in the baseline sizing of Chapter 5 and then explored in Chapter 6, in order to preserve consistency between mission definition and model development, avoiding the imposition of arbitrary constraints before the physical plausibility of the system has been quantitatively assessed.

4. Mass–Energy Analysis Model

4.1 Modeling strategy

4.1.1 Modeling objectives and scope

The target of the model developed in this work is to provide a preliminary analysis tool for assessing the feasibility of a multicopter vehicle operating in the Martian atmosphere, by linking mission requirements, environmental constraints, and the main system-level design variables.
More specifically, the model is intended to provide a consistent estimate of the power required during the main flight phases, the overall mission energy demand, and the mass of the energy-storage system needed to sustain the operational profile considered.
Particular attention is given to the interaction between rotor disk area, thrust requirements, hover power, energy demand, and the overall mass of the system, quantities are strongly coupled in the Martian environment, where the low atmospheric density makes thrust generation particularly demanding and where the available onboard energy remains one of the main limiting factors.
In this chapter, the model is developed as a link between mission definition and configuration design, allowing payload, endurance, and range requirements to be translated into physical quantities that can be directly used in the sizing process.

4.1.2 Model structure and workflow

The model adopted in the present study is organized in a modular form, so as to make explicit the logical sequence that connects the mission profile to the main design quantities of the vehicle. As shown in Figure 4.1.1, the workflow begins with the definition of the mission inputs and the reference environmental conditions, and then it proceeds with the estimation of the required thrust, the power demand in the different flight phases, and the overall mission energy, based on this energy requirement, the battery mass needed to sustain the operational profile is then estimated.

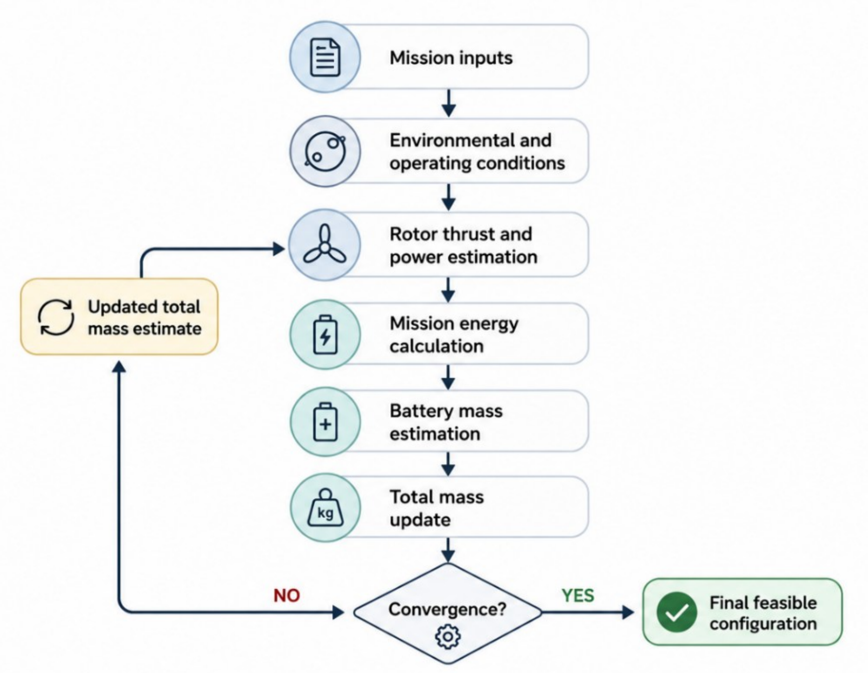

Figure 4.1.1 — Iterative sizing workflow adopted for the preliminary mass–energy model

The key of the model is the coupling between mass, power, and energy: the battery mass is not assigned, since it depends on the energy required by the mission; at the same time, the required energy depends on the overall system mass, because this mass determines the vehicle weight, the thrust required for lift generation, and therefore the power demand throughout the different mission phases [4].
For this reason, in the baseline sizing case the process is applied iteratively: the total mass is updated on the basis of the calculated battery mass, and the procedure is repeated until convergence is achieved.
The workflow can be summarized through the following main steps:

- definition of the mission inputs and environmental parameters;
- estimation of thrust and power in the relevant flight phases;
- integration of the energy demand along the mission profile;
- estimation of the battery mass;
- update of the total system mass;
- verification of solution convergence.

The adopted approach makes it possible not only to obtain a coherent preliminary configuration for the baseline case, but also to explore the sensitivity of the system to the main design parameters. In the following analyses, the same mass–energy logic is used to evaluate the effect of variations in gross mass, disk loading, payload, and available energy capacity, while maintaining a clear distinction between mission inputs, modeling assumptions, and outputs of the sizing process.

4.2 Rotorcraft Power Model

4.2.1 Hover power formulation

For a multicopter configuration operating on Mars, hovering represents the most demanding reference condition from a propulsive standpoint [2], since the entire weight of the vehicle must be supported solely by the thrust generated by the rotors. For this reason, the formulation of hover power constitutes the starting point of the performance model developed in this work and one of the key steps in the mass–energy sizing process.
Hover power is generally decomposed into two main contributions:

- induced power, associated with the energy required to accelerate downward the air mass that produces the necessary thrust;
- profile power, associated with the aerodynamic losses due to the drag of the rotating blades.

This decomposition is explicitly adopted in the Mars Science Helicopter study [2], and the hover power can therefore be written as:

$$P_{hover} = P_i + P_p$$

where P_i represents the induced power and P_p the profile power. Following the formulation reported in the MSH study [2], the induced power is expressed as:

$$P_i = \kappa\, T \sqrt{\frac{T}{2\rho A}}$$

where T is the total thrust required, ρ is the local atmospheric density, A is the total rotor disk area, and κ is the induced power factor, introduced to account for deviations from the ideal momentum-theory prediction. This expression directly highlights one of the central aspects of the design problem: for a given thrust requirement, a reduction in atmospheric density leads to an increase in induced power, whereas an increase in the available rotor disk area helps to reduce it.

The second contribution is the profile power, which in the same reference is written as:

$$P_p = \rho A_b V_{tip}^3 \frac{1}{8} \bar{c}_d$$

where A_b is the total blade area, V_{tip} is the blade tip speed, and $\bar{c}_d$ is a mean drag coefficient used to represent, in a global form, the aerodynamic losses of the rotor blade sections. This term is particularly relevant in the Martian case, since the low Reynolds numbers typical of flight on Mars lead to a significant increase in airfoil drag compared with terrestrial conditions [7], thereby increasing the portion of power associated with profile losses.

The adopted formulation therefore emphasizes the twofold constraint that characterizes rotor design for Mars:

- the low atmospheric density strongly penalizes induced power and drives the design toward large-diameter rotors, corresponding to low disk loading values;
- the need to limit profile power requires careful control of blade tip speed and airfoil aerodynamic performance, also in relation to local Mach number constraints.

The MSH report [2] shows that the P/T ratio decreases as disk loading is reduced and rotor aerodynamic efficiency is improved, confirming the central role of these parameters in preliminary rotorcraft sizing. In the present work, this formulation is adopted as the basis of the rotorcraft power model for two main reasons:

- it preserves a clear physical interpretation, since it explicitly separates the contribution associated with thrust generation from the losses associated with the rotating blade system.
- it remains sufficiently compact to be integrated into a preliminary sizing framework, in which hover power must be recalculated iteratively as total mass, rotor disk area, and mission parameters vary.

Following this logic, the thrust required in hovering is first used to estimate the power demand, which is then integrated over the mission profile to determine the required energy; this energy requirement is finally used to size the energy-storage system.
A further useful parameter for interpreting rotor efficiency in hover is the figure of merit, FM, defined as the ratio between ideal power and actual power [30]: it provides a compact measure of rotor efficiency in hovering and it is commonly used in rotorcraft performance analysis, including preliminary studies of Martian rotorcraft [2].

4.2.2 Induced power estimation

Within the model developed here, the thrust required in hover is assumed to be equal to the vehicle weight,

$$T = W = mg_m$$

thereby linking the induced-power calculation directly to the total system mass. The total rotor disk area is expressed as

$$A = N_r \pi R^2$$

where N_r is the number of identical rotors and R is the rotor radius. With this formulation, the induced-power term is explicitly governed by the main design variables considered in the thesis: vehicle mass, number of rotors, and rotor size. Replacing these relations into the induced-power formulation [30] gives an expression that can be directly implemented within the iterative sizing procedure:

$$P_i = \kappa m g_m \sqrt{\frac{m g_m}{2\rho N_r \pi R^2}}$$

This equation clearly shows that for a given vehicle mass, increasing the total rotor disk area reduces the required power, whereas an increase in mass leads to a nonlinear growth of the induced-power term. The estimation of P_i is therefore one of the central steps of the mass–energy loop developed in this chapter.

Values of the induced power factor κ commonly adopted in hover are of the order of 1.2 [2]. In a similar way, preliminary models for Martian rotorcraft often introduce global efficiency parameters to correct the ideal estimate provided by momentum theory, with figure-of-merit values of approximately 0.6 being used, for example, in comparative analyses of multirotor configurations. In this thesis, κ is therefore treated as a model parameter, selected consistently with the preliminary level of fidelity of the analysis.

4.2.3 Profile power contribution

The total blade area is expressed as a function of rotor solidity:

$$A_b = \sigma A$$

where σ is the rotor solidity and A is the total rotor disk area. Substitution into the profile-power expression gives

$$P_p = \rho \sigma A V_{tip}^3 \, \frac{1}{8} \, \bar{c}_d$$

And, since $A = N_r \pi R^2$,

$$P_p = \rho \sigma N_r \pi R^2 V_{tip}^3 \, \frac{1}{8} \, \bar{c}_d$$

This form is directly suitable for implementation in the model and makes the dependence of profile power on the main rotor design variables explicit: number of rotors, rotor radius, solidity, and blade tip speed. Unlike induced power, the profile-power contribution is not directly driven by the thrust requirement, but it is highly sensitive to blade tip speed, which appears with a cubic dependence. This is especially important in the Martian case, where increasing rotor speed may initially appear to be an attractive way to generate thrust in a rarefied atmosphere. In practice, however, a higher V_{tip} rapidly increases profile power and also brings the rotor closer to the limits imposed by tip Mach number.

A second critical quantity is the mean drag coefficient $\bar{c}_d$:in Martian rotorcraft, the low Reynolds numbers experienced by the blade sections lead to significantly larger viscous losses than in terrestrial conditions [7]. At the very low Reynolds numbers characteristic of flight on Mars, airfoil drag can increase by a factor of approximately 4–5 relative to typical terrestrial helicopter values, with a direct impact on profile power [2]. Similar considerations are also found in studies of the Mars Science Helicopter rotor, where the flow over the blade sections is described as subcritical, with a marked increase in section drag coefficient and a strong sensitivity of performance to low-Reynolds-number effects [2], [8].

For these reasons, profile power is not computed here from a detailed spanwise distribution of blade-section properties, but through a global mean coefficient consistent with the preliminary nature of the model. This keeps the formulation compact enough for parametric analysis while preserving the physical meaning of the profile-power contribution in the overall power balance.

The simultaneous presence of induced and profile power highlights the fundamental compromise involved in rotor design for Mars: increasing the rotor disk area reduces the induced-power contribution, whereas relying on higher rotor speeds to generate thrust tends to increase profile power rapidly. The power model adopted in this work is intended to capture this balance in a compact form, so that it can be incorporated into the mission-energy calculation. The following section combines the contributions introduced so far to define the power profile associated with the different phases of the reference mission.

4.2.4 Power profile for each phase

After defining the hover-power requirement, the model is extended to the main phases of the mission profile: vertical take-off, climb, forward flight toward the target, operational hovering, descent, and landing. The flight profile is discretized into operational segments, each associated with a representative power level: vertical take-off, operational hovering, and landing are treated as hover-dominated conditions, since in these phases the vehicle is supported entirely by the rotors; climb is modeled by adding to the hover power the mechanical power required to increase altitude, using a simplified formulation consistent with momentum-theory-based rotorcraft modeling [30]:

$$P_{climb} = P_{hover} + \frac{W V_{climb}}{\eta_{prop}}$$

where W is the vehicle weight, V_{climb} is the vertical climb speed, and η_{prop} is the overall efficiency of the propulsive chain. Descent is represented in an analogous but opposite manner, as a condition requiring less power than hover because of the favorable contribution of the downward vertical velocity:

$$P_{descent} = P_{hover} - \frac{W V_{descent}}{\eta_{prop}}$$

Forward flight toward the target is described through a dedicated estimate of cruise power, obtained as the sum of three main contributions: induced power in forward flight, profile power corrected for forward motion, and parasite power associated with the aerodynamic drag of the vehicle body [2]:

$$P_{cruise} = P_{i,cruise} + P_{p,cruise} + P_{par,cruise}$$

The aerodynamic drag of the body is estimated using an equivalent drag coefficient and a reference frontal area:

$$D = \frac{1}{2}\rho V_{cruise}^2 C_D S_{ref}$$

or, in aggregated form,

$$D = \frac{1}{2}\rho V_{cruise}^2 C_D S_{ref} = \frac{1}{2}\rho V_{cruise}^2 S_{D,eq}$$

where ρ is th atmospheric density, V_{cruise} is the cruise speed, C_D is the equivalent drag coefficient of the body, and S_{ref} is the reference frontal area. In the aggregated formulation, $S_{D,eq} = C_D S_{ref}$ represents the equivalent drag area of the vehicle. In the baseline case, this parameter is used as a preliminary

estimate of the combined drag contribution of the body, arms, landing gear, and other non-lifting elements, in order to avoid introducing an artificial separation between drag coefficient and frontal area before a definitive geometry is available.
In steady forward flight the multicopter does not generate a purely vertical thrust vector as in hover, instead, the thrust vector is tilted forward so that its vertical component balances the vehicle weight while its horizontal component compensates for the aerodynamic drag of the body.
Figure 4.2.1 illustrates the free-body diagram adopted in the model to represent this condition. In constant-speed cruise, the resultant force must be zero both in the vertical direction and along the direction of motion. Therefore, the model assumes:

$$T_{cruise,y} = W$$
$$T_{cruise,x} = D$$

The module of the total thrust needed in forward flight can be calculated as:

$$T_{cruise} = \sqrt{W^2 + D^2}$$

Starting from this value, the model evaluates the induced-power contribution in forward flight through an iterative estimate of the induced velocity. The profile-power contribution is corrected as a function of the advance ratio, while parasite power is obtained from the product of drag and cruise speed.

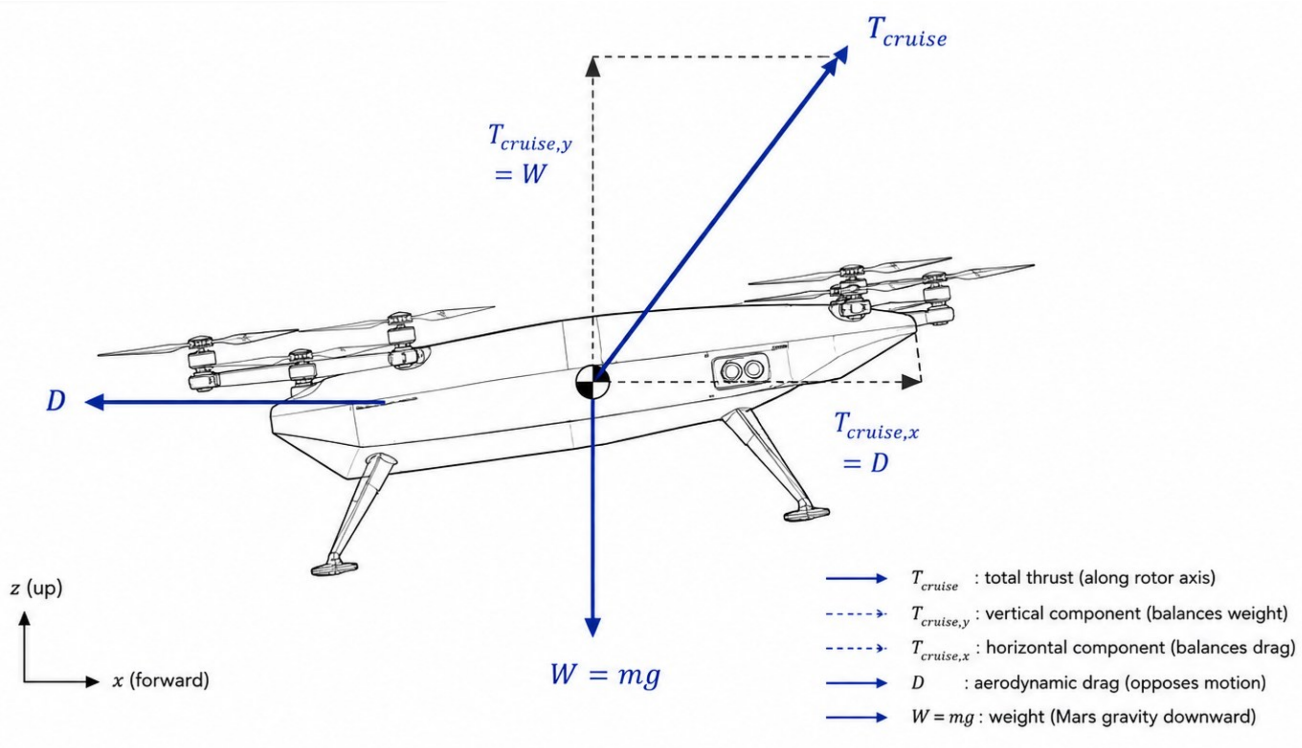

Figure 4.2.1: Mars multicopter steady forward cruise free-body diagram

In compact form, the cruise power used in the model can be written as:

$$P_{cruise} = \frac{k_{i,cruise} T_{cruise} v_i}{\eta_{prop}} + P_{p,hover,eq}(1 + k_\mu \mu^2) + \frac{D V_{cruise}}{\eta_{prop}}$$

where $k_{i,cruise}$ is the correction factor applied to induced power in forward flight, v_i is the induced velocity in forward flight, $P_{p,hover,eq}$ is the equivalent profile power in hover, k_μ is the correction coefficient for the profile-power contribution, and e $\mu = V_{cruise}/V_{tip}$ is the advance ratio.
The mission power profile is then represented as a discrete sequence of power levels associated with the different operational segments:

$$\{P_{to}, P_{climb}, P_{cruise}, P_{hover}, P_{descent}, P_{land}\}$$

This discretization provides the basis for the calculation of the total mission energy, obtained by summing the energy contribution of each phase according to its duration. In this way, the model accounts for the different energetic roles of the operational phases without requiring a high-fidelity trajectory simulation, while maintaining a level of complexity consistent with the preliminary objective of the thesis.

4.2.5 Total mission energy calculation

Once the power profile associated with the different operational phases has been defined, the total mission energy is obtained by integrating the required power over time. In general form,

$$E_{mission} = \int P(t)\, dt$$

Within the simplified piecewise representation adopted for the mission profile, this relation is approximated in discrete form as the sum of the energy contributions of the individual operational segments:

$$E_{mission} \approx \sum_j P_j \ \Delta t_j$$

where P_j is the characteristic power level associated with the j-th phase and Δt_j is its duration. Using the mission profile defined in the previous chapters, the total mission energy can therefore be written as:

$$E_{mission} = P_{to}\Delta t_{to} + P_{climb}\Delta t_{climb} + P_{cruise}\Delta t_{cruise} + P_{hover}\Delta t_{hover} + P_{desc}\Delta t_{desc} + P_{land}\Delta t_{land}$$

This formulation clarifies that the overall energy requirement is not determined only by the maximum-power condition, but by the combined effect of power level and duration across the different mission phases. In the framework of this thesis, it provides the direct link between the rotorcraft power model and the battery sizing model, since the mission energy obtained in this way is used to estimate the required energy-storage capacity and the corresponding mass of the battery system.

4.3 Battery Sizing Model

4.3.1 Battery energy density assumptions

The preliminary sizing of the energy system is carried out by assuming an electrochemical battery as the only source of energy for flight: in this framework, the key parameter linking the mission energy requirement to the mass of the storage system is the battery specific energy, expressed in Wh/kg. This quantity represents the energy effectively available per unit mass of the battery pack and therefore it acts as one of the main drivers of the mass–energy model.

To justify the specific-energy value adopted in the preliminary model, it is useful to compare the main values reported in the most relevant literature on Martian rotorcraft.

Reference	**Battery metric**	**Value**	**Note**
Mars Science Helicopter Conceptual Design [2]	Cell specific energy	278 Wh/kg	JPL technology forecast
Mars Science Helicopter Conceptual Design [2]	Pack specific energy	230 Wh/kg	Including battery management system
Mars Science Helicopter Conceptual Design [2]	End-of-life pack specific energy	218.5 Wh/kg	Conservative sizing value
Systematic methodology for the preliminary design of future rotary VTOL Martian aerobots [4]	Pack specific energy	230 Wh/kg	Used for preliminary sizing
Systematic methodology for the preliminary design of future rotary VTOL Martian aerobots [4]	Cell specific energy	260 Wh/kg	Commercial-cell reference, not direct pack value
A Study of Past, Present and Future Mars Rotorcraft [5]	Cell specific energy	144 Wh/kg	Ingenuity battery reference

Table 4.3.1 — Reference battery specific energy values for Mars rotorcraft preliminary sizing

As shown in Table 4.3.1, the values most suitable for a realistic preliminary sizing are in the range of approximately 220–230 Wh/kg at pack level, whereas higher values generally refer to individual cells and cannot be transferred directly to vehicle battery sizing [2], [4]. For this reason, the model adopts a value consistent with the pack-level references available in the literature, avoiding overly optimistic assumptions [4].
Using a pack-level value rather than an ideal cell-level value prevents an unrealistically favorable estimate of the energy-system mass and makes the sizing process more representative of a configuration that could plausibly be implemented.

From a modeling point of view, this choice provides a direct link between the required energy and the battery mass: once the total mission energy has been estimated, battery specific energy acts as the conversion parameter used to obtain a first estimate of the energy-storage mass. Higher values of battery specific energy therefore improve vehicle feasibility significantly, whereas more conservative values make the mass–energy constraint more severe.
It is important to note that the energy management is not limited to flight operations, but also includes system survival during the Martian night and the following recharge cycle, with a non-negligible portion of the available energy allocated to survival loads and mission margins [2]. In the case of Ingenuity, for example, more than half of the battery capacity was required simply to keep the vehicle systems warm during the Martian night [16].

4.3.2 Battery mass estimation

The battery pack mass is estimated from the total energy required by the mission profile, that also includes auxiliary loads and energy margins needed to represent the operation of the system in a more realistic way. The overall required energy can therefore be expressed as:

$$E_{req} = E_{flight} + E_{aux} + E_{margin}$$

where E_{flight} is the energy associated with the flight phases, E_{aux} includes non-propulsive contributions such as avionics, sensors, communications, data processing, and thermal loads, while E_{margin} represents a conservative margin introduced to account for the uncertainties of the preliminary model. Starting from this required energy, the battery pack mass is estimated as:

$$m_{bat} = \frac{E_{req}}{\eta_{sys}\,\epsilon_{bat}}$$

where ϵ_{bat} is the battery pack specific energy and η_{sys} is a global efficiency factor accounting for the losses between the energy nominally stored in the pack and the energy effectively available for the mission. Written in this form, the model avoids treating the battery as an ideal energy reservoir and allows system losses, usability limits, and operational margins to be included in an aggregate way.
Battery mass is therefore not prescribed a priori, but it emerges as an output of the iterative sizing process [4], and, once estimated, it updates the total vehicle mass and consequently affects thrust, power demand, and mission energy in the following iterations. For this reason, battery sizing is one of the central steps of the mass–energy loop introduced in the chapter workflow.

4.3.3 Auxiliary loads, thermal survival and energy margins

In addition to the propulsive energy required during flight, a Martian multicopter has to include loads related to avionics, sensors, onboard computing, communications, payload operation, thermal management, and survival during non-operational phases. Such contributions are represented through the aggregate term E_{aux} introduced in the definition of the total required energy.

In the Martian environment, the most relevant auxiliary contribution is often associated with thermal survival during ground permanence, due to the low ambient temperatures and the need to keep batteries and electronics within acceptable operating limits. This aspect is particularly evident in the MSH concept, where a significant portion of the onboard energy is allocated to night survival and thermal control of the system [2]. Including this contribution in the model, a scaling law calibrated on the MSH is adopted [2] and according to this relation, the energy required for night survival can be estimated as:

$$E_{night} = 15\, m_{gross}^{1/3} Wh/sol$$

where m_{gross} is the gross mass of the vehicle. Equivalently, assuming a sol duration of approximately 24.6 h, this contribution can be interpreted as an average survival power:

$$P_{night} = 0.518\, m_{gross}^{1/3} W$$

This formulation is not intended to represent a detailed thermal model of the vehicle, rather it provides a practical way to include a realistic non-propulsive energy contribution that scales with system size. In this work, this term is introduced to avoid underestimating battery mass and to make the mass–energy model more representative of Martian operating conditions.
The term E_{margin} is instead used to account, in a conservative manner, for uncertainties associated with the preliminary model, the environmental conditions, and the actual performance of the subsystems.

As a result, the battery pack is sized not only on the basis of the nominal propulsive energy, but on the overall energy requirement of the mission: this approach completes the battery sizing model and closes the mass–energy framework developed in this chapter, providing the basis for the parametric and configuration analyses.

4.4 Coupled Mass–Energy Iteration

4.4.1 Problem formulation

The preliminary sizing of a Martian multicopter involves a direct coupling between total vehicle mass, required power, and mission energy. The mass of the energy-storage system cannot be prescribed independently, since it depends on the energy required by the operational profile, and at the same tim the required energy depends on the total vehicle mass, which itself includes the battery mass. The sizing problem is therefore implicitly coupled and must be solved through an iterative procedure [2], [4].
The total vehicle mass is written as:

$$m_{tot} = m_{fix} + m_{bat}$$

where m_{fix} denotes the sum of the masses assigned or estimated independently of the energy loop, including structure, payload, avionics, actuation, non-battery propulsion components, and other subsystems, while m_{bat} is the battery pack mass, which is determined iteratively. For a given value of m_{tot}, the model first evaluates the thrust required in hover:

$$T = m_{tot} g_M$$

where g_M is the Martian gravitational acceleration. This thrust value is then used to estimate the rotor sizing, the power required during the different mission phases, and the corresponding energy demand. The total required energy is expressed as:

$$E_{req} = E_{flight} + E_{aux} + E_{margin}$$

where E_{flight} is the energy associated with the flight phases, E_{aux} accounts for non-propulsive contributions, and E_{margin} introduces a conservative allowance for preliminary-model uncertainties. In the baseline implementation, the auxiliary term is mainly represented by the night-survival contribution, while other secondary loads are treated in aggregate form or implicitly included through the energy margin. Starting from E_{req}, a direct estimate of the required battery mass is obtained as:

$$m_{bat,direct} = \frac{E_{req}}{\eta_{sys} \epsilon_{bat}}$$

where ϵ_{bat} is the battery pack specific energy and η_{sys} represents, in aggregate form, the usable fraction of the stored energy and the overall losses of the energy system. In the baseline model, this term is implemented as the usable fraction of the nominal battery pack capacity.

The sizing problem is therefore intrinsically coupled: the battery mass depends on the mission energy requirement, which is determined by the total vehicle mass, and at the same time the total mass includes the battery itself. This coupling can be written as a fixed-point relation:

$$m_{\text{bat}} = f(m_{\text{tot}}) = f(m_{\text{fix}} + m_{\text{bat}})$$

The iterative procedure is then used to find a solution in which the battery mass, total vehicle mass, and mission energy requirement are mutually consistent. The problem is formulated in MATLAB through an ordered set of assigned inputs and quantities of interest, as shown in Figure 4.4.1., that summarizes the overall structure of the model: environmental, geometric, energy-related, and mission inputs feed the mass–energy loop, while the main outputs are the converged battery mass, the total vehicle mass, the phase power levels, the overall mission energy, and the estimated operational performance.

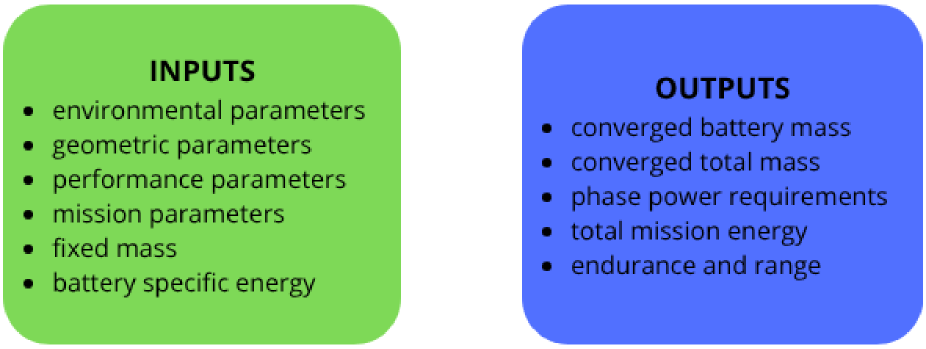

Figure 4.4.1 — Main input and output variables of the preliminary mass–energy sizing model

4.4.2 Iterative solution procedure

The iterative procedure adopted in this work is structured so that it can be implemented directly in MATLAB in a simple and transparent way. Its purpose is to progressively update the battery pack mass and, consequently, the total vehicle mass, until a configuration consistent with the mission profile and the assigned energy parameters is obtained.

The algorithm starts from an initial estimate of the battery mass, $m_{bat}^{(0)}$ From this value, the initial total vehicle mass is calculated as:

$$m_{tot}^{(0)} = m_{fix} + m_{bat}^{(0)}$$

At each iteration k, the model updates the required thrust according to the current total mass:

$$T^{(k)} = m_{tot}^{(k)} g_M$$

Based on this thrust requirement, the rotor sizing, the power levels associated with the different mission phases, and the total required energy are then evaluated:

$$E_{req}^{(k)} = \sum_i P_i^{(k)}\, t_i + E_{aux}^{(k)} + E_{margin}^{(k)}$$

where the term $\sum_i P_i^{(k)}\, t_i$ represents the propulsive energy associated with the flight phases, while $E_{aux}^{(k)}$ and $E_{margin}^{(k)}$ include the non-propulsive contributions and the energy margin, respectively.

The corresponding direct estimate of the required battery mass is then obtained as:

$$m_{bat,direct}^{(k+1)} = \frac{E_{req}^{(k)}}{\eta_{sys} \epsilon_{bat}}$$

In the MATLAB implementation, a relaxation factor λ is introduced to improve the numerical stability of the procedure. The battery mass for the next iteration is therefore calculated as:

$$m_{bat}^{(k+1)} = \lambda m_{bat,direct}^{(k+1)} + (1-\lambda) m_{bat}^{(k)}$$

where $0 < \lambda \leq 1$. When $\lambda = 1$, the algorithm directly adopts the newly estimated battery mass; for lower values, the update is damped, reducing possible oscillations between successive iterations. The total mass is then updated as:

$$m_{tot}^{(k+1)} = m_{fix} + m_{bat}^{(k+1)}$$

and the cycle is repeated until the convergence criterion is satisfied. The calculation sequence can be summarized as follows:

- assign the environmental, geometric, energy-related, and mission inputs;
- initialize the battery mass m_bat^(0);
- compute the total mass m_tot^(k) = m_fix + m_bat^(k);
- compute the required thrust T^(k) = m_tot^(k) g_M;
- update the rotor sizing and the phase power levels;
- compute the required energy E_req^(k);
- estimate the direct battery mass m_bat,direct^(k+1);
- update the battery mass using the relaxation factor;
- update the total mass m_tot^(k+1);
- check convergence; if it is not satisfied, return to the thrust-calculation step.

This structure corresponds to a fixed-point iteration loop: at each iteration, the change in battery mass modifies the system weight, which in turn changes the required thrust and therefore the full power and energy balance.
The procedure aim is to assess the plausibility of a family of configurations as the main design parameters are varied, so such an iterative loop represents the numerical core on which the next parametric analyses are built, including variations in rotor number, rotor radius, battery specific energy, and payload mass.

4.4.3 Convergence criteria

For the iterative procedure described in the previous section to produce a usable solution, the convergence is assessed mainly on the total vehicle mass, since this is the quantity that couples the mass–energy balance with the calculation of thrust and required power. The main criterion is based on the relative difference between two successive iterations:

$$\varepsilon^{(k)} = \left| \frac{m_{tot}^{(k+1)} - m_{tot}^{(k)}}{m_{tot}^{(k)}} \right|$$

The solution is considered converged when:

$$\varepsilon^{(k)} < \varepsilon_{tol}$$

where ε_{tol} is an assigned tolerance, selected consistently with the preliminary level of the analysis. In a MATLAB implementation aimed at parametric studies, values of the order of 10^{-3} or 10^{-4} are generally sufficient to ensure numerical stability without introducing unnecessary computational cost.

Since the fixed mass m_{fix} remains constant during the iteration, convergence of the total mass also implies convergence of the battery mass; however, beyond the numerical criterion itself, it is also useful to monitor the variation of the required energy and of the main mission quantities, so as to verify that the solution is physically consistent and not merely formally converged. In particular, a converged configuration must simultaneously satisfy:

- closure of the mass–energy balance;
- physically meaningful signs and values of the computed quantities;
- no violation of the operational limits imposed by the model, for example in terms of geometric parameters, blade tip speed, or energy constraints;
- consistency between total mass, required power, and available energy.

Failure to converge should therefore not be interpreted only as a numerical issue, but also as a possible indication that the configuration under examination is not feasible. For instance, lack of convergence may indicate that, for a given combination of payload, rotor size, number of rotors, or battery specific energy, the energy balance cannot be closed within the assigned constraints.

In this regard, the convergence criterion has a dual role: it stops the numerical procedure and, at the same time, contributes to the identification of the vehicle feasibility envelope. A converged solution therefore represents a configuration that is preliminarily consistent from a mass–energy point of view, whereas a non-convergent solution points to a region of the design space that may not be practically achievable.

4.5 Model assumptions and preliminary consistency assessment

The model developed in this work is preliminary and is not intended to reproduce the aerodynamic, structural, or dynamic behavior of the vehicle with high fidelity, so its validity must be interpreted in relation to the specific purpose of the work, that is to provide a simple, physically coherent and computationally lightweight tool for exploring the relationship between mass, power, energy, and configuration in a Martian multicopter. The model is not verified through direct comparison with experimental tests on the vehicle under study, but through a preliminary consistency assessment based on two complementary criteria: the first concerns the internal physical consistency of the adopted formulations, which are derived from momentum theory and from established relations in rotorcraft literature, while the second concerns a qualitative and, where possible, quantitative comparison with the orders of magnitude reported in NASA studies and in recent conceptual-design works on Martian rotorcraft [2], [4].

The main assumptions of the model can be summarized as follows:

- the Martian atmosphere is treated as uniform and steady in the nominal case;
- hovering is assumed to be the sizing condition for power;
- induced power is estimated through momentum theory, corrected by means of a figure of merit or an induced power factor;
- profile power is represented through global mean coefficients;
- the mission is represented as a discrete sequence of phases, each associated with a characteristic power level;
- the energy system is modeled through pack-level specific energy and a usable fraction of the stored energy;
- auxiliary loads, thermal survival, and energy margins are treated in aggregate form;
- aerodynamic interactions between rotors, control dynamics, and local atmospheric variations are not modeled explicitly.

These simplifications limit the ability of the model to predict detailed performance, but they are appropriate to build a preliminary sizing and trade-off analysis tool capable of identifying plausible configurations, parametric sensitivities, and feasible regions of the design space.
The results obtained with this framework should therefore be interpreted as preliminary estimates, useful for comparing configurations, evaluating the effect of the main design drivers, and identifying the parameters that are most critical for sizing. Any future design phase would require higher-fidelity aerodynamic models, structural analyses, detailed thermal assessments, investigation of rotor–rotor interactions, and verification of the dynamic and control behavior of the vehicle.

5. Baseline Vehicle Sizing and Reference Configuration

5.1 Definition of the Reference Configuration

5.1.1 Reference mission inputs

Applying the model developed in Chapter 4, a quantitative reference case must first be defined, and it has to be simple enough to allow a coherent preliminary sizing, while still being representative of a scientifically meaningful mission in the context of Martian exploration.

The mission profile considered is a local one-way sortie, in which the vehicle is not required to return immediately to its initial take-off point, indeed after transferring to the target area and completing the scientific hovering phase the multicopter performs a vertical descent to the surface and it remains on the ground during a sleep phase before the next recharge cycle. This operational logic is consistent with the framework adopted in MSH studies [2], where the vehicle performs a sortie, lands, and must then sustain a ground-survival period before the following operational cycle can begin.

The mission inputs adopted for the baseline case therefore follow a structure similar to that used in the reference studies, particularly in terms of the decomposition of the mission into operational phases. However, the values reported in Table 5.1.1 are not intended to reproduce a complete Mars Science Helicopter mission directly, rather they define a more contained reference case, suitable for verifying the preliminary closure of the mass–energy model.

Parameter	**Value**	**Unit**
Take-off hover duration	30.0	s
Climb altitude	200.0	m
Climb speed	3.0	m/s
Cruise distance	1000.0	m
Cruise speed	12.0	m/s
Scientific hover duration	120.0	s
Descent speed	3.0	m/s
Landing duration	20.0	s
Sleep	1.0	sol

Table 5.1.1 — Reference mission parameters adopted for the preliminary energy sizing model

Although the selected profile is relatively limited in terms of range and hover time compared with the more ambitious capabilities investigated for future Martian rotorcraft, it retains the functional elements that are most relevant to the present model: vertical take-off, climb, transfer to a target area, scientific hovering, vertical descent, landing and a final ground permanence phase. It therefore provides a suitable baseline case for obtaining an initial converged configuration and for verifying the behavior of the sizing framework before more extended configurations will be explored in Chapter 6.

The reference environmental conditions are assumed to be representative of Jezero Crater during spring conditions [2], [41], with an atmospheric density of approximately 0.015 kg/m^3 and a temperature of about −50 °C: these values place the system in a regime characterized by low atmospheric density, low Reynolds numbers, and reduced speed of sound.

5.1.2 Selected configuration and baseline assumptions

The reference configuration selected for this chapter is a hexacopter multirotor, consistently with the conclusions drawn in Chapter 2. Among the different multicopter architectures, the hexacopter is selected because, in the Martian context, it offers a favorable compromise between operational simplicity, total rotor disk area, robustness, and controllability.
In the studies related to the Mars Science Helicopter [2], the hexacopter configuration is particularly attractive because it provides lower disk loading than more compact solutions and it can achieve improved rotor efficiency, although at the cost of a heavier airframe compared with the coaxial configuration. In the present study, the reference configuration is intended to provide a first physically plausible converged case, useful for checking the internal consistency of the mass–energy model and for defining the starting point of the parametric analyses.

Figure 5.1.1 — Mars Science Helicopter hexacopter configuration. Source: [2]

The vehicle is therefore described through assumptions that are consistent with a preliminary sizing phase: identical rotors, uniform thrust distribution, almost steady operation during the different mission phases, no explicit modeling of aerodynamic interactions between rotors, and an aggregate representation of propulsive efficiencies.

The baseline explicitly includes three main contributions for the energy required:

- the energy associated with the flight mission;
- an energy reserve applied to the mission energy balance;
- an aggregate night-survival energy contribution, introduced to represent the need to keep the vehicle operational during ground permanence before recharge.

This choice follows the NASA framework closely, since the battery sizing of the MSH [2] includes both a 20 % energy reserve and a separate sleep-energy term calibrated on Mars Helicopter data. As shown by NASA capability studies on the Mars Science Helicopter [2] and the Advanced Mars Helicopter Design [18], increasing range and hover time inevitably requires a larger energy capacity and, consequently, a higher battery mass, with direct effects on total mass, rotor diameter, and required power [22]. The baseline adopted here should therefore be interpreted as an initial reference configuration, useful for verifying model closure and for providing the starting point of the following parametric analyses, while higher-performance configurations, in terms of range, endurance, and energy capacity, are investigated in Chapter 6.

5.1.3 Baseline sizing methodology and input parameters

Starting from the reference mission and the selected hexacopter configuration, the baseline sizing is performed through the model developed in the previous chapter: environmental parameters, main rotor parameters, energy assumptions and the operational mission profile are assigned as inputs, whereas quantities such as battery mass, total mass, rotor disk area, rotor diameter, phase power levels, and required energy are obtained as outputs of the process.
The main parameters assigned to the model are reported in Table 5.1.2.

Parameter	**Symbol**	**Value**	**Unit**
Number of rotors	N_r	6	–
Payload mass	m_{pay}	3.0	kg
Target disk loading	DL_{target}	8.0	N/m^2
Martian gravity	g_m	3.711	m/s^2
Atmospheric density	ρ	0.015	kg/m^3
Speed of sound	a	233.0	m/s
Tip Mach number	M_{tip}	0.65	–
Rotor solidity	σ	0.20	–
Induced power factor	k	1.20	–
Equivalent drag area	$S_{D,eq}$	0.49	m^2
Forward-flight profile correction	k_{mu}	4.65	–
Mean blade drag coefficient	$\bar{c}_d$	0.04	–
Motor/ESC efficiency	$\eta_{\mathrm{mot/ESC}}$	0.90	–
Mechanical efficiency	η_{mech}	0.97	–
Overall propulsive efficiency	η_{prop}	0.873	–
Battery specific energy	ϵ_{bat}	230	Wh/kg
Usable battery fraction	f_{usable}	0.70	–
Energy reserve fraction	f_{res}	0.20	–

Table 5.1.2 — Main baseline sizing parameters adopted in the mass–energy model

The logic of the model can be divided into three main steps:

- a reference non-battery mass is defined by scaling the percentage mass distribution of the Mars Science Helicopter according to the payload mass assumed in this study; an initial provisional estimate of the battery mass is then added only to initialize the iterative process.
- starting from the current total mass, the model calculates the required thrust, the total disk area from the assigned disk loading, the rotor diameter, and the power required during the different phases of the mission.
- the total required energy is converted into an updated battery mass, taking into account the battery pack specific energy, the usable fraction of the stored energy, and the energy reserve. The total mass is then updated and the process is repeated until convergence is reached.

For the mass breakdown, the model uses the percentage distribution of the Mars Science Helicopter as a reference [2], so the payload mass is set equal to 3.0 kg and, starting from this value, a scale mass is defined through the ratio between the selected payload and the payload fraction of the MSH.
The masses associated with structure, systems, propulsion hardware, and contingency are then obtained by applying the corresponding MSH reference fractions to the scaled mass: in this way the model preserves a mass distribution that is compatible with a Martian rotorcraft platform already investigated in the literature, while avoiding the direct imposition of the total vehicle mass.
The propulsion contribution derived from the MSH includes motors and associated hardware, whereas the battery is treated separately as an iterative variable, since its mass depends on the energy required by the mission, which in turn depends on the total vehicle mass.

The disk loading is assumed equal to 8 N/m^2 and it is used as a design input, with whom the model then calculates the total disk area required to support the vehicle weight at the current mass, while the diameter of each rotor is obtained from the updated total mass and from the number of rotors.
The choice of M_{tip} and σ is made so that the baseline remains consistent both with the adopted physical model and with the orders of magnitude reported for reference Martian rotorcraft configurations. The tip Mach number defines the blade tip speed:

$$V_{tip} = M_{tip} a$$

and it directly affects profile power, which scales with the cube of tip speed. An excessively high value would therefore penalize the energy balance and reduce the margin with respect to compressibility effects; on the other side, an excessively low value would artificially reduce profile power but would require the blades to generate the required thrust with insufficient peripheral speed.
For this reason, the selection of M_{tip} is evaluated together with the equivalent rotor solidity; in the baseline case, $M_{tip} = 0.65$ is adopted as a preliminary operating value: it remains lower than the more aggressive values reported in MSH studies, while still being high enough to avoid excessive blade loading.
The solidity is set equal to $\sigma = 0.20$, a value consistent with an MSH-like hexacopter configuration and close to the solidity reported for early MSh configurations. In the absence of a definitive blade geometry, this value represents a prudent choice, since it provides an adequate equivalent blade area without assuming a level of aerodynamic optimization that would not be justified at this stage.

The consistency of the M_{tip}–σ pair is checked through two indicators: the equivalent figure of merit, evaluated a posteriori from the rotor power obtained with the explicit model, and the ratio C_T/σ, used as a preliminary indicator of blade loading. The latter is not treated as a definitive aerodynamic constraint, but as a plausibility check: its purpose is to verify that the required thrust is not obtained through an unrealistic combination of low tip speed and reduced blade area.
The mean blade drag coefficient is assumed equal to:

$$\bar{c}_d = 0.04$$

and it should be interpreted as a global equivalent coefficient, not as a value derived from the polar curve of a specific airfoil of the present rotor. This choice is motivated by the orders of magnitude reported for rotor sections operating in low-Reynolds-number Martian conditions. In the *Mars Science Helicopter Conceptual Design* [2], the profile contribution is explicitly linked to the increase in drag coefficient caused by low Reynolds numbers, and the aerodynamic curves computed for the CLF5605 section of the Mars Helicopter [2] show c_d values of the order of a few hundredths under the operating conditions considered.

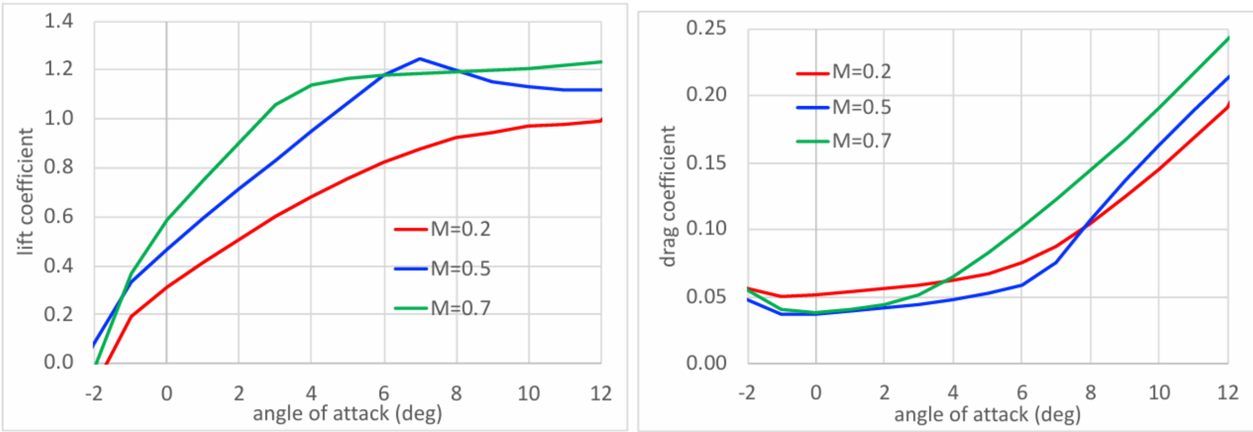

Figure 5.1.2 — Representative lift and drag coefficient values for the CLF5605 Mars Helicopter blade section in Martian low-Reynolds-number conditions. Adapted from [2].

In particular, by observing the drag branch of Figure 5.1.2, c_d values at moderate angles of attack generally fall within the approximate range 0.035–0.06, before the more pronounced increase associated with near-stall conditions. Since the present model does not use a complete polar varying with angle of attack, Mach number, and radial blade position, an effective mean value of $\bar{c}_d = 0.04$ is adopted. This value lies in the lower-to-intermediate part of the range shown by the reference polar and allows non-negligible viscous losses to be represented without introducing an excessive penalty in the preliminary model.

For cruise, the parasite contribution is represented through an equivalent drag area,

$$S_{D,eq} = C_D S_{ref} = 0.49\, m^2$$

rather than by assigning the drag coefficient and frontal area separately. The adopted value is selected by analogy with the MSH hexacopter configuration, for which a drag area of approximately 0.492 m^2 is reported. This approach is more robust than assigning C_D and S_{ref}, independently, since the final geometry of the fuselage, arms, landing gear, and other non-lifting elements is not yet defined. The parameter $S_{D,eq}$ should therefore be interpreted as an aggregated MSH-like estimate of the vehicle body drag in forward flight, useful for including the parasite contribution without attributing to the model a geometric precision that is not yet available.

For the energy system, the battery specific energy is assumed equal to 230 Wh/kg, intended as a pack-level value rather than a cell-level value, and the model also considers a usable battery fraction of 70% and an energy reserve of 20% applied to the overall requirement. The updated battery mass is therefore calculated as:

$$m_{bat,new} = \frac{E_{req}}{\epsilon_{bat} f_{usable}}$$

where E_{req} includes the flight mission, thermal survival and reserve, ϵ_{bat} is the battery pack specific energy, and f_{usable} is the effectively usable fraction of the nominal capacity.

The process is initialized with a first estimate of the battery mass: at each iteration, the model updates the total mass, it recalculates thrust, rotor disk area, power levels, and energy demand, and it obtains a new battery mass. To avoid numerical oscillations, the update is relaxed through a weighted combination of the current battery mass and the value directly calculated from the energy requirement. The solution is considered converged when the relative variation of the total mass between two successive iterations falls below the assigned tolerance, so the final baseline result is a configuration in which total mass, battery mass, and energy requirement are mutually consistent.

5.2 Baseline Mass Breakdown

To analyse the preliminary configuration identified in the previous section more clearly, it is useful to examine how the vehicle mass is distributed among the main subsystem groups. At this stage of the design process, the mass breakdown is not yet obtained from a complete bottom-up sizing of individual components, but from a baseline mass allocation derived from a reference configuration available in the literature. The main reference adopted for this purpose is the baseline hexacopter presented by Johnson et al. [2], in which the authors divide the vehicle mass into five main categories: structure, propulsion, systems & equipment, contingency, and payload, for a total vehicle mass of 17.656 kg.

The mass fractions reported in Table 5.2.1 are therefore adopted as baseline fractions for the present preliminary analysis: such values provide a consistent starting point for the mass-estimation model and allow the plausibility of the initial configuration to be assessed. The distribution shown in Figure 5.2.1 highlights that the largest share of the mass is associated with the structure, which alone accounts for more than one third of the total mass. This is followed by the propulsion group and contingency, while systems & equipment and payload have a smaller relative contribution. This distribution shows that, in the Martian environment, the need to ensure structural stiffness, rotor integration, resistance to operational loads, and adequate margins against preliminary-design uncertainty inevitably leads to a significant mass penalty.

Mass category	**Reference MSH mass [kg]**	**Mass fraction [%]**
Structure	6.405	36.3
Propulsion	3.460	19.6
Systems and equipment	2.644	15.0
Contingency	3.127	17.7
Payload	2.020	11.4
Total	17.656	99.97

Table 5.2.1 — Mars Science Helicopter subsystem mass breakdown and mass fractions. Derived from: [2]

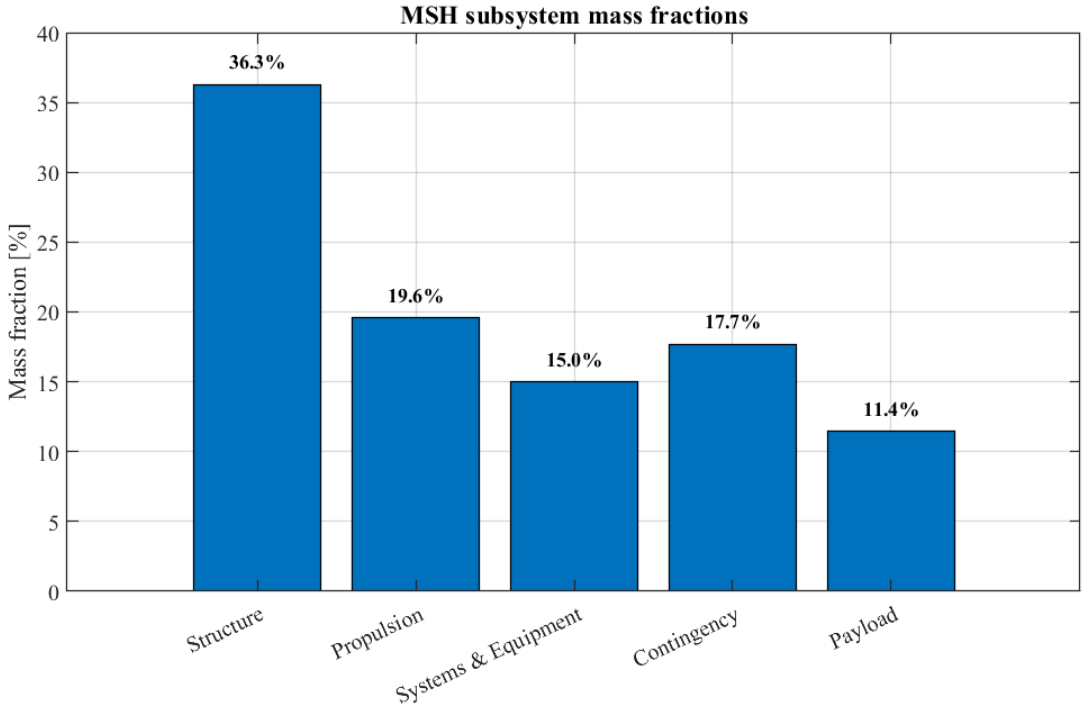

Figure 5.2.1 — Mars Science Helicopter subsystem mass fraction distribution. Derived from: [2]

5.2.1 Propulsion group

In the reference vehicle, the propulsion category has a mass of 3.460 kg, corresponding to approximately 19.6% of the total mass. This category does not include only the motors, but the complete set of main elements directly involved in the generation and management of propulsive power; in particular, the breakdown provided by Johnson et al. [2] divides this mass into three main sub-items: motor = 0.741 kg, battery = 1.522 kg, and solar cell = 1.197 kg.

Within the propulsion group, the dominant contribution is therefore represented by the battery, followed by the solar cells, while the motors have a more limited mass impact, a result that is particularly significant because it highlights a typical feature of electric Martian aircraft: the mass of the propulsion system is not dominated primarily by the actuators, but by the energy architecture required to sustain the mission.

5.2.2 Structure, avionics and payload

In the mass breakdown of the MSH [2], the structure does not include only the primary structure of the vehicle, but also a significant portion of the rotor system. In particular, for the hexacopter configuration, this category is divided into rotor group, fuselage group, and alighting gear. The rotor group itself includes blades, hubs, shafts, and rotor supports, so in the present preliminary model the rotor mass is included within the structure category, consistently with the classification adopted in the MSH reference study [2].

The systems & equipment category has a mass of 2.644 kg, equal to 15.0% of the total vehicle mass: this group includes subsystems such as flight controls and avionics, which, although not dominant in absolute terms,they still represent a non-negligible contribution and they reflect the functional complexity of the vehicle.

In conclusion, the payload has a mass of 2.020 kg, corresponding to approximately 11.4% of the total mass. Unlike the other categories, however, it is not mainly determined by internal architectural constraints of the vehicle, but by the mission objectives, so in the present study the payload is treated as a mission-driven input, separate from the other items of the mass breakdown, although it still contributes substantially to the definition of the initial system mass.

5.2.3 Battery mass fraction

In the reference baseline case, the battery mass is equal to 1.522 kg, corresponding to approximately 8.6% of the gross mass: this value provides a useful first-order reference for interpreting the results obtained in the present study, especially in relation to the trade-off between mass, endurance, and available energy capacity. It should be emphasized, however, that this value cannot be treated as a fixed constraint or as a definitive design target, since battery mass fraction is strongly affected by the mission profile, the duration of the operational phases, the fraction of energy required for flight, and the possible need to cover additional survival conditions or operational margins.
For the present analysis, this baseline remains useful because it helps placing the following results within a realistic range, but if other configurations are required to provide greater range or endurance, an increase in battery mass and, consequently, in its fraction of the total mass should be expected.

5.3 Baseline sizing results

Table 5.3.1 reports the mass distribution obtained for the baseline configuration after the sizing procedure, based on the application of the mass fractions derived from the baseline hexacopter of the Mars Science Helicopter study [2].

Mass category	**Baseline mass [kg]**	**Mass fraction [%]**
Structure	9.5124	35.738
Propulsion hardware	2.8782	10.813
Systems and equipment	3.9267	14.753
Contingency	4.6441	17.448
Payload	3	11.271
Battery	2.6555	9.9769
Total	26.617	100

Table 5.3.1 — Baseline subsystem masses and mass fractions obtained from the MSH-scaled allocation method

5.3.1 Converged gross mass and battery mass

The application of the mass–energy model to the baseline case defined in the previous section provides a first converged configuration for the reference vehicle. As shown in Figure 5.3.1, the iterative process converges regularly toward an overall gross mass of approximately 26.62 kg, associated with a battery mass of about 2.66 kg, and the monotonic convergence of both total mass and battery mass indicates that, within the assumptions adopted, the coupling between mass, required power, and available energy leads to a numerically stable and physically consistent solution.
The battery mass remains relatively limited because the operational profile considered is short and it includes a limited cruise distance of 1 km and a scientific hovering time of 120 s. At the same time, the baseline case is not a simple “flight-only” test, since it also includes a night-survival contribution and an energy reserve, so the configuration obtained occupies an intermediate position: it is sufficiently complete to verify the behavior of the mass–energy model, while not yet representing the higher-endurance configurations that will be investigated in the parametric analyses.

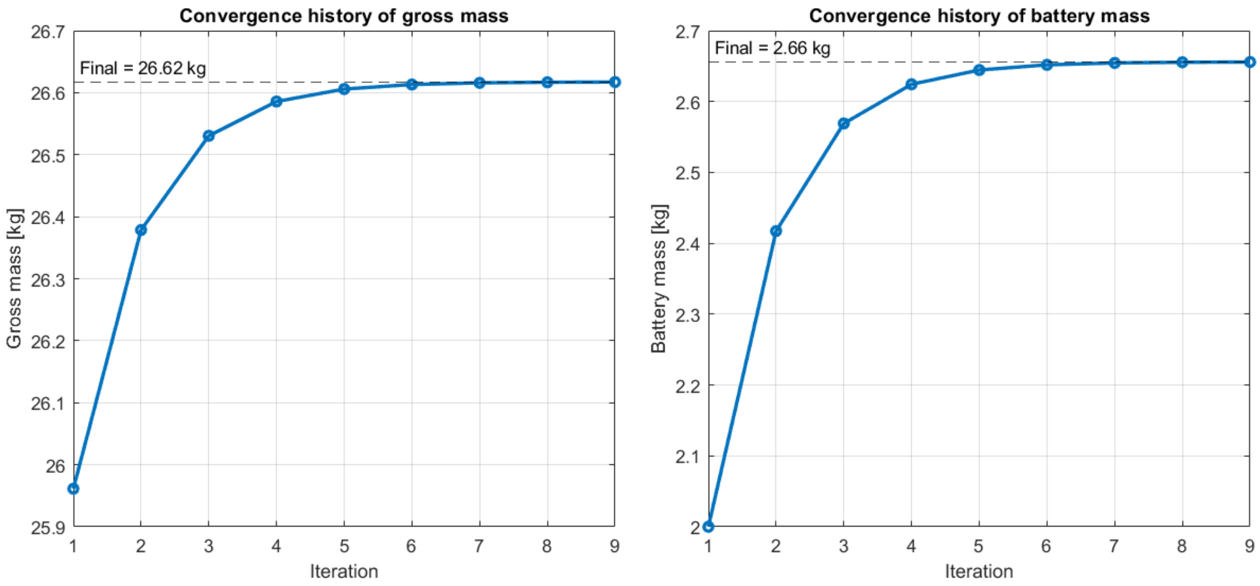

Figure 5.3.1 — Iterative convergence of gross mass and battery mass obtained from the baseline mass–energy sizing procedure.

Parameter	**Value**	**Unit**
Fixed non-battery mass	23.961	kg
Gross mass	26.617	kg
Battery mass	2.656	kg
Battery mass fraction	9.98	%
Rotor diameter	1.619	m
Total disk area	12.347	m^2
Disk loading	8.000	N/m^2
Ideal hover power	1613	W
Induced hover rotor power	1935.6	W
Profile hover rotor power	643.4	W
Total hover rotor power	2579.0	W
Hover electric power	2954.2	W
Climb power	3293.6	W
Cruise power	2706.1	W
Flight energy	311.56	Wh
Night survival energy	44.79	Wh
Required energy including reserve	427.61	Wh
Mission duration	6.44	min
One-way cruise distance	1.00	km

Table 5.3.2 — Main sizing and performance results obtained for the baseline configuration.

The main results obtained from the baseline sizing process are summarized in Table 5.3.2., and they show that the iterative process converges toward a baseline configuration with a gross mass of approximately 26.6 kg and a battery mass of about 2.66 kg, corresponding to a battery fraction close to 10%.

The rotor diameter is determined by the final total mass, the number of rotors, and the assigned disk-loading target, and it is approximately 1.62 m for each rotor, with a total disk area of about 12.35 m^2. This value is larger than that of the initial MSH hexacopter configuration, which has a rotor radius of approximately 0.64 m, but the difference is consistent with the higher gross mass of the baseline analyzed here and with the decision to maintain a disk loading of the same order as the MSH-like reference case. The imposed value, DL = 8 N/m^2, corresponds to approximately 2.16 kg/m^2 under Martian gravity, very close to the value of about 2.29 kg/m^2 reported for the MSH hexacopter.
The resulting rotor diameter should therefore be regarded as physically plausible from the standpoint of the aerodynamic balance, although further packaging and structural-integration checks would be required. The difference between ideal power, rotor power, and actual electrical power highlights the role of rotor and propulsive losses in the sizing process: starting from an ideal hover power of approximately 1.61 kW, the total rotor power increases to about 2.58 kW, while the required electrical power reaches approximately 2.95 kW. This confirms that the baseline is not governed only by the thrust requirement, but also by the aerodynamic and propulsive inefficiencies associated with flight in the Martian atmosphere.
Overall, the table defines a stable and physically plausible reference configuration, which can be used as the starting point for a more detailed analysis of the power and energy distribution across the different mission phases.

5.3.2 Hover power and mission energy

Figure 5.3.3 shows the power required during the main phases of the baseline mission profile.

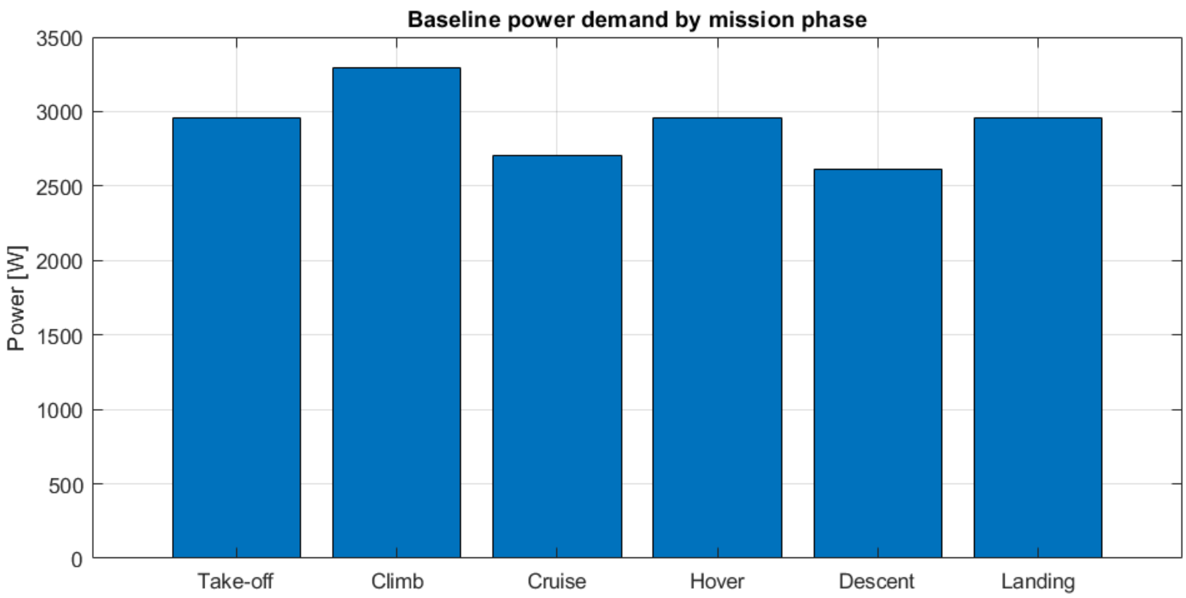

Figure 5.3.3 — Baseline power demand by mission phase

The most demanding phase in terms of instantaneous power is climb, with a requirement of approximately 3.29 kW, an expected result since the power needed to support the vehicle is combined with the additional contribution associated with the increase in potential energy. Take-off, scientific hovering and landing instead require values close to the electrical hover power, approximately 2.95 kW, since they are dominated by vertical or almost-steady flight conditions.

Cruise requires a slightly lower power, of approximately 2.71 kW, but it remains of the same order of magnitude as hover. This behavior is consistent with the multicopter configuration adopted: in the absence of lifting surfaces, the rotors must continue to support almost the entire vehicle weight even during forward flight. The parasite drag contribution of the body is included in the model, but at the moderate cruise speeds considered in the baseline it remains secondary compared with the power associated with thrust generation. Descent also shows a lower power requirement than hover, of about 2.61 kW, because the downward vertical motion partially reduces the propulsive demand relative to the stationary condition.

Figure 5.3.4 reports the distribution of the energy required by the different mission phases, and unlike power the energy depends not only on the instantaneous power level, but also on the duration of each phase. For this reason, scientific hovering represents the largest energy contribution among the flight phases, with approximately 98.5 Wh, since it combines a high power level with a significant duration of 120 s. Climb and cruise also provide relevant contributions, equal to approximately 61.0 Wh and 62.6 Wh, respectively, whereas take-off and landing contribute less, about 24.6 Wh and 16.4 Wh, because of their shorter duration.

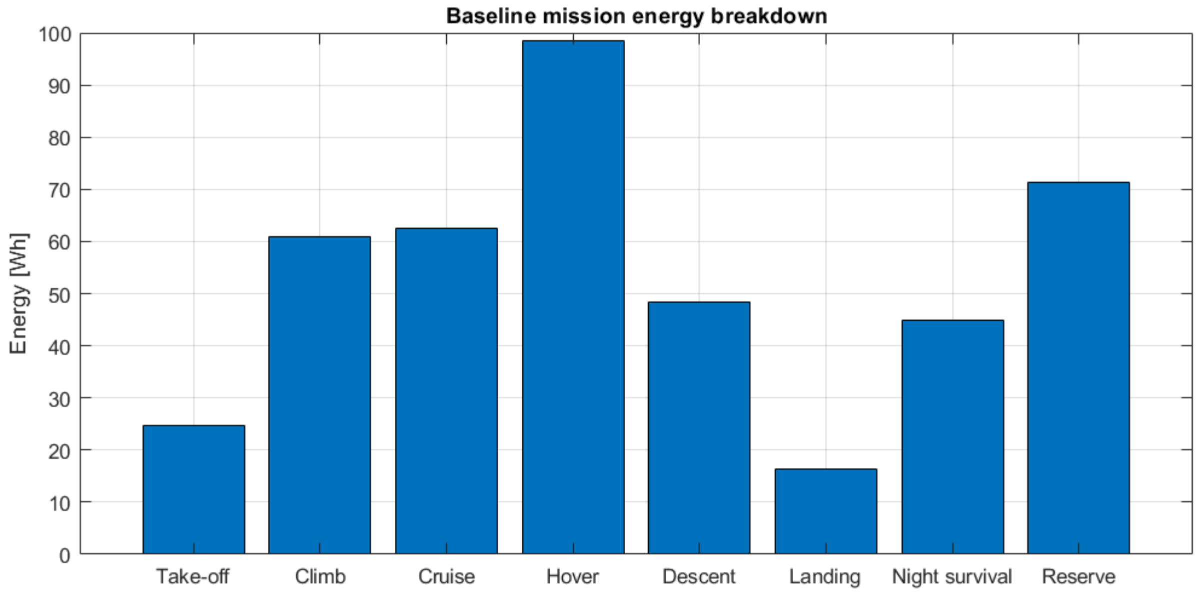

Figure 5.3.4 — Baseline energy contribution by mission phase

The descent phase requires approximately 48.4 Wh, an intermediate value between the short take-off/landing phases and the longer climb, cruise, and hovering phases. Considering the flight phases alone, the required energy is approximately 311.6 Wh, while the night-survival contribution is about 44.8 Wh. Finally, with a 20% energy reserve, equal to approximately 71.3 Wh, the total energy required by the baseline reaches about 427.6 Wh.

Taken together, the figures 5.3.3 and 5.3.4 clarify the different information provided by power and energy: power identifies the critical phases for the instantaneous sizing of the propulsion system, with climb representing the most demanding case; the energy instead determines the battery capacity required to close the mission. In the baseline case, scientific hovering dominates the energy balance among the propulsive phases, while night survival and reserve show that battery sizing cannot be based on flight alone, but it must also include auxiliary loads and operational margins.

5.3.3 Baseline rotor consistency assessment

In addition to the global mass, power, and energy results, the baseline configuration was checked through a set of rotor-consistency indicators. This verification is particularly important because the adopted sizing model does not impose a Figure of Merit directly. Instead, the hover power is computed through an explicit formulation including induced and profile power contributions. Therefore, an a posteriori check is required to verify that the selected combination of tip Mach number, rotor solidity, mean blade drag coefficient, and disk loading leads to a rotor configuration that is not only numerically convergent, but also physically plausible from a preliminary rotor-design standpoint.

Two main indicators are considered in this assessment:

- the equivalent Figure of Merit, FM_{eq}, obtained by comparing the ideal hover power with the total rotor power predicted by the model; this quantity provides a compact indication of the effective hover efficiency associated with the adopted explicit power formulation
- the blade-loading coefficient, expressed through the ratio C_T/σ. In rotorcraft aeromechanics, this parameter is commonly used as a compact measure of the aerodynamic loading required on the rotor blades [47], [48].

Using the baseline rotor assumptions reported in Table 5.1.2, the derived consistency indicators are summarized in Table 5.3.3.

Parameter	Symbol	Value
Thrust coefficient	C_T	0.0233
Blade loading	C_T/σ	0.1163
Minimum tip Mach from screening criterion	$M_{tip_{min}}$	0.6398
Equivalent Figure of Merit	$\mathrm{FM_{eq}}$	0.625
Reference Figure of Merit	$\mathrm{FM_{ref}}$	0.600

Table 5.3.3 — Derived rotor consistency indicators for the baseline configuration

The results indicate that the baseline rotor sizing remains within a plausible preliminary design region, indeed the equivalent Figure of Merit is approximately $FM_{eq} = 0.625$, which is close to the conservative reference value $FM_{ref} = 0.600$, so that confirms that the explicit hover-power formulation does not lead to an excessively optimistic estimate of rotor efficiency. In other words, the power obtained from the induced and profile contributions remains consistent with the level of efficiency that would be expected from a global Figure-of-Merit-based correction.

The blade-loading parameter is equal to $C_T/\sigma = 0.1163$: this quantity is useful because it can be related, in preliminary rotorcraft analysis, to an approximate mean blade lift coefficient. For a hovering rotor, the mean blade lift coefficient may be estimated as [47]

$$\bar{C_l} \approx 6\frac{C_T}{\sigma}$$

which gives, for the present baseline,

$$\bar{C_l} \approx 6 \cdot 0.1163 \approx 0.70.$$

This result indicates that the rotor blades are required to operate at a relatively high average lift coefficient, but that is non unrealistic for a preliminary sizing analysis. Practical blade-loading limits for helicopter rotors are commonly reported around $C_T/\sigma \approx 0.12 - 0.14$, although the actual stall margin depends on blade geometry, airfoil characteristics, reynolds number, and mach number [48].
The obtained value is therefore close to the upper part of the preliminary acceptable range, but it remains below typical practical limits. Values of the same order of magnitude are also adopted in rotorcraft design studies, where blade loadings around $C_T/\sigma = 0.10$ are used as representative design values [49], and experimental/numerical rotorcraft analyses include operating conditions in the approximate range $C_T/\sigma = 0.089 - 0.128$ [50].

Therefore, the value $C_T/\sigma = 0.1163$ should not be interpreted as a definitive aerodynamic validation of the rotor, rather it is used as a screening indicator showing that the selected combination of tip Mach number and solidity does not lead to an excessive blade-loading requirement within the simplified sizing model. This point is especially relevant for the Martian environment, where the low atmospheric density and low Reynolds number conditions may significantly affect the available section lift and stall margin.

The minimum tip Mach number obtained from the screening procedure is $M_{tip,min} = 0.6398$, which is slightly lower than the adopted baseline value $M_{tip} = 0.65$. The margin is therefore limited, but still sufficient according to the adopted screening criterion. This confirms that the selected tip speed is just adequate to keep the blade loading within the preliminary screening range, without introducing an unnecessary excess in rotor peripheral speed.

Overall, these indicators do not replace a detailed aerodynamic design of the rotor, but they provide a useful consistency check for the mass–energy sizing model. The baseline configuration can therefore be considered coherent with the preliminary objectives of the analysis, but a definitive rotor validation would require blade-element or CFD-based calculations, dedicated low-Reynolds-number aerodynamic polars, and a more detailed definition of the blade geometry.

5.4 Reference Configuration Summary

5.4.1 Final baseline layout

Based on the results obtained in the previous sections, the baseline case can be interpreted as a first converged reference configuration, useful for verifying the consistency of the mass–energy model developed in Chapter 4. The sizing process leads to a hexacopter configuration with a gross mass of approximately 26.6 kg, a payload of 3.0 kg, a battery mass of about 2.66 kg, a rotor diameter of approximately 1.62 m, and an electrical hover power of the order of 2.95 kW.
The main significance of this configuration does not lie in the absolute values of this single case, but in the fact that it demonstrates the existence of an internally consistent solution within the adopted assumptions. The baseline shows that, for the selected mission profile, it is possible to obtain an MSH-like configuration in which total mass, rotor sizing, required power, energy capacity, and preliminary rotor-plausibility constraints are mutually compatible.

It is important to emphasize that this configuration does not represent an optimized design or a definitive prediction of the performance of a Martian multicopter, but it should be regarded as a nominal reference case, developed to verify the behavior of the sizing framework and to provide a quantitative starting point for the following analyses. In this sense, the baseline is a working configuration:

sufficiently realistic to be physically plausible, but still intentionally preliminary and open to parametric variation. A relevant aspect of the baseline is the consistency between the explicit rotor-power formulation and the control indicators introduced a posteriori: the equivalent figure of merit, close to 0.625, is comparable with the conservative reference value $\mathrm{FM_{ref}} = 0.60$, while the ratio C_T/σ , approximately equal to 0.116, confirms that the selected combination of tip Mach number and solidity does not lead to an unrealistic aerodynamic loading of the blades. This supports the use of the baseline configuration as a reference for design exploration, although it does not replace a future detailed aerodynamic analysis.

5.4.2 Key design drivers emerging from the baseline case

The baseline case makes it possible to identify several key drivers that govern the preliminary feasibility of the Martian multicopter.

The first driver is the coupling between total mass, rotor disk area, required power, and battery mass, indeed even for a relatively limited mission closing the mass–energy balance requires an iterative procedure, since any increase in mass raises the required thrust, modifies the power demand, and directly affects the battery mass.

The second driver is the rotor sizing, represented at first order by disk loading: the value imposed in the baseline, equal to 8 N/m^2 ,leads to relatively large rotors, but remains consistent with the need to limit induced power in an extremely rarefied atmosphere. At the same time, rotor sizing cannot be pushed arbitrarily toward increasingly larger disk areas, since mass, integration, packaging, and structural-complexity constraints must also be considered.

The third driver concerns the choice of the rotor parameters M_{tip}, σ, and $\bar{c}d$. The baseline shows that an excessive reduction in tip speed may lead to an underestimation of profile power and to an implausible blade loading, whereas excessively high tip Mach values increase the profile-power contribution and reduce the margin with respect to compressibility effects. The selected configuration therefore represents a preliminary compromise between energy efficiency, aerodynamic blade loading, and physical plausibility of the model.

The fourth driver is the energy system, since the baseline confirms that battery sizing does not depend only on flight energy, but also on auxiliary loads, night survival, and operational margins. Even for a short mission, the night-survival and reserve-energy contributions have a noticeable effect on the overall energy requirement, showing that vehicle autonomy cannot be assessed solely from the propulsive phases.

Finally, the baseline analysis shows that improvements in range and endurance cannot be achieved by modifying a single design parameter in isolation: increasing the battery capacity, reducing the disk loading, changing the payload mass, or adopting a battery with higher specific energy all affect the mass–energy balance simultaneously, often producing coupled and competing effects on the final vehicle performance.

For this reason, Chapter 6 extends the baseline sizing process through a set of parametric analyses, in which the total mass, payload mass, disk loading, battery specific energy and auxiliary loads are varied systematically in order to assess how each parameter influences the overall design. The objective is to understand the main trends governing the system and to determine whether higher-performance solutions can be obtained while preserving a physically plausible closure of the mass–energy balance.

6. Parametric Design Exploration and Sensitivity Analysis

6.1 Analysis Setup

After defining an internally consistent baseline configuration in the previous chapter, the analysis is extended here to a parametric exploration of the design space, in which the baseline case is used as a quantitative reference, while selected parameters are varied to assess their influence on vehicle sizing, energy demand, and preliminary feasibility.

The purpose of this chapter is to identify the main sensitivities of the mass–energy model and to determine under which conditions the Martian multicopter can maintain a plausible physical and energetic closure. In this sense, the results are intended to provide design insight into the dominant trade-offs of the system, such as the coupling between mass, rotor sizing, battery requirements, and mission performance.

The logic followed in the analysis is summarized in Figure 6.1.1.: starting from the baseline case, one independent parameter is varied at a time, while the remaining inputs are kept fixed unless otherwise specified. For each value of the selected parameter, the full mass–energy model is rerun, so that all dependent quantities are updated consistently. The resulting configurations are then assessed in terms of both numerical outputs and physical plausibility, using the evaluation metrics defined in Section 6.1.3. In this way, the chapter addresses the central question of which parameters most strongly affect the feasibility and performance of the Martian multicopter, and under which assumptions the baseline concept can be scaled toward more demanding mission requirements.

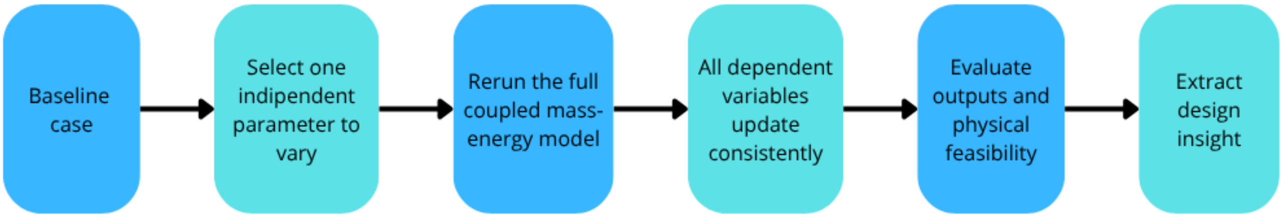

Figure 6.1.1 — Parametric analysis workflow adopted to evaluate the effect of individual design variables on the mass–energy model outputs

6.1.1 Varied parameters

The parametric exploration is carried out by varying a set of quantities that, based on the baseline results and on the reference literature, are expected to have the strongest influence on the preliminary sizing of the vehicle. These parameters are selected to investigate the effects of vehicle scale, mission-driven payload requirements, rotor disk loading, battery technology, and non-propulsive energy demand.

Gross mass is first varied as a synthetic scaling variable, and it is used to study how rotor size, hover power, battery mass, and overall performance evolve with vehicle class, and this allows the scaling behaviour of the multicopter to be evaluated before considering more specific design changes.

Payload mass is then varied because it represents one of the most direct mission-driven requirements. Unlike purely internal design parameters, the payload mass affects the initial system mass and it propagates through the entire sizing loop, influencing battery mass, rotor dimensions, power demand, and achievable range. For this reason, it is treated as a key variable in the assessment of mission capability.

Disk loading is also included in the parametric analysis because it directly controls the compromise between rotor size and induced power: lower calues of disk loading generally reduce hover power, but

they require larger rotor areas, with possible implications for packaging, structural design, and geometric feasibility. Higher disk loadings have the opposite effect, reducing rotor size but increasing the power required to generate lift in the low-density Martian atmosphere.
Battery specific energy, auxiliary power demand, and thermal loads are also varied, since they represent key drivers of the vehicle energy balance. A higher battery specific energy increases the amount of energy available for a given battery mass, whereas auxiliary and thermal loads reduce the fraction of stored energy that can be allocated to flight. Varying these quantities makes it possible to quantify how sensitive the final configuration is to battery technology assumptions and to the severity of the Martian operating environment.

6.1.2 Fixed parameters

To isolate the effect of each variable, the parametric analysis is performed by keeping the reference mission, environmental assumptions, and core modelling approach fixed, unless otherwise stated in the individual sections. This choice allows the influence of each parameter to be interpreted without introducing additional changes in the operating scenario or in the structure of the sizing model.
The fixed assumptions include the Martian gravity, atmospheric density, reference speed of sound, overall electromechanical efficiencies, hover-power formulation, induced and profile power contributions, and the rotor-consistency parameters adopted in the baseline case. The baseline mission profile and the general structure of the mass–energy model developed in Chapter 4 are also retained as a common basis for the analysis. As a result, power, energy, and battery-mass estimates remain comparable across the different cases.
Keeping these parameters fixed does not imply that they are universally valid for every possible Martian mission, rather this choice defines a homogeneous basis for comparison. The results obtained in Chapter 6 should therefore be interpreted in relative terms: they are intended to reveal trends, sensitivities, and feasibility thresholds consistent with the case study considered, rather than to provide absolute performance values valid for all possible mission scenarios.

6.1.3 Evaluation metrics

To compare the different configurations consistently, the parametric analysis is based on a set of evaluation quantities directly related to mass closure, energy demand, rotor sizing, and mission performance. Depending on the specific analysis, the total mass is either used as a scaling variable or obtained through the iterative mass–energy closure. In both cases, the corresponding battery mass and battery mass fraction are evaluated, since they indicate how strongly the configuration is driven by the energy-storage system.
Rotor-related quantities, such as rotor diameter, total disk area, and disk loading, are used to assess the aerodynamic and geometric implications of each solution. These parameters are important because a configuration may be energetically favourable while requiring rotor dimensions that are difficult to justify from a preliminary design perspective.
The operational relevance of each case is evaluated through hover power, total mission energy, mission duration, and achievable range, and these quantities make it possible to distinguish between solutions that only converge numerically and configurations that also have practical interest for local Martian exploration missions. Finally, each configuration is checked against the physical and operational limits adopted in the model, including battery fraction, rotor size, disk loading, and tip Mach number, so the assessment is not based on a single performance index, but on the combined interpretation of mass, energy, rotor geometry, and mission capability. This approach provides the basis for identifying a preliminary feasibility envelope for the Martian multicopter.

6.2 Effect of Gross Mass

6.2.1 Rotor diameter scaling

For a multicopter operating in the Martian atmosphere, an increase in gross mass leads directly to a higher total thrust requirement in hover, since the vehicle must satisfy the condition $T \approx mg_M$. In an environment characterized by very low atmospheric density, this increase cannot be efficiently compensated by keeping the rotor geometry unchanged, because doing so would increase disk loading and, consequently, the induced power required to sustain the vehicle. For this reason, as vehicle mass increases, the design naturally tends to require a larger total disk area and therefore, for a fixed number of rotors, a larger rotor diameter: this represents the first and most immediate scaling effect of the system [2]. Empirical scaling studies on terrestrial rotorcraft also show that rotor diameter increases with mass according to a sublinear law, with an exponent of the order of $m^{0.4}$, corresponding to a disk area that scales approximately as $m^{0.8}$ [21]. Although this relation cannot be transferred directly to the Martian case, because of the strong differences in atmospheric density, Reynolds number, and Mach constraints, it remains useful as a qualitative indication: an increase in mass does not only imply a higher thrust requirement, but also a progressive growth of the rotor scale in order to maintain disk-loading levels compatible with efficient operation [21].
In the Martian case, this tendency becomes even more severe: studies on the Mars Science Helicopter [2] show that reducing the P/T ratio requires low values of T/A, namely low disk-loading values, which can only be achieved through large-diameter rotors. In the same study, preliminary sizing results for vehicles with masses of around 20 kg lead to rotor diameters of the order of 2.5–2.7 m for the coaxial configuration and 1.0–1.4 m for the individual rotors of a hexacopter configuration, highlighting how an increase in vehicle scale is rapidly accompanied by an increase in the required rotor geometry.

Overall, rotor diameter scaling cannot be interpreted as a purely geometric law, but rather as the result of a compromise between competing constraints [2], [8]: on the one hand, increasing rotor diameter helps reduce induced power and improve the energetic sustainability of flight; on the other hand, rotor diameter growth is limited by aeroshell packaging constraints, the complexity of folding and deployment mechanisms, and tip Mach limitations. In this work, the effect of gross mass on rotor sizing is analyzed by keeping the other independent inputs of the case study fixed and running the mass–energy model again for each mass value considered, so that rotor diameter is not imposed as an arbitrary parameter, but it emerges as a response variable of the sizing process. The aim is to show directly how, as vehicle mass increases, the system progressively requires larger rotors in order to maintain acceptable disk-loading levels and a plausible closure of the energy balance.

Figure 6.2.1 illustrates this effect by showing the required rotor diameter as a function of gross mass, for different numbers of rotors and different target values of disk loading. The plot is derived directly from the definition of disk loading: by setting the total thrust required in hover equal to the vehicle weight, $T = mg_M$,and writing the total disk area as

$$A_{tot} = \frac{T}{DL}$$

this area can be distributed among N_r identical rotors, each assumed to have a circular disk geometry. The corresponding rotor radius is therefore obtained as:

$$R = \sqrt{\frac{m g_M}{DL\, N_r\, \pi}}$$

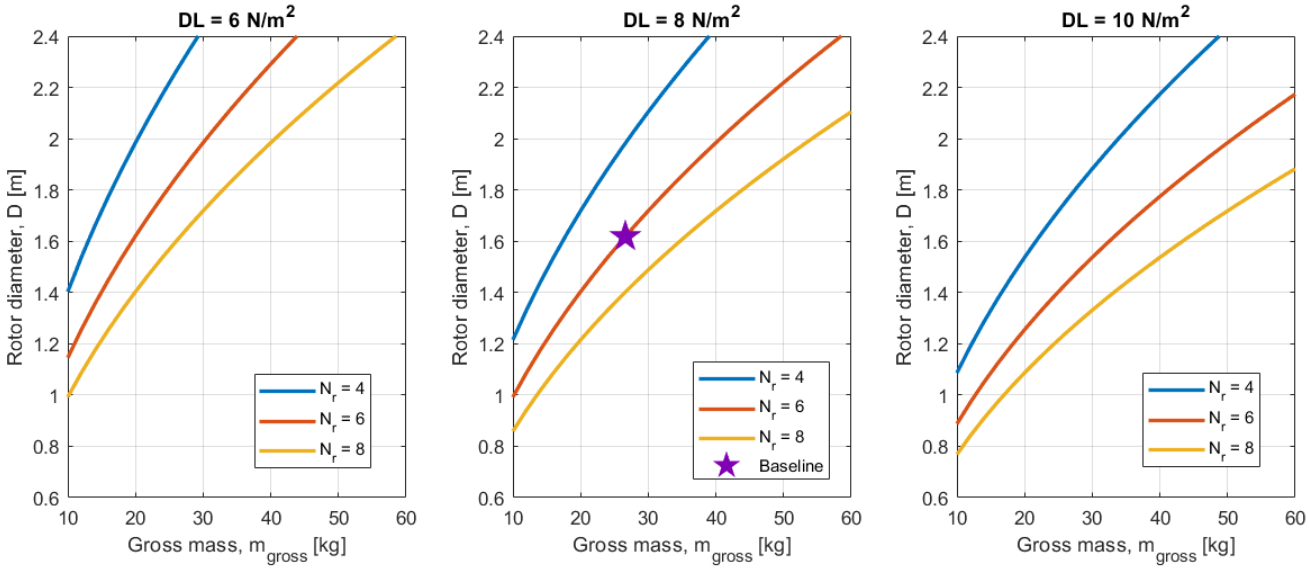

Figure 6.2.1 — Rotor diameter scaling with gross mass for different rotor numbers and disk loading targets

Three main indications emerge from the figure:

- for each disk-loading value considered, the required rotor diameter increases monotonically with vehicle gross mass
- for a given mass and disk loading, increasing the number of rotors reduces the diameter required for each rotor, since the total thrust is distributed over a larger overall disk surface.
- lower disk-loading targets systematically require larger rotor diameters.

Overall, the figure shows that the rotor scaling depends simultaneously on vehicle scale, number of rotors and the imposed disk-loading level, highlighting the fundamental geometric compromise between reducing induced power and increasing packaging and integration constraints [4].

6.2.2 Hover power scaling

While the previous section showed how increasing gross mass requires a larger rotor scale, the hover-power analysis makes it possible to assess whether this growth remains sustainable from a propulsive point of view. The geometric sizing of the rotor system, indeed, cannot be separated from the energetic cost of lift generation, since hover power is one of the main drivers of the energy-system sizing [2].

In the complete model discussed in Chapter 4, hover power is described through a formulation that accounts for rotor losses by means of the figure of merit and the overall propulsive efficiency; however, the following plot is not built using the full hover-power model, but rather a simplified induced-dominated formulation, in order to isolate, in a transparent way, the role of mass and disk loading, allowing the relationship between vehicle scale, disk loading, and propulsive severity to be interpreted directly.

In this simplified form, derived from momentum theory [30], hover power is written as:

$$P_{hover} = \kappa T \sqrt{\frac{T}{2\rho A_{tot}}}$$

where $T = m_{gross} g_M$ is the thrust required in hover, ρ is the Martian atmospheric density, A_{tot} is the total rotor disk area, and κ is a correction factor applied to induced power. Substituting the definition of disk loading as ratio of thrust T to total area , A_{tot} it gives:

$$P_{hover} = \kappa T \sqrt{\frac{DL}{2\rho}} = \kappa m_{gross} g_M \sqrt{\frac{DL}{2\rho}}$$

It follows that, for a given atmospheric density, the hover power estimated in this way scales linearly with vehicle mass and with the square root of disk loading. Figure 6.2.2 shows the variation of hover power with disk loading for a set of representative gross masses, highlighting two main trends:

- first, for a fixed disk loading, heavier configurations require substantially higher lift power.
- second, for a fixed mass, increasing disk loading produces a systematic increase in the required power.

The geometric advantage associated with higher disk-loading values is therefore paid through a higher propulsive cost in hover.

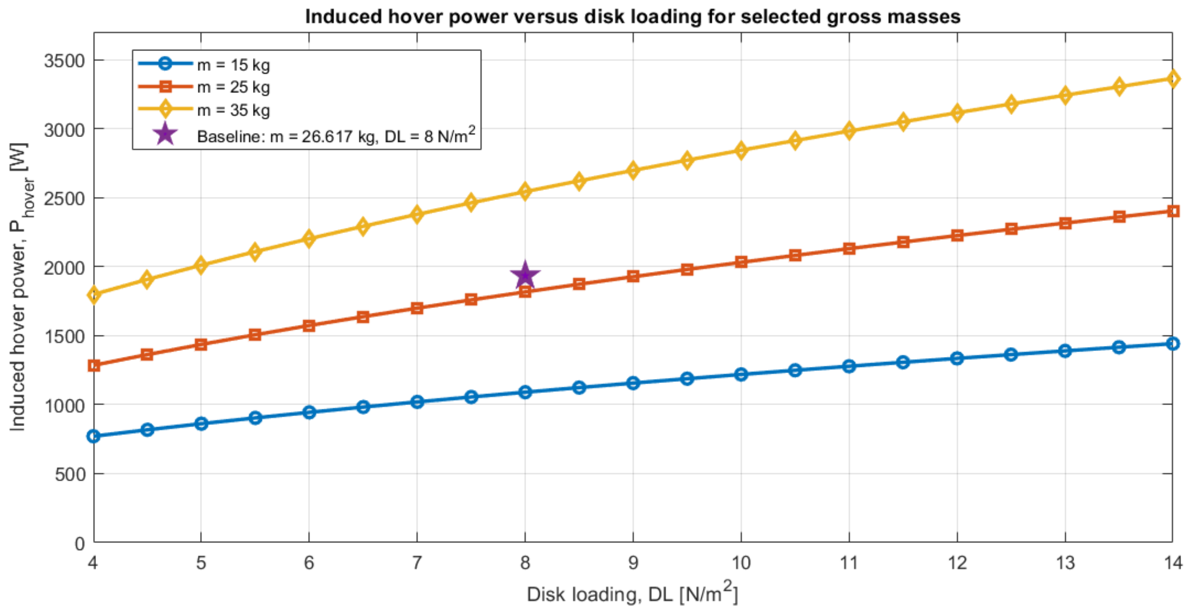

Figure 6.2.2 — Hover power variation with disk loading for selected gross mass values

The baseline case lies in an intermediate region of the plot, consistently with the disk-loading value adopted in the preliminary sizing. Overall, the figure confirms that disk loading cannot be interpreted merely as a geometric parameter, but rather as a true design lever that controls the compromise between system compactness and propulsive severity. This result is consistent with the indications reported for the MSH where hover power is mainly related to the induced cost associated with thrust generation and with the corresponding available disk area [2].

The counterpart of this result has already emerged in the previous section: reducing disk loading helps contain hover power, but it requires larger rotors and introduces more severe constraints in terms of mass, volume, and integration. This trade-off provides a natural link with the following parametric analyses, where an increase in required power translates into a higher overall energy penalty and, consequently, into a greater battery-mass requirement.

6.2.3 Energy storage and mission capability

The energy-storage analysis is set up to evaluate how variations in gross mass affect, at the same time, the onboard energy capacity, the required power, and the achievable performance in terms of range and endurance. Unlike the baseline case, in this phase the total mass is not interpreted as a fixed value, but as a design variable, in order to assess whether increasing the scale of the vehicle leads to an actual improvement in mission capability, or whether the additional energy is progressively absorbed by the higher power demand.

The first step of the model links battery mass to total mass through an assigned battery mass fraction:

$$m_{bat} = f_{bat} m_{gross}$$

Three battery mass fractions are therefore considered in this study.

- the value $f_{bat} = 0.10$ represents the case closest to the baseline configuration of Chapter 5, for which the battery mass is approximately 10% of the total mass.
- the values $f_{bat} = 0.12$ and $f_{bat} = 0.15$ represent two moderately more favorable energy-allocation cases, useful for evaluating how small increases in the fraction of mass assigned to the battery may affect mission capability.

The nominally storable energy is then estimated from the battery pack specific energy:

$$E_{bat} = m_{bat} e_{spec}$$

where m_{bat} is the battery mass and e_{spec} is the battery pack specific energy.

However, not all the nominal stored energy is considered effectively usable during the mission: to account for the admissible depth of discharge and for the need to preserve an operational margin, a usable energy fraction $\mathrm{f_{usable}}$ is introduced. The usable energy is therefore calculated as

$$\mathrm{E_{usable} = f_{usable} E_{bat}}$$

Concurrently, for each gross-mass value, the energy required by the mission profile is computed. Mission energy is obtained by summing the contributions of the different operational phases:

$$\mathrm{E_{mission} = E_{takeoff} + E_{climb} + E_{cruise} + E_{hover/science} + E_{descent} + E_{landing}}$$

To this value, the energy contribution required for night survival is added:

$$\mathrm{E_{nominal} = E_{mission} + E_{night}}$$

Consistently with the conservative approach adopted in the model, the energy reserve is applied to the overall requirement associated with the nominal mission and night survival:

$$\mathrm{E_{reserve} = f_{res}(E_{mission} + E_{night})}$$

The total required energy therefore becomes

$$E_{required} = (E_{mission} + E_{night})(1 + f_{res})$$

The residual energy margin is finally calculated as the difference between the usable onboard energy and the total required energy:

$$E_{residual} = E_{usable} - E_{required}$$

A positive value of $E_{residual}$ indicates that, for the assumed battery mass fraction, the vehicle has enough energy to complete the reference mission, including night survival and the energy reserve.
A negative value, however, does not imply that a lower-mass configuration is impossible in absolute terms, but it only means that the energy balance cannot be closed with the specific battery allocation considered. The same mass could become feasible by slightly increasing the battery mass fraction, reducing the payload, modifying the mission profile, or improving system efficiency.
In parallel with the energy balance, a preliminary rotor-area sizing is performed for each gross-mass value, and to prevent the rotor radius from varying arbitrarily with mass, the target disk loading used in the baseline case is kept constant:

$$\mathrm{DL} = 8\ \mathrm{N/m^2}$$

From the definition of disk loading as the ratio between total required thrust and rotor disk area, the rotor area can be obtained. In hover, the total required thrust is assumed to be equal to the vehicle weight in the Martian environment:

$$T = m_{gross} g_{Mars}$$

Consequently, once the total vehicle mass is known, the required total rotor disk area is calculated as

$$A_{tot} = \frac{T}{DL} = \frac{m_{gross} g_{Mars}}{DL}$$

Once the required total area is known, the radius of each rotor is obtained by distributing this area over the six rotors of the hexacopter configuration:

$$\mathrm{R} = \sqrt{\frac{\mathrm{A_{tot}}}{\mathrm{N_{rotors}} \pi}}$$

$$D = 2R$$

In this way, the increase in mass is accompanied by a coherent update of the rotor scale: a higher gross mass requires greater thrust, but keeping disk loading constant allows this increase to be compensated by a larger rotor disk area. A maximum rotor diameter of 2.50 m is also considered, as a preliminary plausibility constraint related to packaging, integration, and compatibility with aeroshell-type architectures.
Positive residual energy is then interpreted as energy potentially available to extend mission capability: such energy can be allocated, alternatively, to increasing the cruise segment or to extending the hover/science time over the site of interest. In the first case, the residual energy is converted into extra cruise time:

$$t_{extra,cruise} = \frac{E_{residual}}{P_{cruise}}$$

and the corresponding additional range is calculated as

$$R_{extra} = V_{cruise} t_{extra,cruise}$$

The total range estimated is therefore:

$$R_{total} = R_{nominal} + R_{extra}$$

In the second case, the same residual energy can be used to extend the hover phase during scientific operations. The extra hover time is estimated as

$$t_{extra,hover} = \frac{E_{residual}}{P_{hover}}$$

and the potential overall endurance is calculated by adding this contribution to the nominal mission duration:

$$\mathrm{t_{total} = t_{nominal} + t_{extra,hover}}$$

The two quantities, estimated maximum one-way range and potential endurance, should not be interpreted as simultaneously achievable performance figures, but as two alternative ways of using the residual energy. In other words, the excess energy can be used either to fly farther or to remain longer in hover over the site of interest, depending on the operational priority of the mission. For this reason, the following results are discussed as potential capability estimates, not as a new optimized operational mission or as guaranteed performance values.

Finally, to avoid an excessively rigid interpretation of the energy-feasibility threshold, the battery mass fraction required to close the reference mission is also calculated:

$$\mathrm{f_{bat,required} = \frac{E_{required}}{e_{spec} f_{usable} m_{gross}}}$$

Rotor diameter

The first check concerns the geometric compatibility of the configurations obtained as gross mass is varied: since disk loading is kept constant at the baseline value, an increase in total mass requires an increase in the total rotor disk area: as a consequence, the diameter of each rotor also increases with mass.

As shown in Figure 6.2.3, the rotor diameter increases progressively over the mass range considered. The value corresponding to the baseline configuration, approximately 1.62 m, falls within the analyzed range and it is consistent with the sizing obtained in Chapter 5. The imposed maximum diameter of 2.50 m is not exceeded, although the heavier configurations progressively approach this threshold.

This result highlights a first important constraint associated with mass scaling, so that increasing gross mass may allow more energy to be carried onboard and may potentially improve mission capability, but it also requires progressively larger rotors. Beyond a certain range, therefore, configuration feasibility would no longer be limited only by the energy balance, but also by packaging, structural integration, geometric compatibility, and deployment constraints.

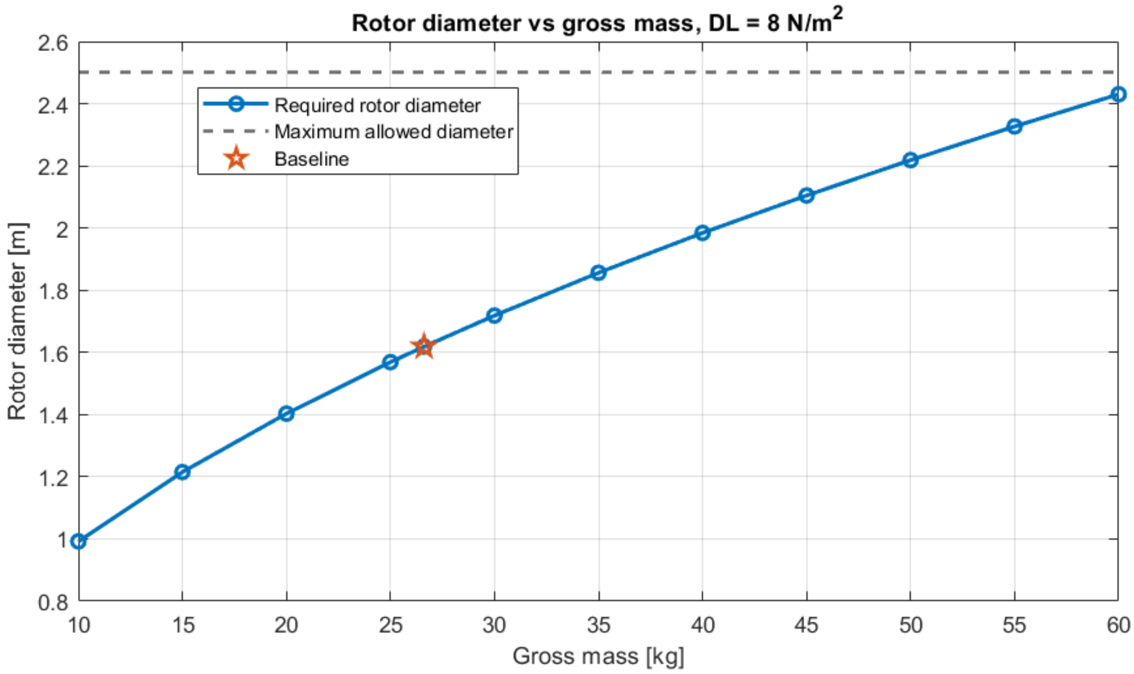

Figure 6.2.3 — Rotor diameter variation with gross mass at fixed disk loading of $DL = 8\ N/m^2$

Endurance and Range

Figure 6.2.4 shows the combined effect of gross mass and battery mass fraction on the potential performance of the multicopter, expressed in terms of potential endurance and estimated maximum one-way range. Three battery mass fractions are considered in this analysis, $f_{\text{bat}} = 0.10, 0.12$, and 0.15, selected to represent configurations close to the mass allocation of the baseline case rather than strongly energy-extended scenarios.

The trends show that increasing the fraction of mass allocated to the battery produces a clear increase in both potential endurance and estimated range; however, the improvement is not proportional, because an increase in gross mass also implies a higher thrust requirement and, consequently, a higher power demand during both hovering and cruise.

For the case closest to the baseline, $f_{\text{bat}} = 0.10$, the performance remains close to the nominal mission in the lower part of the mass range. This does not mean that lighter configurations are intrinsically impossible, but rather that, with the battery representing 10% of the total mass, the available energy margin for extending the mission is very limited or absent. As mass increases, the battery mass increases proportionally and the residual energy margin becomes positive, allowing a gradual increase in both estimated range and potential endurance.

The curves corresponding to $f_{\text{bat}} = 0.12$ and $f_{\text{bat}} = 0.15$ show that even modest increases in the fraction of mass assigned to the battery can lead to a significant improvement in mission capability. In particular, moving from a baseline-like configuration to a moderately more favorable energy allocation makes it possible to obtain higher range and endurance without relying on excessively high battery fractions. Even in these cases, however, the curves progressively tend to flatten, since an increasing part of the additional energy is absorbed by the higher propulsive demand of the heavier vehicle.

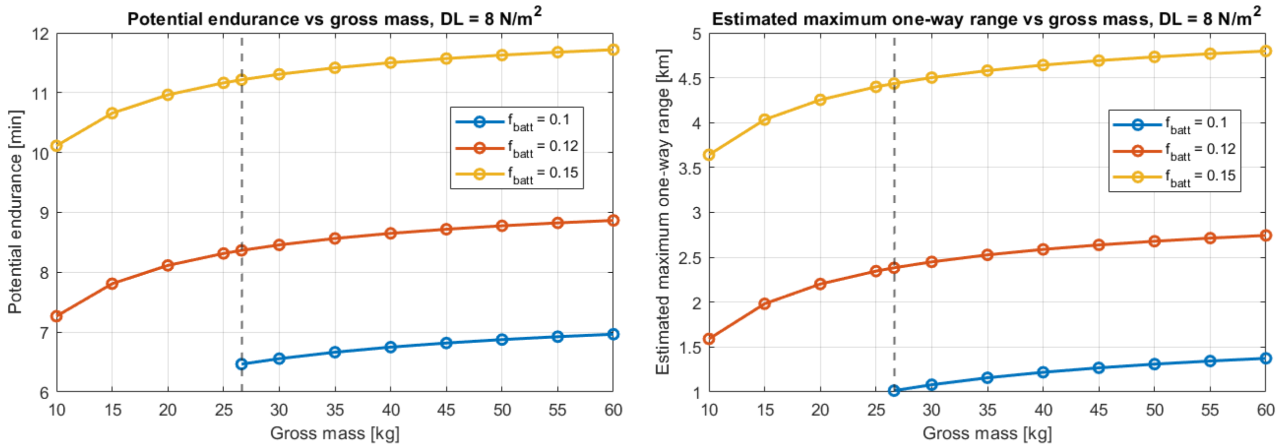

Figure 6.2.4 — Potential endurance and estimated maximum one-way range as a function of gross mass for different battery mass fractions

Energy budget

The Figure 6.2.5 shows the evolution of the energy budget as gross mass is varied for the baseline-like case, $f_{\text{bat}} = 0.10$, while keeping disk loading constant at $DL = 8\,\text{N/m}^2$. The plot compares four quantities: the usable battery energy, the energy required by the nominal mission and night survival, the total required energy including the 20% reserve, and the residual energy.

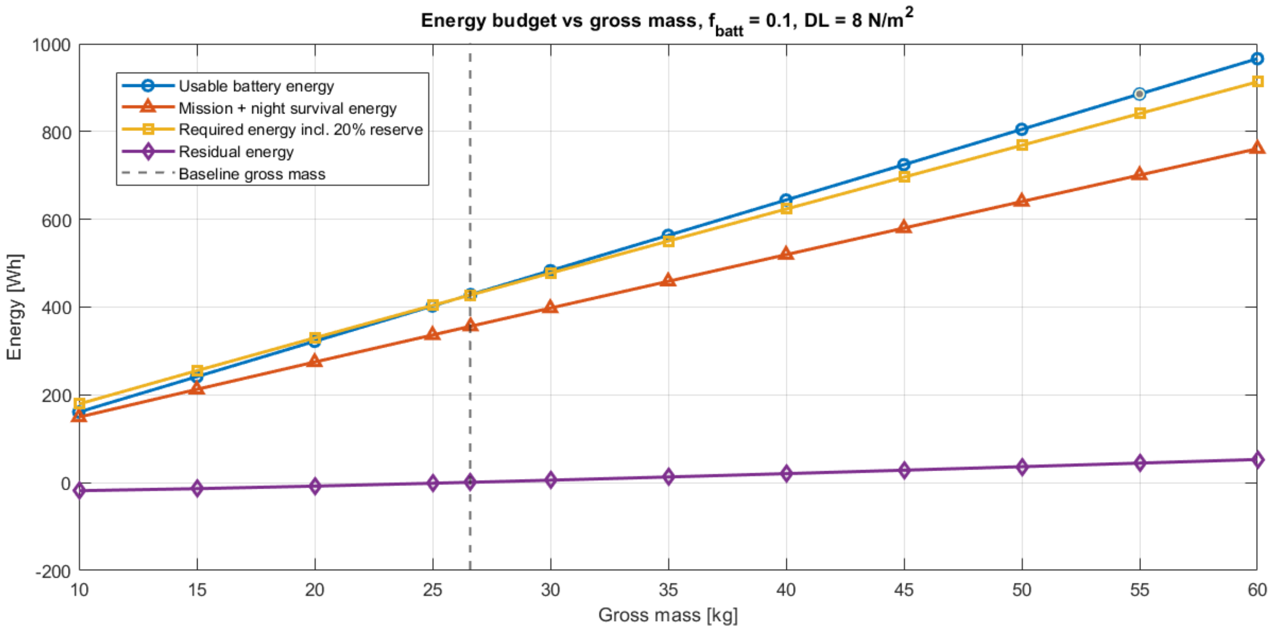

Figure 6.2.5 — Energy budget variation with gross mass for $f_{\text{batt}} = 0.1$ and fixed disk loading

Usable energy increases with gross mass, since battery mass is calculated as a fraction of total vehicle mass; at the same time, the energy required by the mission also increases, because a heavier vehicle requires greater thrust and therefore higher power during the flight phases. The comparison between the usable-energy curve and the required-energy curve including reserve makes it possible to assess whether the mission energy balance closes for the specific battery allocation considered.

For masses lower than the baseline value, the usable-energy curve is very close to, or slightly below, the required-energy curve including reserve: this indicates that, with $f_{\text{bat}} = 0.10$, these configurations do not have a sufficient energy margin to complete the reference mission with the same reserve policy.

Near the baseline mass, the two curves are almost coincident and the residual energy becomes slightly positive, confirming that the reference configuration is sized consistently with the mission profile and with the battery fraction obtained in Chapter 5. For higher masses, the energy margin increases progressively, because the battery grows proportionally with total mass. Again, however, this benefit should not be interpreted as an automatic improvement caused by mass itself, but as the result of the simultaneous scaling of total mass, battery mass, and rotor disk area.

Required battery mass fraction

To avoid an excessively rigid interpretation of the energy-closure threshold, the battery mass fraction required to complete the reference mission is also calculated:

$$f_{\text{bat,required}} = \frac{E_{\text{required}}}{e_{\text{spec}} f_{\text{usable}} m_{\text{gross}}}$$

This quantity makes it possible to estimate, for each gross-mass value, the fraction of the total mass that would need to be allocated to the battery in order for the vehicle to close the energy balance of the nominal mission, including night survival and reserve. The comparison between $f_{\text{bat,required}}$ and the battery fraction of the baseline case therefore makes it possible to distinguish between a configuration that is energetically closed with a baseline-like mass allocation and a configuration that would require a different internal mass distribution.

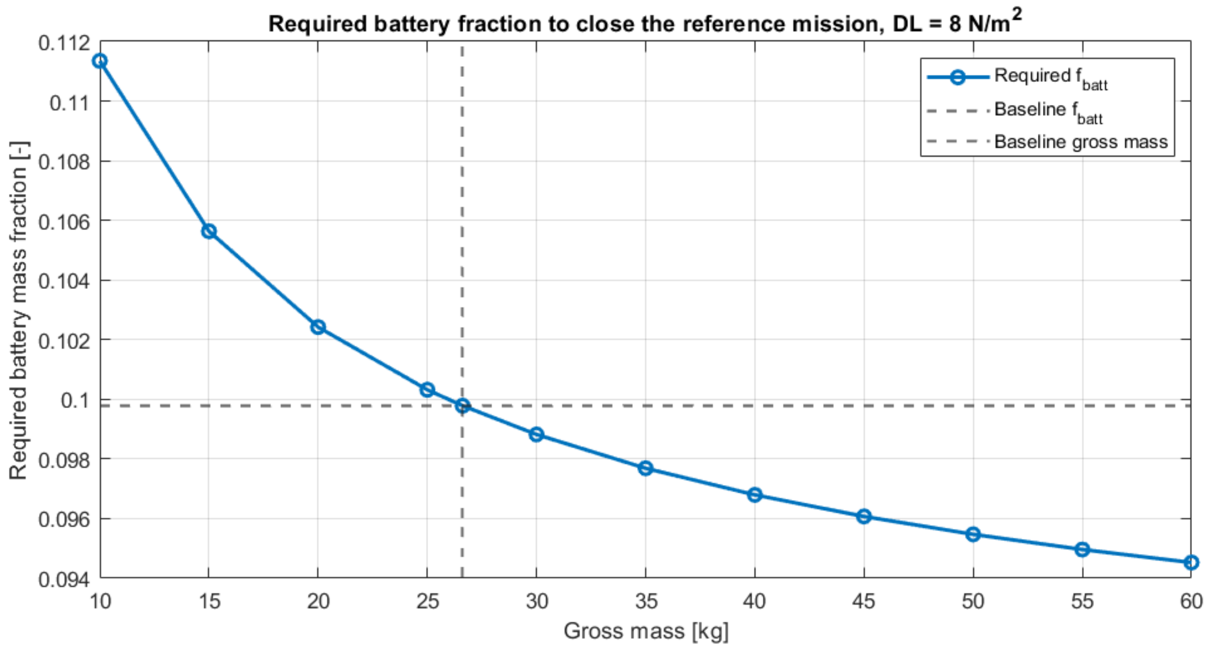

Figure 6.2.6 — Required battery mass fraction for reference mission closure

Figure 6.2.6 shows that the required battery mass fraction decreases as gross mass increases: this occurs because, in the adopted scaling approach, some contributions to the energy budget have a higher relative weight in lighter configurations. In particular, night survival has a proportionally stronger impact on lower-mass vehicles, whereas for larger masses the battery contribution grows more favorably relative to the overall energy requirement.

The main result is that the required battery fraction remains close to the baseline value over the entire mass range analyzed. For masses below the baseline, a battery fraction slightly higher than 10% would be required, whereas for higher masses the required fraction tends to decrease slightly.

Concluding remarks on gross mass variation

The Tables 6.2.1 and 6.2.2 summarize the main results of the gross mass scaling analysis and make it possible to distinguish between two different effects: the increase in total vehicle mass and the variation of the fraction of mass allocated to the battery.

Table 6.2.1 shows that, when the battery mass fraction is kept equal to $f_{\mathrm{bat}} = 0.10$, increasing gross mass leads to an increase in usable energy, from 428.5 Wh in the baseline case to 966.0 Wh for a mass of 60 kg. However, the improvement in potential performance remains limited: the estimated maximum range increases from 1.01 km to 1.37 km, while potential endurance increases from 6.46 min to 6.96 min. This trend shows that the additional energy available on board is not fully converted into useful performance, because the increase in mass also produces a higher power requirement during the flight phases.

Gross mass [kg]	Usable battery energy [Wh]	Residual energy [Wh]	Estimated maximum one-way range [km]	Potential endurance [min]
26.617	428.5	+0.9	1.01	6.46
30	483.0	+5.7	1.08	6.56
40	644.0	+20.6	1.22	6.75
50	805.0	+36.5	1.31	6.87
60	966.0	+52.9	1.37	6.96

Table 6.2.1 — Performance summary for energetically closed configurations with $\boldsymbol{f_{bat} = 0.10}$ and fixed disk loading $\boldsymbol{DL = 8\ \mathrm{N/m^2}}$

Table 6.2.2 instead highlights the effect of battery mass fraction with reference to the baseline-mass configuration. In this case, the impact on performance is more pronounced: increasing f_{bat} from 0.10 to 0.15 raises the residual energy from 0.9 Wh to 215.2 Wh, the estimated maximum range from 1.01 km to 4.44 km, and the potential endurance from 6.46 min to 11.22 min. This result confirms that the baseline-like configuration is sized close to the energy-closure condition of the reference mission, and for this reason even moderate increases in the mass assigned to the battery produce a significant increase in the available margin.

Battery mass fraction [-]	Usable battery energy [Wh]	Residual energy [Wh]	Estimated maximum one-way range [km]	Potential endurance [min]
0.10	428.5	+0.9	1.01	6.46
0.12	514.2	+86.6	2.38	8.37
0.15	642.8	+215.2	4.44	11.22

Table 6.2.2 — Performance summary at baseline gross mass for different battery mass fractions

Overall, the analysis shows that gross mass cannot be evaluated as an isolated parameter, since a heavier vehicle can carry more energy, but it also requires larger rotors and higher propulsive power; as a result, the gain in range and endurance remains limited if the battery fraction is kept constant.

Conversely, a different internal mass allocation toward the energy-storage system can have a more direct effect on mission capability, but it reduces the mass available for payload, structure, and other subsystems.

The results therefore suggest that vehicle sizing must be approached as a compromise between total mass, battery fraction, payload, rotor scale, and energy margins. The baseline configuration represents a coherent solution for the nominal mission, but any increase in range or endurance requires a reassessment of the mass allocation between the battery and the other subsystems. This consideration introduces the following analysis dedicated to payload, where the effect of payload mass on the overall closure of the design is evaluated.

For the following analyses, a reference gross mass of 30 kg is adopted as a representative case for the fixed-mass studies, since this value represents a rounded mass slightly higher than the baseline, capable of providing a wider energy margin while keeping rotor dimensions and propulsive requirements within the design domain considered. In this way, the 30 kg case provides a useful reference for evaluating, in the following sections, the trade-off between payload, battery mass, and mission capability without simultaneously changing the overall scale of the vehicle.

6.3 Effect of Payload Mass

6.3.1 Payload as design variable

After analyzing the effect of the gross mass variation, the focus is shifted to the payload as an internal variable of the mass budget: unlike the previous sweep, in which the total vehicle mass was varied and the system was rescaled accordingly, this section considers a reference platform with fixed total mass. In this way, changes in payload mass are not interpreted as a simple increase in the overall vehicle mass, but rather as a different allocation of the available mass within the vehicle.

Payload is a critical element in the design of a Martian multicopter, because it is directly linked to the scientific capability of the mission, since a heavier payload may allow the integration of more complex sensors, redundant instruments, or more advanced data-acquisition systems. However, for a fixed gross mass, any increase in payload mass necessarily reduces the mass available for other subsystems, particularly the energy-storage system. For this reason, payload competes directly with the battery and can significantly affect range, endurance, and energy margin [4].

The overall mass budget can be expressed as:

$$m_{\text{gross}} = m_{\text{battery}} + m_{\text{payload}} + m_{\text{propulsion}} + m_{\text{structure}} + m_{\text{avionics}} + m_{\text{thermal}} + m_{\text{communications}} + m_{\text{margin}}$$

Assuming that the total vehicle mass is fixed and that the minimum masses required for the main subsystems remain constant, the mass available for the battery can be obtained as:

$$m_{\text{battery}} = m_{\text{gross}} - m_{\text{payload}} - m_{\text{other}}$$

where m_{other} includes propulsion, structure, avionics, communications, thermal control, and margins not directly associated with the payload. This formulation highlights the direct relationship between an increase in payload mass and a reduction in the available energy-storage capacity, so in the present model, the main effect of payload is therefore not a direct increase in required power, since gross mass is kept constant, but a reduction in battery mass and therefore in the energy available to complete the mission profile. As a consequence, a heavier payload may reduce range, endurance, and residual energy margin, even if hover and cruise power remain approximately unchanged. At a preliminary level, it is also assumed that more complex payloads may require additional integration mass, associated with structural supports, harnesses, thermal insulation, mechanical interfaces, and data-management resources. This effect can be represented by introducing an effective payload mass:

$$m_{\text{payload,eff}} = m_{\text{payload}}(1 + k_{\text{support}})$$

where k_{support} represents a penalty associated with payload integration. Similarly, the electrical consumption of the payload during the scientific phase can be included as an additional energy contribution:

$$E_{\text{payload}} = P_{\text{payload}} t_{\text{science}}$$

These elements show that payload must be treated as a design variable to be sized according to the scientific objectives of the mission, since a heavier payload may increase scientific return, but it may also reduce the available energy to the point of penalizing flight performance and operational margin. Based on the conceptual studies available for Martian rotorcraft, payload fractions of the order of 10% of the total mass can be considered representative for a preliminary sizing phase, while values close to

15% describe configurations more strongly oriented toward scientific capability [2], [22]. For the 30 kg reference platform, a payload range between 1 kg and 4 kg is therefore adopted, corresponding to approximately 3.3% – 13.3% of the total mass, while the nominal value is set to 3 kg, equal to 10% of the reference gross mass.

6.3.2 Impact on mass closure

To account for the indirect effect of payload on the supporting subsystems, a linear penalty law with respect to the nominal case is introduced to avoid compensating for an increase in payload mass exclusively through a reduction in battery mass, while neglecting the auxiliary masses required for its integration. In a real vehicle, a heavier or more complex payload does not require only additional useful mass, but also structural supports, thermal interfaces, harnesses, electrical connections, avionics resources, and additional integration margins.

The variation of the mass of the subsystems affected by the payload is therefore described by the following relation:

$$m_i = m_{i,\mathrm{ref}} + k_i(m_{\mathrm{payload}} - m_{\mathrm{payload,ref}})$$

where $m_{i,\mathrm{ref}}$ is the mass of the subsystem in the reference case, $m_{\mathrm{payload,ref}} = 3\,\mathrm{kg}$ is the nominal payload mass, and k_i is a penalty coefficient expressed in kg/kg. This coefficient represents the increase in subsystem mass required to accommodate each additional kilogram of payload relative to the nominal case.

The adopted coefficients are introduced as preliminary parametric factors consistent with the conceptual level of the analysis, and their use is in line with the approach adopted in MSH studies, where sizing is developed through simplified mass, power, and energy models, and subsystem-mass sensitivities are assessed through parametric factors and uncertainty margins [2]. In a similar way, in the present model the coefficients k_i are used to represent the system-level effect of increasing payload mass on the masses required for its integration.

Subsystem	$\boldsymbol{k_i}$ **[kg/kg]**	**Physical meaning**
Structure	0.15	Additional supports, brackets, interfaces and local reinforcement
Thermal control	0.08	Additional insulation, thermal interfaces and local thermal accommodation
Avionics	0.05	Additional processing, interfaces and data handling allowance
Harness	0.04	Additional wiring, connectors and power/data distribution

Table 6.3.1 — Payload-driven subsystem mass penalty coefficients adopted in the preliminary mass-budget closure model

Table 6.3.1 reports the adopted coefficients: the structure receives the highest coefficient, equal to $0.15\,\mathrm{kg/kg}$, since a heavier payload requires mechanical supports, brackets, interfaces, and local reinforcements. Thermal control is penalized by $0.08\,\mathrm{kg/kg}$, to account for insulation, thermal interfaces, and possible dissipation or heating requirements. Avionics and harnesses are assigned lower coefficients, equal to $0.05\,\mathrm{kg/kg}$and $0.04\,\mathrm{kg/kg}$, respectively, associated with processing, data handling, cabling, and power distribution.

Overall, the total penalty is:

$$k_{\mathrm{tot}} = 0.15 + 0.08 + 0.05 + 0.04 = 0.32\,\mathrm{kg/kg}$$

This means that, in the adopted model, each additional kilogram of payload entails approximately 0.32 kg of auxiliary mass distributed among structure, thermal control, avionics, and harnesses.
Figure 6.3.1 shows the effect of the penalty law on the main subsystems influenced by payload mass, and as expected the largest increase affects the structure, while thermal control, avionics, and harnesses show smaller variations, associated respectively with thermal accommodation, data management, cabling, and power distribution.

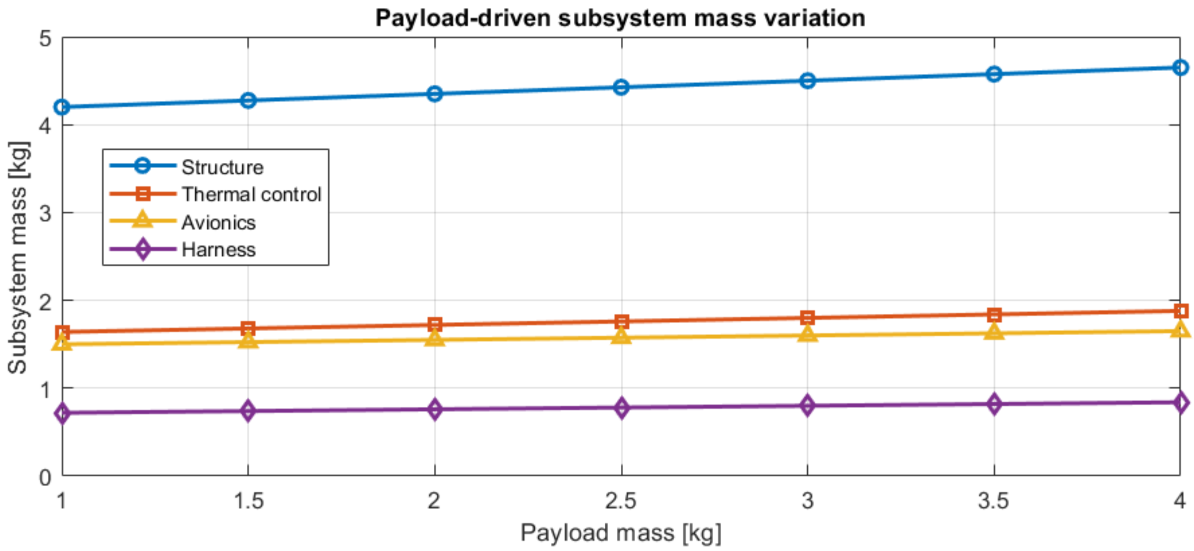

Figure 6.3.1 — Subsystem mass variation induced by payload mass increase

Once this penalty is introduced, it is possible to evaluate how payload variation modifies the residual mass available for the battery: since gross mass is kept constant at 30 kg, increasing the payload directly reduces the mass that can be allocated to the energy-storage system; conversely, reducing the payload allows a larger fraction of the total mass to be assigned to the battery.
Figure 6.3.2 shows this effect in terms of battery mass fraction.

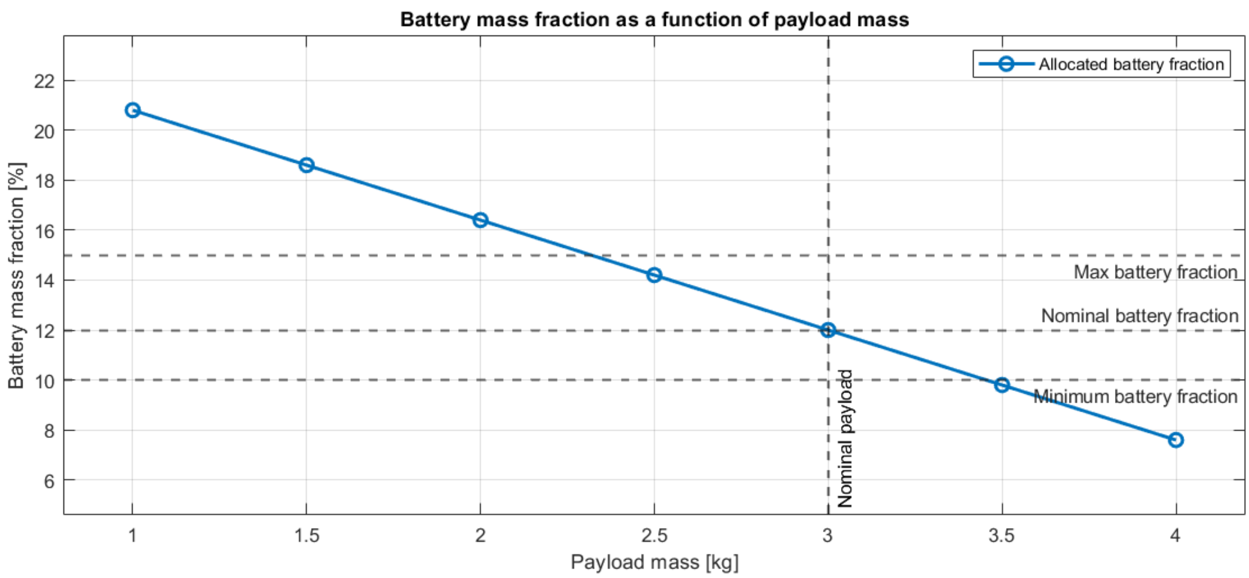

Figure 6.3.2 — Battery mass fraction variation with payload mass at fixed gross mass

The horizontal lines represent values used to interpret the result: 10% indicates a baseline-like configuration, 12% represents the nominal value adopted for the 30 kg platform, and 15% identifies a configuration moderately more oriented toward energy capacity.

The nominal case, $m_{\mathrm{payload}} = 3\,\mathrm{kg}$, lies on the 12% reference, while for lower payload masses, the battery fraction increases significantly, exceeding 15% and indicating configurations that are more favorable from an energy point of view, although less oriented toward scientific capability. For higher payload masses, instead, the battery fraction decreases rapidly, falling below the baseline-like 10% reference in the most demanding case. The result therefore highlights the main trade-off of this section: for a fixed total mass, increasing payload improves the potential scientific return, but reduces the energy margin available for range, endurance, and operational flexibility.

6.3.3 Impact on endurance and range

After assessing the effect of payload mass on mass-budget closure, the analysis is extended to mission performance in terms of range and endurance, in order to quantify the associated penalty and identify a payload-mass interval compatible with an adequate energy margin.
In this analysis, the vehicle gross mass is kept fixed at 30 kg: higher payload masses therefore reduce the mass available for the battery and slightly increase the masses associated with supporting subsystems, such as structure, thermal control, avionics, and harnesses. This approach makes it possible to isolate the effect of payload as an internal mass-budget variable, distinguishing it from the gross-mass sweep discussed in Section 6.2.
For each payload value, the battery mass is computed according to the closure model introduced in the previous section, and the electrical consumption of the payload is included during the hover/science phase. Since no specific instrument architecture is defined at this preliminary stage, the payload power is approximated as proportional to mass:

$$P_{\mathrm{payload}} = 17 m_{\mathrm{payload}}$$

The adopted coefficient is derived from the MSH study [2], where a payload mass of approximately 2.02 kg is associated with an equipment power of about 35 W, corresponding to approximately 17.3 W/kg. The energy required by the payload is then applied only to the scientific phase:

$$E_{\mathrm{payload}} = P_{\mathrm{payload}} t_{\mathrm{hover/science}}$$

The residual energy is calculated by subtracting from the available energy after reserve the energy required by the nominal mission, night survival, and payload operation:

$$E_{\mathrm{residual}} = E_{\mathrm{available}} - E_{\mathrm{mission}} - E_{\mathrm{night}} - E_{\mathrm{payload}}$$

When this margin is positive, it is converted into an extension of the cruise phase:

$$t_{\mathrm{extra}} = \frac{E_{\mathrm{residual}}}{P_{\mathrm{cruise}}}$$
$$R_{\mathrm{extra}} = V_{\mathrm{cruise}} t_{\mathrm{extra}}$$

The total range and endurance are then estimated as:

$$t_{\mathrm{endurance}} = t_{\mathrm{mission,nominal}} + t_{\mathrm{extra}}$$
$$R_{\mathrm{total}} = R_{\mathrm{nominal}} + R_{\mathrm{extra}}$$

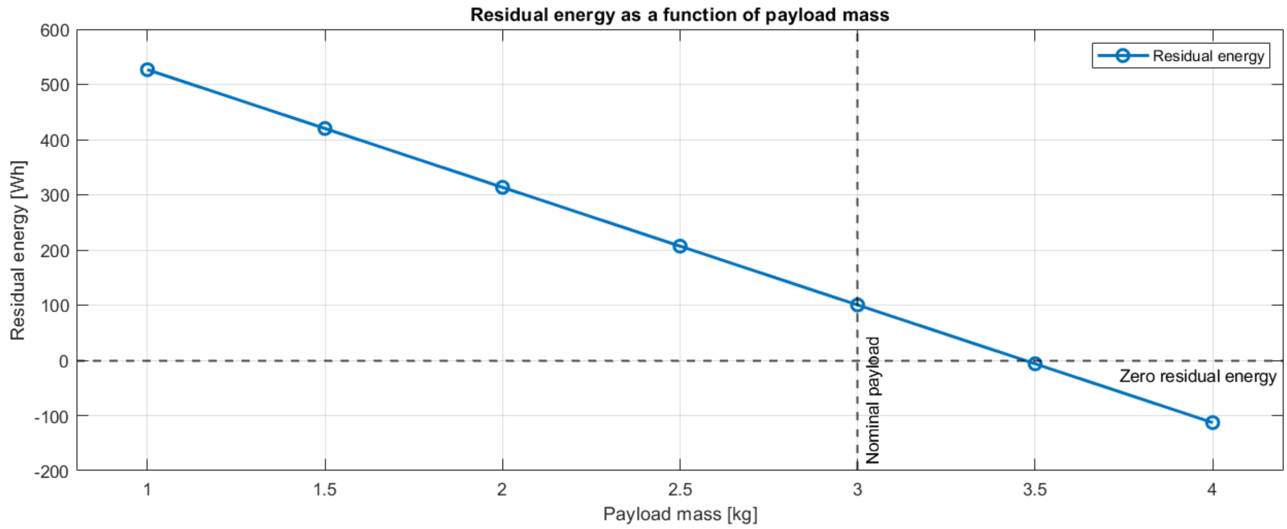

Figure 6.3.3 — Residual energy as a function of payload mass

In the figure 6.3.3 the variation of residual energy with payload mass is shown, and the result highlights an almost monotonic reduction in the available energy margin: as payload increases, more mass is assigned to the useful load and to its supporting subsystems, while the residual mass that can be allocated to the battery decreases. Since gross mass is kept constant, the penalty does not mainly arise from an increase in propulsive power, which remains essentially linked to the fixed total mass, but from the reduction in onboard available energy.

For payload masses below the nominal value of 3 kg, residual energy remains positive and increases significantly, so lighter-payload configurations allow a larger fraction of the total mass to be assigned to the battery, resulting in a wider energy margin. Conversely, for payload masses above the nominal value, the residual margin decreases rapidly, indeed around 3.5 kg the configuration approaches energy closure, while at 4 kg the residual energy becomes negative. In this condition, the vehicle no longer has enough energy to complete the reference mission with the reserve assumed in the model.

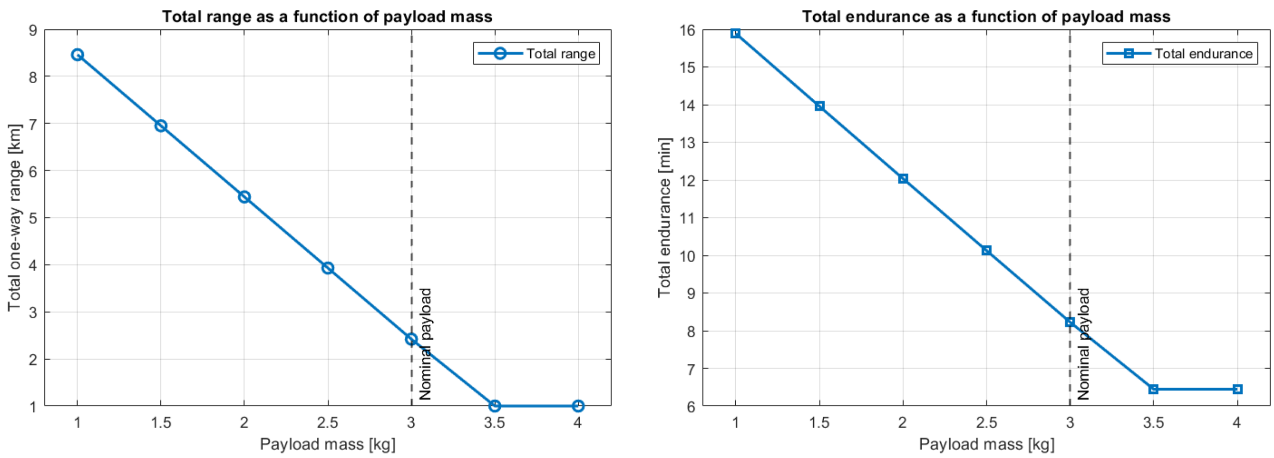

Figure 6.3.4 — Effect of payload mass on total one-way range and endurance at fixed gross mass

The same trend is reflected in Figure 6.3.4, which reports the estimated total one-way range and total endurance as payload mass varies: both quantities decrease as payload mass increases, confirming that payload competes directly with the battery within the mass budget. Lightweight-payload configurations show significantly higher performance since the residual energy can be converted either into an extension of the cruise phase or into additional hover/science time. The nominal 3 kg case instead represents an intermediate compromise between scientific capability and energy margin.

It is important to clarify that the reported range and endurance values do not represent simultaneously achievable performances, but two alternative ways of using the residual energy, since in the first case, the energy margin is converted into an extension of the cruise phase, while in the second it is used to increase the hover time during the scientific phase. When the residual energy is zero or negative, the mission extension is not possible and the configuration must be interpreted as energetically critical or not closed, depending on the sign of the margin.

The nominal case of $m_{\text{payload}} = 3\ \text{kg}$ therefore lies in a region that is still energetically closed, although with a limited margin: lower payload masses allow a significant increase in range and endurance, but reduce the scientific capability carried by the vehicle; higher payload masses, instead, increase the potential scientific return of the mission, but progressively penalize the operational flexibility of the platform, eventually compromising energy closure in the most demanding case analyzed. A summary of the main results is reported in Table 6.3.2.

Payload mass [kg]	**Battery fraction [%]**	**Residual energy [Wh]**	**Estimated maximum one-way range [km]**	**Potential endurance [min]**
2.0	16.4	+313.5	5.40	12.04
2.5	14.2	+206.9	3.93	10.13
3.0	12.0	+100.3	2.42	8.22
3.5	9.8	−6.3	Not closed	Not closed
4.0	7.6	−112.9	Not closed	Not closed

Table 6.3.2 — Performance impact of payload mass variation at fixed gross mass of 30 kg.

Concluding remarks on payload variation

The analysis carried out in this section shows that, for a fixed gross mass, payload mass is a critical variable of the mass budget. Unlike the gross-mass sweep, in this case increasing the payload does not rescale the whole vehicle, but it changes the internal distribution of the available mass, so any increase in payload reduces the residual mass that can be allocated to the battery and therefore the usable onboard energy.

The results show that payload masses below the nominal value of 3 kg provide significantly higher energy margins. In particular, for $m_{\text{payload}} = 2\ \text{kg}$, the battery mass fraction increases to 16.4% and the residual energy reaches approximately 313.5 Wh, allowing an estimated maximum one-way range of 5.40 km and a potential endurance of 12.04 min. However, this higher operational capability is obtained at the expense of the carried useful mass and therefore of the potential scientific return of the mission.

The nominal 3 kg case, associated with a battery mass fraction of 12%, instead represents an intermediate configuration that maintains a positive energy margin of approximately 100.3 Wh and allows an estimated maximum range of 2.42 km and a potential endurance of 8.22 min. This configuration can therefore be interpreted as a compromise between scientific capability and flight performance within the 30 kg reference platform.

For payload masses above the nominal value, the energy penalty becomes more pronounced:

- at 3.5 kg, the battery fraction decreases to 9.8 % and the residual energy becomes slightly negative;
- at 4 kg, the reduction of the battery fraction to 7.6
- % leads to a more evident energy deficit.

These configurations therefore do not close the energy balance with the reserve assumed in the model, although the total vehicle mass remains unchanged.

Overall, payload should not be interpreted only as an additional mass, but as a design variable that directly modifies the balance between scientific return and energy capability. A larger payload can increase the scientific value of the mission, but reduces the operational flexibility of the platform. Conversely, a lighter payload improves range, endurance, and energy margin, but limits the instrument capability. The nominal value of 3 kg therefore appears consistent with the objective of maintaining a configuration that is scientifically meaningful while remaining energetically closed.

This analysis confirms that payload selection must be evaluated together with battery mass and available energy margins. In the following sections, this result provides a useful basis for interpreting the sensitivity analyses, in which vehicle performance is assessed with respect to other design and technological parameters.

6.4 Disk Loading Sensitivity and Feasible Design Window

6.4.1 Analysis setup and literature-based range

After analyzing the effects of gross mass and payload mass, the focus is now shifted to disk loading as a design variable; unlike in section 6.2, where disk loading was mainly used to highlight rotor-diameter scaling as vehicle mass varied, in this section the total mass is kept fixed and disk loading is varied directly, with the aim of assessing the trade-off between geometric compactness, required power, and energy margin [4]. The analysis is performed using the same reference platform adopted in the previous section, defined by:

$m_{gross} = 30 \text{ kg}$	$N_{rotors} = 6$	$m_{payload} = 3 \text{ kg}$	$f_{batt} = 0.12$

In this way, the effect of the disk loading is isolated from the effects associated with the overall scale of the vehicle and with different payload-mass allocations. For each disk-loading value considered, the model recalculates the total rotor disk area, the diameter of each rotor, the power required in the main mission phases, and the corresponding energy balance. The disk-loading range is selected so as to include both values slightly more conservative than the baseline and more compact configurations that are expected to be more demanding from an energy standpoint.
The interval considered in this study is therefore:

$$DL = 6 - 12 \text{ N/m}^2$$

with a nominal value of:

$$DL_{base} = 8 \text{ N/m}^2$$

This choice is consistent with the values reported in the MSH literature [2], where the hexacopter configuration has a mass of approximately 17.66 kg, a total disk area of 7.72 m^2, and a disk loading of 2.29 kg/m^2, corresponding to approximately 8.5 N/m^2 [2]. In addition, for several representative Martian sites, the same hexacopter architecture maintains disk-loading values in the range of approximately 8.2 – 10.1 N/m^2 [2].

The adopted range is therefore not an arbitrary interval, but a parametric window centered around the values already used in the reference studies [2], [30]:

- values lower than 8 N/m^2 make it possible to evaluate configurations that are more favorable in terms of induced power, but require larger rotors
- values higher than 8 N/m^2, instead, represent more compact configurations, potentially easier to integrate from a geometric standpoint, but more severe in terms of propulsive and energy requirements.

The objective of this section is to define a design window in which the configuration remains compatible with the main constraints of the model, so the assessment is multi-parametric: a disk-loading value is not considered favorable only because it reduces rotor diameter, nor only because it reduces required power, but according to the overall compromise between geometric sizing, propulsive severity, and mission-energy closure.
To make the structure of the analysis explicit, the Table 6.4.1 summarizes the main parameters adopted in the disk-loading sweep; the quantities related to the configuration, mission profile, and vehicle mass

are kept constant, so that the effect of disk loading alone can be isolated. The quantities listed as computed outputs are instead recalculated by the model for each disk-loading value considered and represent the metrics used to assess the compromise between geometric compactness, required power, and energy margin. This approach allows disk loading to be treated not as a simple geometric parameter, but as a design variable coupled with the propulsive and energy balance of the vehicle.

Parameter	**Value / Range**	**Type**	**Role in the analysis**
Gross mass	30 kg	Fixed input	Reference mass of the vehicle
Number of rotors	6	Fixed input	Hexacopter baseline configuration
Payload mass	3 kg	Fixed input	Nominal scientific payload
Battery mass fraction	12 %	Fixed input	Nominal energy allocation
Disk loading	6-12 N/m^2	Varied input	Main design variable of the analysis
Baseline disk loading	8 N/m^2	Reference value	Nominal value used for comparison
Total rotor disk area	Computed	Output	Rotor area required by each DL value
Rotor diameter	Computed	Output	Geometric compactness indicator
Hover power	Computed	Output	Propulsive severity indicator
Mission energy	Computed	Output	Energy demand of the flight profile

Table 6.4.1 — Fixed inputs, varied parameter and computed outputs used in the disk loading sensitivity analysis

6.4.2 Effect on rotor diameter, hover power and mission energy

Starting from the setup defined in the previous section, the direct effect of disk loading is evaluated on the main design quantities of the hexacopter configuration. Gross mass, number of rotors, payload mass, and battery mass fraction are kept constant, so that varying disk loading affects only the distribution of the total rotor disk area. Assuming six identical rotors, the diameter of each rotor is obtained as:

$$D_{\text{rotor}} = 2\sqrt{\frac{A_{\text{tot}}}{N_r \pi}}$$

The hover power is estimated using the formulation already introduced in the energy model, based on momentum theory [30] and corrected through the figure of merit and the overall efficiency of the propulsive chain:

$$P_{\text{hover}} = \frac{W^{3/2}}{FM\,\eta_{\text{prop}}\sqrt{2\rho A_{\text{tot}}}}$$

This analysis is useful because it shows how much the reduction in rotor size is paid for in terms of hover power and mission energy requirement, and the Figure 6.4.1 reports the variation of rotor diameter, hover power, and mission energy as disk loading changes.

The gray band highlights the disk-loading range obtained from the MSH hexacopter cases [2] reported in the design tables. In particular, the MSH baseline case has $DL = 2.29\,\text{kg/m}^2$, corresponding to approximately $8.5\ \mathrm{N/m^2}$, while the cases associated with representative Martian sites cover approximately the interval $8.2 - 10.1\ \mathrm{N/m^2}$.

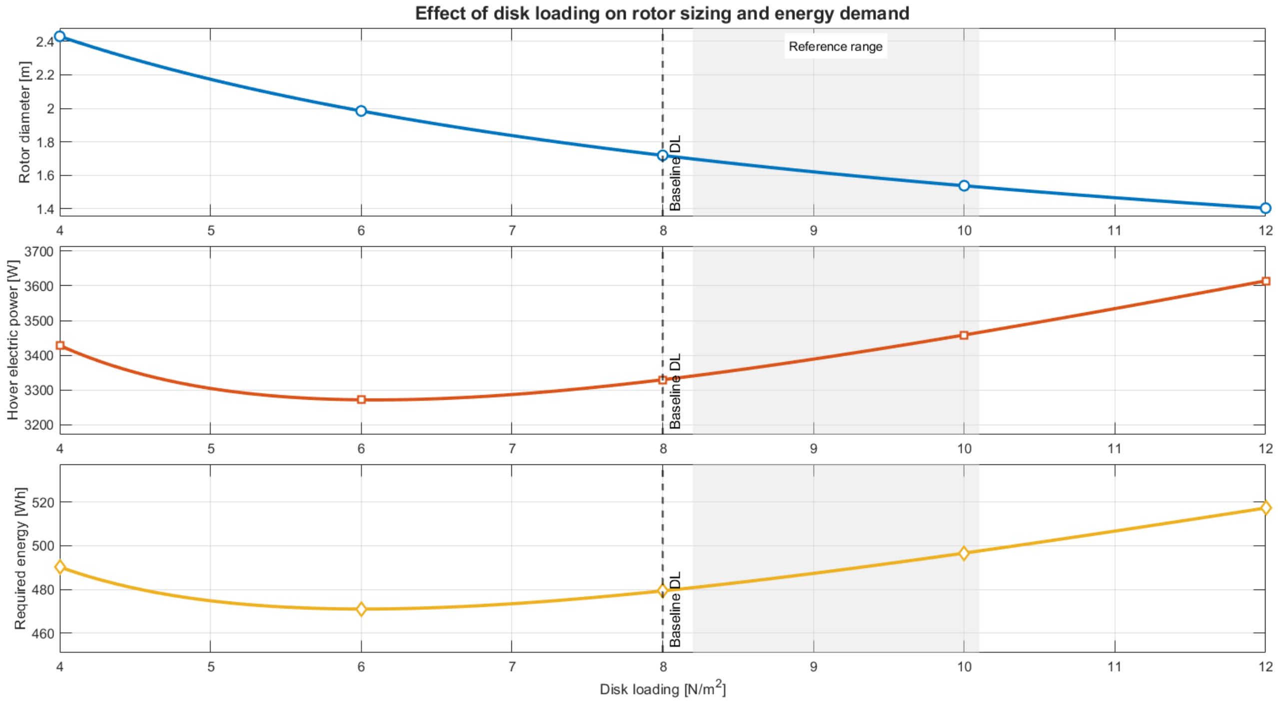

Figure 6.4.1 — Effect of disk loading on rotor diameter, hover power and mission energy for the reference hexacopter configuration.

The first trend shown in the figure is directly linked to the definition of disk loading itself, indeed for a fixed mass increasing DL values reduce the total rotor disk area and therefore the diameter of each rotor. As a result, higher-disk-loading configurations are geometrically more compact, whereas lower values require larger rotor diameters.

The behavior of hover power and mission energy, however, is not purely monotonic:

- at low disk-loading values, the larger rotor area reduces induced power, but it also implies a larger blade area and therefore a higher profile-power contribution
- as disk loading increases, the rotor becomes more compact and the profile power decreases, while induced power rises because of the smaller available disk area.

Disk loading (DL) [N/m^2]	Rotor diameter [m]	Hover power [W]	Required energy [Wh]	Rotor diameter variation vs baseline [%]	Hover power variation [%]	Required energy variation [%]
5.0	2.174	3304.6	474.81	+26.5	−0.8	−0.9
6.0	1.984	3271.7	471.05	+15.5	−1.7	−1.7
8.0	1.719	3329.6	479.34	0.0	0.0	0.0
8.5	1.667	3357.7	483.14	−3.0	+0.8	+0.8
10.0	1.537	3458.5	496.60	−10.6	+3.9	+3.6
12.0	1.403	3614.4	517.21	−18.4	+8.6	+7.9

Table 6.4.2 — Effect of disk loading variation on rotor diameter, hover power and mission energy for the reference hexacopter configuration.

The results reported in Table 6.4.2 show that lower disk-loading values allow a slight reduction in hover power and required energy, but at the cost of a significant increase in rotor diameter.
For $DL = 6\ \mathrm{N/m^2}$, for example, the required energy decreases by approximately 1.7% with respect to the baseline, while rotor diameter increases by 15.5%. This indicates that the energy benefit obtained by reducing disk loading is relatively limited compared with the associated geometric penalty.
Conversely, values of DL higher than the baseline reduce rotor diameter and therefore lead to a more compact configuration, but with a progressive increase in required power and mission energy. For $DL = 10\ \mathrm{N/m^2}$, rotor diameter decreases by 10.6%, while required energy increases by 3.6%. In the more aggressive case, $DL = 12\ \mathrm{N/m^2}$, the diameter reduction reaches 18.4%, but the energy penalty increases to 7.9%.
Overall, the baseline value $DL = 8\ \mathrm{N/m^2}$represents a compromise choice, since it does not coincide with the absolute energy minimum predicted by the model, but it keeps power and energy requirements close to the minimum region while reducing rotor diameter compared with lower-disk-loading configurations. The choice of disk loading must therefore be assessed not only in terms of energy efficiency, but also in relation to geometric compactness, structural integration, and platform packaging constraints.

6.4.3 Feasible disk loading window

Based on the results shown in Figure 6.4.1 and quantified in Table 6.4.2, disk loading can be interpreted as a compromise variable rather than as a parameter to be minimized or maximized in an absolute sense. The analyzed interval does not reveal a sharp feasibility threshold, but it makes it possible to distinguish different design regions.
Values below the baseline, particularly $DL = 5 - 6\ \mathrm{N/m^2}$, offer a slight energy advantage, but require a significant increase in rotor diameter: these configurations are therefore attractive in terms of required power, but less favorable from the standpoint of geometric integration. In other words, the reduction in required energy is obtained by shifting the difficulty toward a larger rotor scale.

The region close to the baseline, approximately between $DL = 8$ and $DL = 8.5\ \mathrm{N/m^2}$, appears more balanced. In this interval, indeed, the reduction in rotor diameter relative to the baseline remains moderate and the energy penalty is still limited. The case $DL = 8.5\ \mathrm{N/m^2}$, for example, reduces rotor diameter by about 3%, with an increase in power and energy below 1%. This region therefore represents a possible conservative design window, in which both compactness and energy requirement remain within moderate variations.

Higher values, such as $DL = 10 - 12\ \mathrm{N/m^2}$, become attractive mainly if reducing rotor size is given priority in the design. However, the geometric benefit is accompanied by an increasing energy penalty. The case $DL = 10\ \mathrm{N/m^2}$ remains relatively moderate, with a rotor-diameter reduction of 10.6% and an energy increase of 3.6%. By contrast, $DL = 12\ \mathrm{N/m^2}$ represents a more aggressive condition, where greater compactness is achieved at the cost of a more evident energy penalty.
For the present study, the most meaningful window can therefore be placed approximately between $DL = 8$ and $DL = 10\ \mathrm{N/m^2}$, a reasonable design region in which rotor diameter can be contained without introducing an excessive increase in required power and mission energy.

6.4.4 Implications for the selected baseline

Given the previous analysis, the baseline value adopted in this work,

$$DL_{\text{base}} = 8 \text{ N/m}^2$$

can be regarded as a cautious and coherent choice for the preliminary phase. It does not correspond to the absolute energy minimum indicated by the model, but it lies in a region where the required power and energy remain close to their minimum values, while avoiding the larger rotor diameter associated with lower disk-loading values.

Compared with $DL = 6 \text{ N/m}^2$, the baseline introduces only a limited energy penalty, but it reduces rotor diameter from approximately 1.98 m to about 1.72 m. This aspect is relevant because, in a Martian multirotor platform, rotor compactness affects not only aerodynamics, but also structure, packaging, stowage, and overall system integration.

At the same time, the analysis shows that slightly higher values, particularly $DL = 8.5 \text{ N/m}^2$, could be considered in later design iterations if more stringent geometric constraints emerged. The associated energy increase is still very limited. More aggressive configurations, such as $DL = 10 - 12 \text{ N/m}^2$, offer greater compactness, but require a more careful assessment of the available energy margin.

Overall, $DL = 8 \text{ N/m}^2$ represents a robust reference value for the following analyses. It favors an energetically cautious configuration without excessively penalizing system compactness. Nevertheless, disk loading remains an open design lever, to be reassessed in later phases if integration, packaging, or stowage constraints prove more restrictive than the available energy margin.

6.5 Effect of the Battery Technology

6.5.1 Sensitivity to battery specific energy

The battery specific energy is one of the most influential parameters in the mass–energy model, since it directly determines the usable energy available for cruise extension, hovering capability, and operational margins. In this section the battery technology is therefore represented through a set of specific-energy scenarios, ranging from conservative pack-level values consistent with Martian rotorcraft studies to more advanced scenarios associated with lithium-metal or solid-state batteries, which are currently being investigated for electric aviation applications. The objective is not to assume that very high-specific-energy cells are immediately available for a Mars-qualified system, but to quantify how improvements in effective pack-level specific energy could expand the feasible mission envelope.

An important distinction concerns the level at which specific energy is defined, since in the model developed in this thesis the battery mass is treated as a system-level variable; therefore, specific energy should be interpreted as an effective pack-level value, including, at least in aggregate form, inactive elements such as structure, interconnections, battery management system, operational margins, and possible penalties associated with thermal control [4]. The MSH study [2] adopts this distinction explicitly: the battery model is based on a JPL technology projection and reports approximately 278 Wh/kg at cell level, 230 Wh/kg at pack level, including the battery management system, and 218.5 Wh/kg at end of life. In addition, the usable energy is limited to 70% of the nominal capacity, considering a depth-of-discharge window between 10% and 80%.
These values are particularly relevant for the present study because they are derived from a Martian rotorcraft concept of larger scale than Ingenuity; at the same time, the experience of Ingenuity [16] shows that, in the Martian environment, the battery cannot be assessed only in terms of specific energy, since power capability, operating temperature, and night survival must also be considered. In the case of Ingenuity, the available data [16] indicate a six-cell battery with an estimated beginning-of-life energy of 44.4 Wh at 25 °C and 38.8 Wh at 0 °C, a continuous power capability of 360 W and a peak power capability of 510 W, together with specific thermal operating windows for high-power discharge and survival.

To analyze the possible impact of technological evolution, more advanced scenarios are also considered in addition to the conservative values consistent with MSH. The DOE Battery500 program [15], [17] targets the development of high-specific-energy lithium-metal cells, with an objective of up to approximately 500 Wh/kg at cell level, focusing in particular on chemistries based on lithium-metal anodes and high-capacity cathodes. NASA SABERS [13] investigates solid-state battery architectures for electric aviation applications, with the aim of overcoming some of the limitations of conventional lithium-ion batteries in terms of energy, safety, packaging, and scalability; the technology is described as being oriented toward the performance and safety requirements of electric aviation. More ambitious programs, such as ARPA-E PROPEL-1K [14], target specific energies of the order of thousands of Wh/kg and can be mentioned as a long-term perspective, but they are not adopted as a main reference here because they represent research targets rather than technologies already available or qualified for Martian missions.
Based on these references, the scenarios reported in Table 6.5.1 are defined in this study.

Scenario	Battery specific energy [Wh/kg]	Interpretation	Main reference
Conservative pack level assumption	220	Conservative value close to the pack-level end-of-life value reported for the MSH	MSH NASA [2]
Reference pack-level assumption	230	Nominal pack-level value adopted as the primary reference for the model.	MSH NASA [2]
Moderately improved Li-ion pack	250	Slightly optimistic scenario compared with the pack-level reference, useful for assessing a moderate improvement in battery technology.	Model sensitivity assumption
Advanced Li-metal pack-equivalent	350	Advanced but still intermediate scenario, representative of potential near-future developments based on lithium-metal technologies.	Battery500-related Li-metal development [15] [17]
Future aviation-oriented battery	500	Advanced scenario associated with high-specific-energy cells/prototypes and solid-state technologies aimed at electric aviation applications.	Battery500 / NASA SABERS [13] [15] [17]
Long-term exploratory target	1000	Highly ambitious long-term target, not considered flight-ready and not used as the primary scenario in the model.	ARPA-E PROPEL-1K [14]

Table 6.5.1 — Battery specific energy scenarios adopted for the parametric analysis

In the following analysis, the main specific-energy values considered are 220, 230, 250, 350, and 500 Wh/kg. The value of 1000 Wh/kg is retained only as a long-term exploratory reference and is not interpreted as a technology available or qualifiable for a Martian mission in the short-to-medium term [14]. This approach makes it possible to evaluate two distinct effects:

- the first concerns the increase in performance for a fixed battery mass: for the same mass allocated to the energy-storage system, a higher specific energy increases the available energy and can therefore extend range, endurance, or residual margin
- the second concerns the battery-mass trade-off: for the same mission and required energy margin, a more advanced technology could reduce the required battery mass, freeing mass for payload, structure, margins, or auxiliary systems.

In this sense, improvement in battery technology can be interpreted both as a performance multiplier and as a mechanism for system mass reduction.

6.5.2 Impact on range and endurance

Starting from the specific-energy scenarios defined in the previous section, the impact of battery technology on the operational performance of the vehicle is now evaluated. In this analysis, battery mass is kept constant and equal to the mass fraction adopted for the reference platform:

$$m_{\mathrm{batt}} = f_{\mathrm{batt}} m_{\mathrm{gross}}$$

with $f_{\mathrm{batt}} = 0.12$ and $m_{\mathrm{gross}} = 30\ \mathrm{kg}$. The resulting battery mass is therefore:

$$m_{\mathrm{batt}} = 3.6\ \mathrm{kg}$$

The variation in specific energy therefore acts only on the nominal energy that can be stored for a fixed mass allocated to the energy-storage system:

$$E_{\mathrm{batt}} = m_{\mathrm{batt}} e_{\mathrm{spec}}$$

The effectively usable energy is then calculated by considering an available fraction equal to 70 % of the nominal battery-pack energy:

$$E_{\mathrm{available}} = E_{\mathrm{batt}} f_{\mathrm{usable}}$$

with $f_{\mathrm{usable}} = 0.70$, consistently with the assumptions adopted in the previous sections. The residual energy margin is finally determined by subtracting from the available energy the total energy requirement of the nominal mission, including flight energy, night survival, and operational reserve:

$$E_{\mathrm{residual}} = E_{\mathrm{available}} - E_{\mathrm{required}}$$

where:

$$E_{\mathrm{required}} = (E_{\mathrm{flight}} + E_{\mathrm{night}})(1 + f_{\mathrm{reserve}})$$

For the 30 kg reference platform, this value is approximately 479.34 Wh. In this way, the analysis does not define a completely new mission resized for each battery technology, but rather quantifies how much additional energy would remain available after completing the already defined nominal profile. The residual energy can be interpreted in different ways: it may be retained as an operational margin, or it may be converted, alternatively, into cruise extension or additional scientific hovering time. It is important to emphasize that the range extension and the increase in hovering time are not intended as simultaneously available performance figures, but as two possible uses of the same energy margin.

The potential cruise extension is calculated as:

$$\Delta t_{\mathrm{cruise}} = \frac{E_{\mathrm{residual}}}{P_{\mathrm{cruise}}}$$

$$\Delta R = \Delta t_{\mathrm{cruise}} V_{\mathrm{cruise}}$$

whereas the equivalent increase in hovering time is estimated as:

$$\Delta t_{\mathrm{hover}} = \frac{E_{\mathrm{residual}}}{P_{\mathrm{hover}} + P_{\mathrm{payload}}}$$

where P_{cruise}, P_{hover}, and P_{payload} are kept constant with respect to the reference configuration. This choice makes it possible to isolate the effect of battery specific energy alone, without introducing simultaneous variations in total mass, rotor geometry, or the propulsion model.
Figure 6.5.1 shows the variation of residual energy and the corresponding operational extensions as battery specific energy changes. Since battery mass is kept constant, the storable energy increases linearly with e_{spec}; as a result, both residual energy and the additional performance derived from it also show an almost linear trend. A summary of the results is reported in Table 6.5.2.
In the reference case, corresponding to $e_{\mathrm{spec}} = 230\ \mathrm{Wh/kg}$, the usable energy is approximately 579.6 Wh, while the residual margin after closure of the nominal mission is about 100.3 Wh. If this margin were used entirely to extend cruise, the vehicle could achieve an additional range of approximately 1.42 km, increasing the estimated maximum one-way range from 1 km to about 2.42 km. If the same margin were

instead allocated to scientific hovering, it would correspond to about 1.78 additional minutes, leading to an overall potential endurance of approximately 8.22 min.

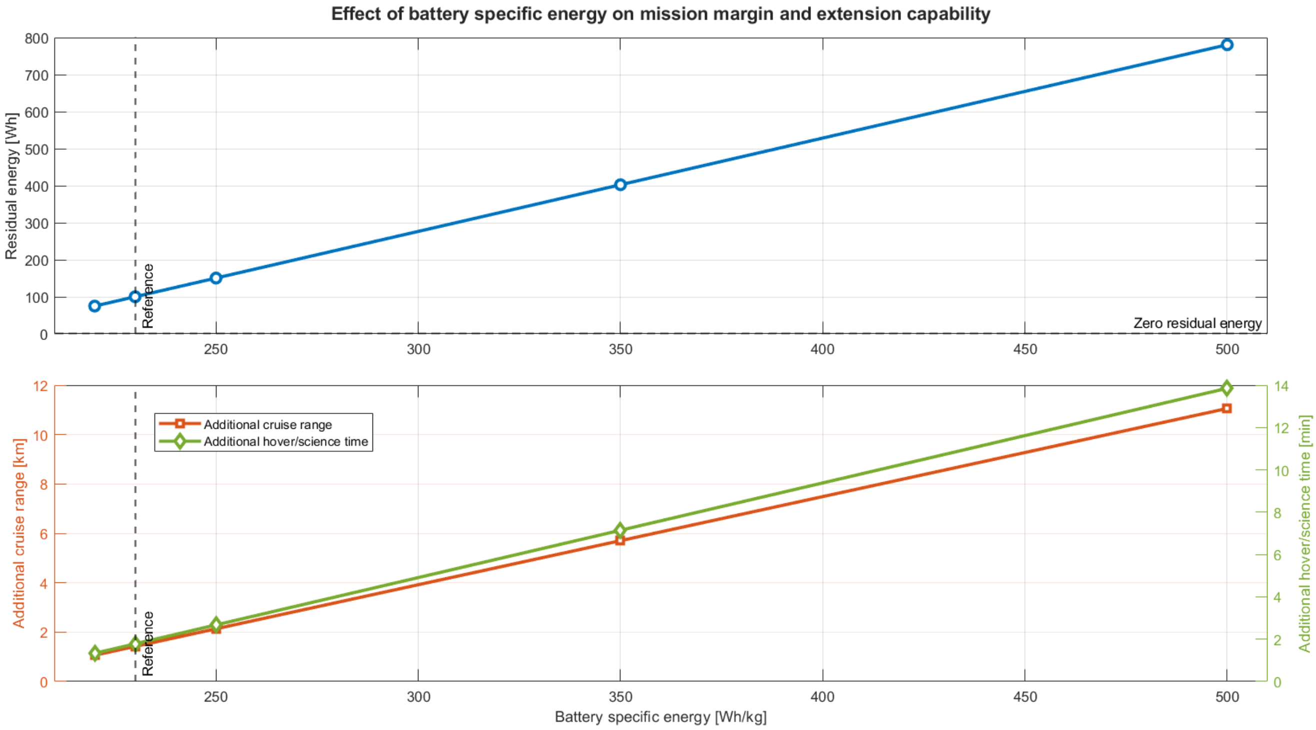

Figure 6.5.1 — Effect of battery specific energy on residual energy, additional cruise range and additional hover time at fixed battery mass.

Battery specific energy [Wh/kg]	Usable battery energy [Wh]	Residual energy [Wh]	Additional cruise range [km]	Additional hover time [min]	Estimated maximum one-way range [km]	Potential endurance [min]
220	554.4	75.1	1.03	1.33	2.03	7.78
230	579.6	100.3	1.42	1.78	2.42	8.22
250	630.0	150.7	2.13	2.67	3.13	9.12
350	882.0	402.7	5.70	7.15	6.70	13.59
500	1260.0	780.7	11.06	13.85	12.06	20.30

Table 6.5.2 — Effect of battery specific energy on residual energy and potential operational extension at fixed battery mass.

Compared with the conservative 220 Wh/kg scenario, which provides a residual margin of approximately 75.1 Wh, moving toward more advanced values significantly increases the energy available after the nominal mission has been completed. For 250 Wh/kg, the residual margin increases to about 150.7 Wh; for 350 Wh/kg, it reaches approximately 402.7 Wh; and in the more ambitious 500 Wh/kg scenario, it rises to about 780.7 Wh. This last case, however, should be interpreted as a highly optimistic technology scenario rather than as an immediately available solution for a qualified Martian platform.

The main result of this section is therefore the quantification of the operational margin associated with different battery-technology scenarios: batteries with higher specific energy do not directly modify the power required by the vehicle, but they increase the energy available after completion of the nominal mission, and this energy can be used to extend exploration range, increase observation time over the target, or preserve larger safety margins against atmospheric, thermal, or operational uncertainties.
In this sense, improvement in battery technology acts as a multiplier of the mission envelope, but it does not remove the need for a proper balance between battery mass, energy margin, and required performance. The following section therefore examines the complementary problem: for the same nominal mission and required energy demand, it evaluates how much the battery mass could be reduced as the available specific energy increases.

6.5.3 Battery mass trade-off

After analyzing the effect of specific energy on possible mission extension for a fixed battery mass, the complementary problem is now considered: determining how much battery mass would be required to close the nominal mission as the storage technology varies. In this case, therefore, battery mass is no longer assumed to be constant; instead, the energy requirement imposed by the mission profile is kept fixed. The required battery mass is calculated by keeping fixed the energy demand of the nominal profile, already defined in the previous section, which includes flight energy, night survival, and operational reserve:

$$E_{\text{required}} = (E_{\text{flight}} + E_{\text{night}})(1 + f_{\text{reserve}})$$

with $E_{\text{flight}} = 352.85\ \text{Wh}$, $E_{\text{night}} = 46.61\ \text{Wh}$, and $f_{\text{reserve}} = 0.20$, giving:

$$E_{\text{required}} \approx 479.34\ \text{Wh}$$

Since only a fraction of the energy nominally stored in the battery pack is considered usable, the minimum battery mass required for each specific-energy value is estimated as:

$$m_{\text{batt,req}} = \frac{E_{\text{required}}}{e_{\text{spec}} f_{\text{usable}}}$$

where e_{spec} is the battery pack specific energy and $f_{\text{usable}} = 0.70$ represents the fraction of nominal energy that is effectively available. The corresponding battery mass fraction is therefore:

$$f_{\text{batt,req}} = \frac{m_{\text{batt,req}}}{m_{\text{gross}}}$$

In the comparison between scenarios, the case $e_{\text{spec}} = 230\ \text{Wh/kg}$ is taken as the nominal pack-level reference. The mass saving associated with more advanced technologies is therefore calculated with respect to the battery mass required in the reference case:

$$\Delta m_{\text{batt}} = m_{\text{batt,req}}(230) - m_{\text{batt,req}}(e_{\text{spec}})$$

This formulation makes it possible to isolate the effect of specific energy on the minimum mass of the storage system, without modifying the mission profile, the overall platform mass, or the propulsion model. Figure 6.5.2 compares the battery mass required in the different specific-energy scenarios with the nominal battery mass allocated in the reference platform, equal to 3.6 kg. In this case, the comparison is not made with respect to the minimum mass needed to close the mission, but with respect to the battery pack mass adopted in the model at 230 Wh/kg, corresponding to 12% of the total mass of the 30 kg platform. By construction, for $e_{\text{spec}} = 230\,\text{Wh/kg}$, the equivalent battery mass coincides with the nominal value of 3.6 kg. The conservative 220 Wh/kg case would instead require a slightly higher mass, approximately 3.76 kg, to provide the same usable energy, while scenarios with higher specific energy make it possible to maintain the same energy capacity while progressively reducing the mass of the storage system: approximately 3.31 kg for 250 Wh/kg, 2.37 kg for 350 Wh/kg, and 1.66 kg in the more optimistic 500 Wh/kg case.

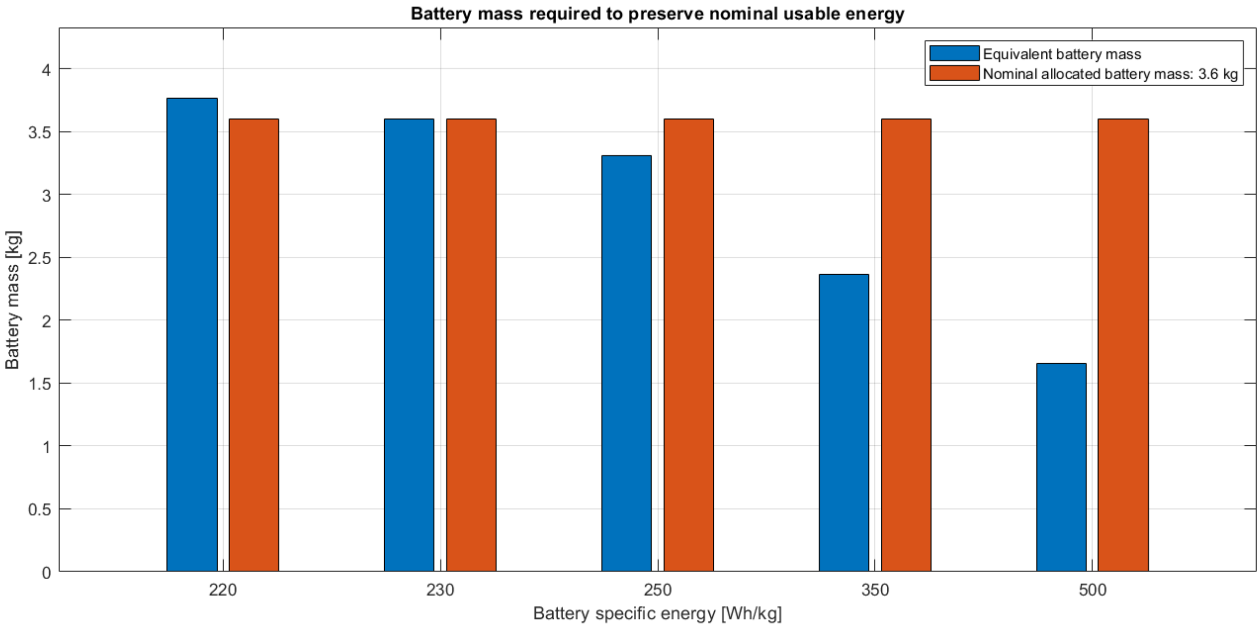

Figure 6.5.2 — Battery mass required to preserve the nominal usable energy capability as a function of battery specific energy

This representation makes it possible to interpret the improvement in specific energy not as a direct extension of performance, but as a potential reduction in battery mass for the same available energy. A more advanced technology could therefore preserve the same energy margin as the nominal configuration while reducing the mass allocated to the storage system, or alternatively freeing mass for other subsystems, payload, or design margins. Figure 6.5.3 provides a complementary interpretation of the trade-off. In this case, the analysis does not consider the minimum battery mass required to close the mission, but the battery mass required to maintain the same usable energy as the nominal 3.6 kg pack at $230\,\text{Wh/kg}$. This usable energy is equal to:

$$E_{\text{available,ref}} = 3.6 \cdot 230 \cdot 0.70 = 579.6\,\text{Wh}$$

The equivalent battery mass is therefore calculated as:

$$m_{\text{batt,eq}} = \frac{E_{\text{available,ref}}}{e_{\text{spec}} f_{\text{usable}}}$$

This second representation makes it possible to evaluate how much mass could be saved while preserving the usable energy capacity of the nominal case. By construction, the reference value of $230\,\text{Wh/kg}$corresponds to $3.6\,\text{kg}$, or 12% of the total mass. At $350\,\text{Wh/kg}$, the same usable energy could be obtained with approximately $2.37\,\text{kg}$ of battery, while at $500\,\text{Wh/kg}$ the equivalent mass would decrease to approximately $1.66\,\text{kg}$. A quantitative summary of the results for the equivalent battery mass, calculated at constant usable energy with respect to the nominal 3.6 kg pack, is reported in Table 6.5.3.

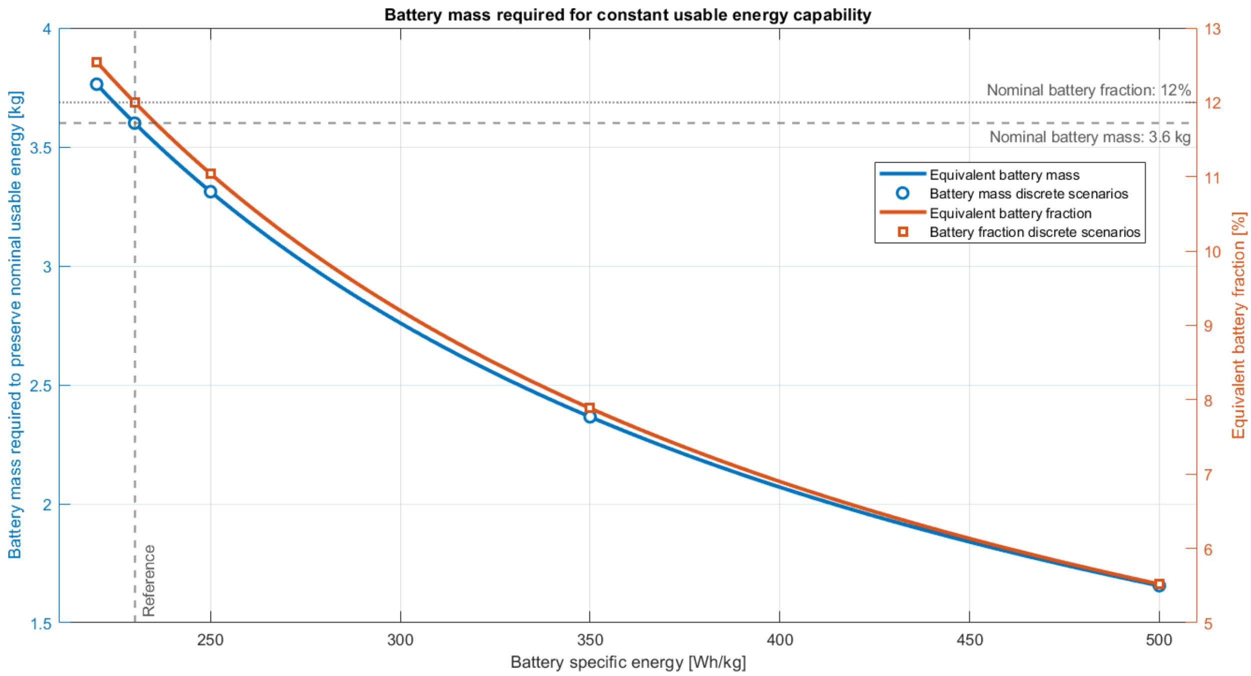

Figure 6.5.3 — Battery mass and battery mass fraction required to preserve the nominal usable energy capability as a function of battery specific energy.

Battery specific energy [Wh/kg]	Battery mass for same usable energy [kg]	Equivalent battery fraction [%]	Battery mass saving vs nominal 3.6 kg [kg]
220	3.764	12.55	-0.164
230	3.600	12.00	0.000
250	3.312	11.04	0.288
350	2.366	7.89	1.234
500	1.656	5.52	1.944

Table 6.5.3 — Battery mass reduction associated with increasing battery specific energy

In the nominal case at 230 Wh/kg, the battery mass corresponds to the value adopted for the reference platform, namely 3.6 kg, equal to 12% of the total mass. The conservative 220 Wh/kg case, representative of a less performing pack-level condition, would instead require approximately 3.76 kg to provide the same usable energy, with an increase of about 0.16 kg relative to the reference.

The more advanced technology scenarios show a progressive reduction in the mass required to maintain the same nominal usable energy capacity: for 250 Wh/kg, the equivalent battery mass decreases to approximately 3.31 kg, corresponding to a mass saving of about 0.29 kg; for 350 Wh/kg, the required mass decreases to approximately 2.37 kg, freeing about 1.23 kg. In the more optimistic 500 Wh/kg case, the same usable energy could be provided by approximately 1.66 kg of battery, corresponding to a saving of about 1.94 kg relative to the nominal battery.

These results do not indicate the minimum mass required only to close the mission, but the mass required to preserve the same usable energy capacity as the nominal configuration, so the benefit associated with higher specific energy can be interpreted as a potential reduction in storage-system mass for the same energy margin, or as mass freed for payload, subsystems, structural margins, or auxiliary functions. In this regard, the 3.6 kg of battery remains the design reference for the platform, while the higher-specific-energy scenarios quantify how much this allocation could be reduced while keeping the available usable energy unchanged.

Concluding remarks

The analysis carried out in this section shows that battery technology should be interpreted as a design variable capable of modifying the overall balance of the platform: for a fixed mass allocated to the storage system, an increase in specific energy expands the operational margin available after closure of the nominal mission; for a fixed energy requirement, instead, the same technological improvement can be converted into a reduction of the required battery mass.

In the context of a Martian VTOL platform, the most appropriate choice does not necessarily coincide with maximizing range or minimizing battery mass, indeed a more realistic approach is to assess how the additional energy margin can be distributed among performance, operational robustness, and system margins. In the Martian environment, a significant fraction of the available energy may be absorbed by functions that are not directly propulsive, such as thermal management, avionics, communications, battery heating, and ground survival. Consequently, the availability of higher-performance batteries does not remove the need for careful management of auxiliary loads.

A further aspect concerns technology maturity: the higher specific-energy values considered in the analysis make it possible to explore the potential benefit of future technologies, but they should not be interpreted as assumptions immediately available for a qualified Martian mission. The distinction between cell-level values, pack-level values, and energy effectively usable in the operating environment therefore remains central. A high nominal specific energy may be partly offset by penalties associated with packaging, thermal management, safety, degradation, and qualification.

For these reasons, the $230\ \mathrm{Wh/kg}$reference case adopted in this study remains a cautious and coherent choice for the preliminary level of the analysis, while more advanced scenarios do not replace the baseline, but they allow the sensitivity of the system to storage-technology evolution to be quantified. The battery therefore emerges as one of the main elements in the trade-off between performance, mass, and operational margin, but its effective benefit depends on the ability to integrate the technology within the overall energy balance of the vehicle. This consideration naturally introduces the need to analyze, in the following sections, the contribution of auxiliary loads and ground-survival requirements.

6.6 Effect of night-survival thermal loads

6.6.1 Night-survival energy model

In the energy model adopted in the previous chapters, the mission energy requirement is not limited to the propulsive flight phases, but it also includes a contribution associated with vehicle night survival before the next recharge cycle, consistently with the MSH framework [2]. In this work, the night-survival contribution is modeled through the preliminary relation adopted in the MSH study, where sleep energy scales with the cubic root of the vehicle gross mass:

$$E_{\text{night}} = 15\, m_{\text{gross}}^{1/3}\ [\text{Wh/sol}]$$

Equivalently, the average power associated with night survival is:

$$P_{\text{night}} = 0.518\, m_{\text{gross}}^{1/3}\ [\text{W}]$$

where m_{gross} is expressed in kg. In the MSH reference study [2], this relation is calibrated on the Mars Science Helicopter and it assumes a sol duration of 1477 min, including a battery efficiency of 85%. The contribution is also treated as equipment power, and therefore as an auxiliary load supplied directly by the battery [2]. The total energy required by the vehicle is therefore calculated as:

$$E_{\text{req}} = (E_{\text{flight}} + E_{\text{night}})(1 + f_{\text{reserve}})$$

where E_{flight} is the energy associated with the flight phases, E_{night} is the night-survival contribution, and f_{reserve} is the energy reserve fraction. These formulations, summarized in Table 6.6.1, allow an energy penalty consistent with vehicle permanence on the Martian surface to be included in the sizing process.

Quantity	Expression / value	Unit
Night-survival energy	$E_{night} = 15\, m_{gross}^{1/3} [Wh/sol]$	Wh/sol
Night-survival power	$P_{night} = 0.518\, m_{gross}^{1/3} [W]$	W
Required energy	$E_{req} = \left(E_{flight}+E_{night}\right)(1+f_{res})$	Wh
$f_{reserve}$	0.20	

Table 6.6.1 — Night-survival energy model parameters and assumptions

The need to account for night survival is also confirmed by the experience of Ingenuity, for which a significant portion of the available energy capacity was allocated to thermal maintenance during the Martian night [5], [16]. Similarly, the battery systems developed for Perseverance and Ingenuity highlight the importance of thermal control, temperature monitoring, and survival heaters within the battery assembly architecture [16]. In this section, the night load is therefore retained as an aggregate auxiliary contribution, not to estimate the detailed thermal losses of the vehicle, but to assess how the energy allocated to survival affects the margin available for range, hovering, and operational capability.

This approach also makes it possible to introduce a relevant architectural alternative: instead of designing the multicopter as a fully autonomous system also during the night, it is possible to assume that, at the end of the sortie, the vehicle lands on a support platform or inside a dedicated shelter. In such a configuration, part of the thermal protection, recharge, and environmental-isolation functions would be transferred from the aerial vehicle to a surface infrastructure; the comparison between these two approaches, self-survival and sheltered survival, is developed in the following section.

6.6.2 Self-survival and sheltered-survival architectures

The night-survival model introduced in the previous section can be interpreted according to two different architectural approaches:

- the self-survival architecture considers the multicopter as an autonomous system, capable of surviving the Martian night without external assistance;
- the sheltered-survival architecture transfers part of the thermal-protection, recharge and energy-management functions to a surface support platform or to a dedicated shelter.

Self-survival architecture

In the self-survival architecture, the multicopter must carry onboard the energy, insulation and thermal-control systems required to survive the Martian night without external assistance.

This approach is consistent with the reference profile adopted for the MSH [2], in which the vehicle does not necessarily return to a lander after completing the mission, but must remain on the surface during the night and subsequently recharge through solar cells.

The main advantage of this architecture is the operational independence: the vehicle may land close to the scientific target, remain on the surface and resume operations after recharge, without being constrained by the presence of a fixed support base.

This approach is therefore particularly suitable for autonomous, distributed and itinerant missions.

However, this autonomy introduces design penalties, since the battery sizing must include the energy required for night survival, and besides the multicopter must incorporate thermal protection, insulation and thermal-management strategies compatible with Martian nighttime temperatures.

Sheltered-survival architecture

In the sheltered-survival architecture, part of these functions is transferred to a surface infrastructure, so the multicopter completes the sortie, returns to a support platform or lands inside a dedicated shelter, transferring to this infrastructure part of the thermal-protection and recharge functions.

In this case, the vehicle does not necessarily need to carry onboard all the energy required for night survival, since part of the thermal load is transferred from the flying system to the surface platform.

This approach finds a conceptual reference in *The Future of Rotorcraft and Other Aerial Vehicles for Mars Exploration* [11], in which the authors identify two relevant limitations for Martian robotic aerial systems:

- a significant fraction of the available energy may be absorbed by survival heating during cold Martian nights;
- solar-recharge systems are vulnerable to dust deposition on the panels, with a consequent reduction in the available power.

For these reasons, the authors propose the use of "automated base stations" [11], described as hangars for small Martian rotorcraft, designed to host the vehicle during non-operational phases, protect it from the external environment and support recharge operations. Figures 6.6.1 and 6.6.2 show, respectively, a possible hangar with a retractable roof and a functional scheme of the subsystems envisioned for an automated base supporting Martian VTOL vehicles.

In this work [11] the shelter is assumed to be an infrastructure capable, at least ideally, of absorbing the nighttime thermal load that, in the self-survival configuration, would instead be allocated to the multicopter battery

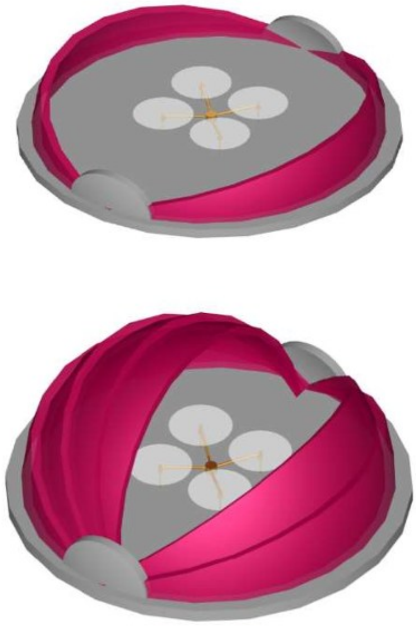

Figure 6.6.1 — Automated base station concept with retractable clamshell roof for Mars rotorcraft. Adapted from: [11].

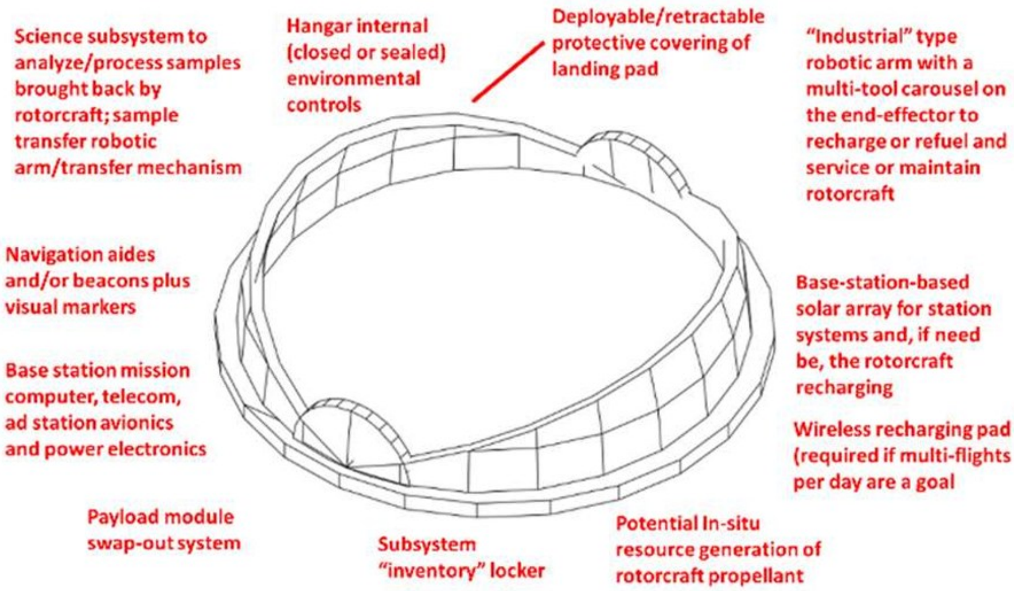

Figure 6.6.2 — Functional layout of an automated base station supporting Mars vertical-lift aerial vehicles. Adapted from: [11]

Consequently, the vehicle may be sized primarily with respect to flight energy and operational reserve, while night survival becomes a function assigned to the surface support platform: this doesn't erase the energy problem at mission level, but it changes its allocation, since part of the complexity is transferred from the multicopter to the surface infrastructure.
The difference between the two architectures can be expressed as follows.

- in the self-survival case, the energy required onboard the multicopter includes both flight and night-survival contributions:

$$E_{\mathrm{req,self}} = \left(E_{\mathrm{flight}} + E_{\mathrm{night}}\right)(1 + f_{\mathrm{res}})$$

- in the ideal sheltered-survival case, instead, the night-survival load is no longer entirely allocated to the multicopter battery, since the shelter provides thermal protection and recharge support:

$$E_{\mathrm{req,sheltered}} = E_{\mathrm{flight}}(1 + f_{\mathrm{res}})$$

In a realistic configuration, small residual onboard energy contributions may still be required, for example for safe-mode operation, docking, minimum communications or the maintenance of critical subsystems.

The sheltered-survival architecture therefore reduces the energy that the vehicle must reserve for thermal maintenance, and this may result in a lower onboard battery mass or, for the same battery mass, in a larger energy margin that may be used to extend the range, increase the scientific hovering time or improve the operational margin.
In addition, the support platform may reduce the vehicle's exposure to dust, thermal cycles and severe environmental conditions, while facilitating recharge through dedicated solar surfaces [9].
In the following analysis, the two architectures are treated as limiting cases used to quantify the effect of night-survival allocation on the available energy margin: the self-survival configuration represents the most autonomous but energetically demanding case, whereas the sheltered-survival configuration represents a more infrastructure-dependent solution that may be advantageous for local and repeated missions.

6.6.3 Energy margin impact of night-survival allocation

After defining the two architectures, the effect of the different allocation of the night-survival contribution can be evaluated quantitatively. The objective is to estimate how the multicopter energy balance changes when the term $E_{\mathrm{night}}$is retained onboard, as in the self-survival case, or ideally transferred to the surface infrastructure, as in the sheltered-survival case.
The analysis is performed over a reference gross-mass range between 10 and 60 kg, while maintaining the aerodynamic and propulsive assumptions adopted in the previous model. The sheltered-survival configuration is represented by the ideal limiting case in which the onboard night-survival contribution is set equal to zero: this is a simplifying assumption, but it allows the maximum theoretical benefit associated with transferring the night-survival function from the aerial vehicle to the surface platform to be quantified.
Figure 6.6.3 compares the onboard energy required by the two architectures: the sheltered-survival curve remains below the corresponding self-survival curve over the entire investigated mass range because the term E_{night} is no longer included in the multicopter energy demand. The distance between the two curves therefore represents the reduction in onboard energy requirement obtained when the night-survival function is transferred to the shelter.
To highlight this difference more clearly, Table 6.6.2 reports the night-survival contribution and the corresponding reduction in onboard energy requirement. The latter is defined as

$$\Delta E_{\mathrm{onboard}} = E_{\mathrm{req,self}} - E_{\mathrm{req,sheltered}}$$

Since the difference between the two configurations is associated with the removal of the night-survival load from the aircraft battery, the adopted model gives

$$\Delta E_{\text{onboard}} = E_{\text{night}}(1+f_{\text{reserve}})$$

Table 6.6.2 therefore reports both the night-survival energy and the effective reduction in required onboard energy, including the adopted operational reserve.

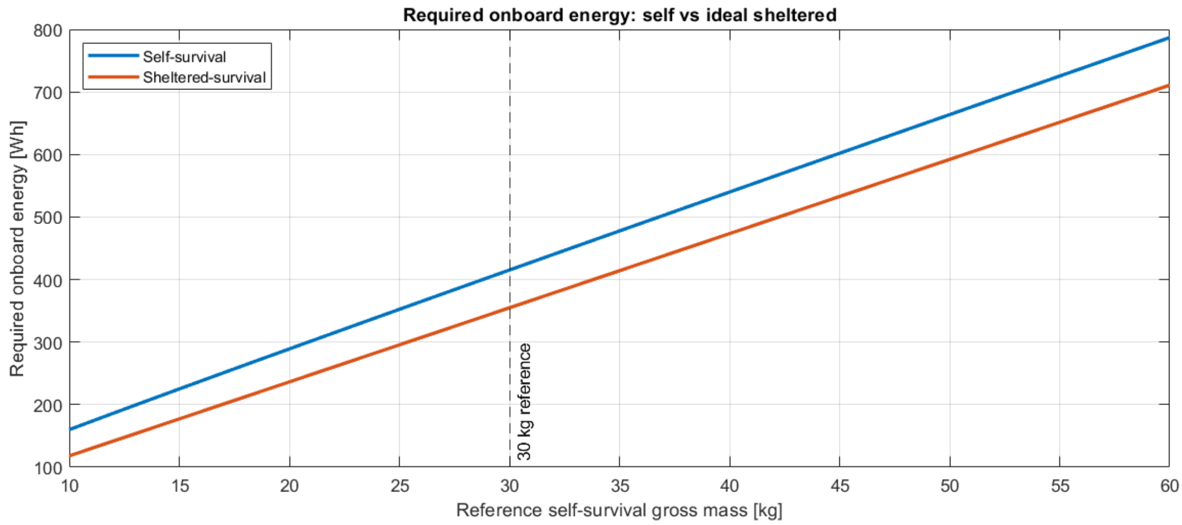

Figure 6.6.3 — Required onboard energy as a function of reference self-survival gross mass

Gross mass [kg]	Night-survival energy E_{night} [Wh]	Onboard energy reduction $\Delta E_{onboard}$ [Wh]
10	32.3	41.877
20	40.7	52.761
30	46.6	60.396
40	51.3	66.475
50	55.3	71.608
60	58.7	76.094

Table 6.6.2 — Reduction of onboard energy requirement enabled by sheltered-survival

The results show that the absolute energy benefit associated with the sheltered-survival configuration increases with vehicle gross mass, indeed for a 10 kg platform the reduction in required onboard energy is approximately 41.9 Wh, whereas for a 60 kg platform it reaches approximately 76.1 Wh. This increase is not linear because the adopted night-survival contribution scales according to

$$E_{\text{night}} = 15 m_{\text{gross}}^{1/3}$$

Consequently, the sheltered-survival architecture provides an increasing absolute benefit as vehicle size grows, but the increase remains sub-linear with respect to gross mass. The energy no longer allocated to night survival can be interpreted according to two alternative approaches:

- in the mass-saving mode, the mission profile is maintained unchanged and the removal of E_{night} is used to reduce the required battery mass;

- in the performance-extension mode, battery mass is maintained unchanged and the recovered energy is made available to extend the flight capability of the vehicle.

Mass-saving mode

In the first scenario, the benefit of the sheltered-survival configuration is not used to increase range or endurance, but to reduce the vehicle mass relative to the self-survival case.
To maintain consistency with the coupled mass–energy model, the calculation is not limited to directly subtracting the night-survival energy from the battery capacity, instead the required battery mass is updated iteratively: a lower energy requirement produces a lower battery mass, which in turn reduces total vehicle mass and consequently the power and energy required during flight.
This approach therefore captures, in simplified form, the coupling between vehicle mass, propulsive power and stored energy, and the most relevant quantity for this interpretation is not the absolute battery mass in the two cases, but the battery-mass saving obtained when moving from the self-survival to the sheltered-survival configuration. This quantity is defined as

$$\Delta m_{\text{bat}} = m_{\text{bat,self}} - m_{\text{bat,sheltered}}$$

where $m_{\text{bat,self}}$ is the battery mass required when the vehicle must autonomously provide its night-survival energy, whereas $m_{\text{bat,sheltered}}$ is the corresponding battery mass when this contribution is transferred to the surface infrastructure.

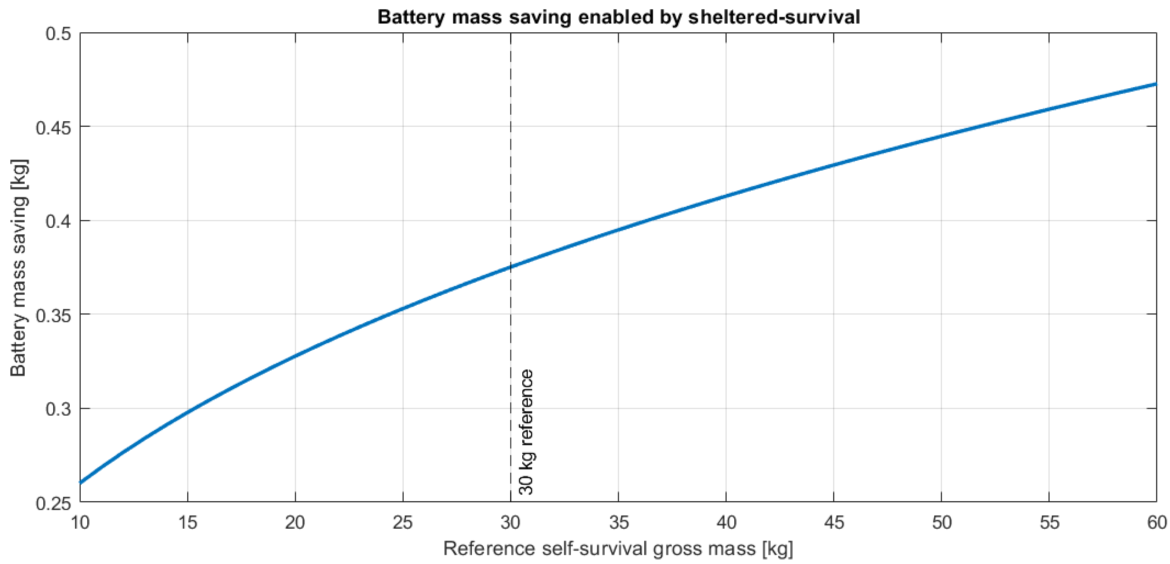

Figure 6.6.4 — Battery mass saving enabled by the sheltered-survival architecture

Figure 6.6.4 shows that the battery-mass saving increases with the reference gross mass, although it remains limited over the investigated range: this behaviour is consistent with the adopted scaling law for the night-survival contribution,

$$E_{\text{night}} = 15 m_{\text{gross}}^{1/3}$$

since the survival-energy term grows only with the cube root of vehicle mass. The benefit associated with its removal therefore increases as vehicle size increases, but more slowly than the total vehicle mass, so the mass-saving mode provides a real but non-dominant reduction in vehicle mass. Even a limited decrease in battery mass contributes to reducing rotor loading, power demand and required stored energy.

Performance-extension mode

In the second scenario, the battery capacity of the self-survival case is maintained unchanged in the sheltered-survival configuration, so the energy no longer reserved for night survival can be interpreted as an additional margin available for extending flight operations. As a first-order approximation, this recovered energy can be allocated to either an increase in scientific hovering time or an extension of cruise distance, two quantities that represent alternative uses of the same recovered energy and should therefore not be interpreted as simultaneously achievable. The additional hovering time can be estimated as

$$\Delta t_{\text{hover}} = \frac{E_{\text{night}}}{P_{\text{hover}}}$$

whereas the additional cruise range can be expressed as

$$\Delta R_{\text{cruise}} = \frac{E_{\text{night}}}{P_{\text{cruise}}} V_{\text{cruise}}$$

Reference self-survival gross mass [kg]	**Battery mass saving $\Delta \mathbf{m}_{\text{bat}}$ [kg]**	**Additional hover time Δt_{hover} [min]**	**Additional cruise range ΔR_{cruise} [km]**
10	0.260	1.948	1.642
20	0.327	1.259	1.035
30	0.375	0.969	0.790
40	0.413	0.804	0.653
50	0.445	0.695	0.563
60	0.473	0.616	0.498

Table 6.6.3 — Equivalent performance extension from reallocated night-survival energy

The results reported in Table 6.6.3 show an apparently counterintuitive trend: the equivalent increase in hover time and cruise range decreases as gross mass increases, but this behaviour is consistent with the model because E_{night} increases slowly with $m_{\text{gross}}^{1/3}$, whereas the power required during hover and cruise grows more rapidly with vehicle mass. Consequently, the same type of recovered energy contribution has a greater effect on smaller vehicles and a progressively smaller effect on heavier platforms. Two main conclusions can therefore be drawn:

- the direct performance benefit of sheltered survival is more relevant for small and medium-sized multicopters, for which the night-survival energy represents a larger fraction of the total flight-energy demand;
- for larger platforms, the recovered energy remains useful, but it is increasingly absorbed by the higher power required to sustain the vehicle during hover and cruise.

Within the adopted model, the sheltered-survival architecture therefore does not produce a major increase in single-sortie performance, instead the direct gains in range and hovering time remain moderate, as shown in Table 6.6.3 Nevertheless, the analysis demonstrates that the allocation of night-survival energy is not negligible and may influence battery sizing and operational margin. The possible use of an external shelter as part of the final mission architecture, including its role in recharge and environmental protection, is discussed in Chapter 7.

6.6.4 Recharge-area sensitivity and architectural implications

The results of the previous section show that, when the sheltered-survival architecture is assessed only in terms of removal of the night-survival contribution E_{night} from the onboard energy balance, the benefit for a single sortie remains moderate, but this energetic comparison does not fully describe the possible role of an external support station. As discussed by Young et al. in *The Future of Rotorcraft and Other Aerial Vehicles for Mars Exploration* [11], an automated base station should not be interpreted only as a thermal shelter, but as a surface-support infrastructure capable of hosting and protecting one or more aerial vehicles during non-operational phases.

One of the main operational limitations of a Martian multicopter is the restricted photovoltaic area that can be carried onboard without introducing excessive mass, volume, packaging and aerodynamic penalties. In a conventional configuration, such as for the MSH [2], the photovoltaic cells are installed directly on the vehicle and must therefore remain compatible with the geometric and structural constraints of the rotorcraft. By contrast, a fixed surface station may accommodate a larger photovoltaic area that is not directly constrained by the flight configuration.

In the MSH model [2], the recharge is provided through photovoltaic cells mounted on the vehicle, and the equivalent daily photovoltaic-energy production per unit area is assumed to be

$$e_{\mathrm{solar,sol}} = 540\ \mathrm{Wh/m^2/sol}$$

with a total solar-cell area of

$$A_{\mathrm{solar}} = 0.62\ \mathrm{m^2}$$

The capability of a photovoltaic array to provide energy over one Martian sol can be estimated as

$$E_{\mathrm{solar,sol}} = A_{\mathrm{solar}} e_{\mathrm{solar,sol}}$$

Since $e_{\mathrm{solar,sol}}$ already represents an equivalent daily energy production of the photovoltaic array, photovoltaic-conversion efficiency is not applied a second time. Instead, the recharge-chain efficiency η_{charge} and a solar-availability factor β are introduced.

The factor β represents, in aggregated form, non-ideal operating conditions such as dust deposition on the panels, non-optimal array orientation, seasonal variation in solar irradiance and additional installation losses. The ideal case corresponds to $\beta = 1$, whereas lower values represent progressively more penalising environmental conditions. The equivalent recharge time, expressed in Martian sols, can therefore be estimated as

$$N_{\mathrm{sol,recharge}} = \frac{E_{\mathrm{req}}}{A_{\mathrm{solar}} e_{\mathrm{solar,sol}} \eta_{\mathrm{charge}} \beta}$$

where E_{req} is the energy that must be restored after the mission. This formulation makes it possible to quantify the potential advantage of an external recharge platform: whereas the solar area installed directly on the multicopter is constrained by vehicle mass, packaging and rotor interference, a surface-based system may accommodate larger collection areas and therefore reduce the recharge time between consecutive sorties. The analysis can also be inverted to determine the photovoltaic area required to complete recharge within a prescribed time:

$$A_{\mathrm{solar,req}} = \frac{E_{\mathrm{req}}}{N_{\mathrm{sol,target}} e_{\mathrm{solar,sol}} \eta_{\mathrm{charge}} \beta}$$

where $N_{\mathrm{sol,target}}$ is the maximum target recharge time, expressed in sols. The evaluation is performed for the 30 kg reference platform previously adopted in the parametric analyses of Chapter 6, and for this platform the updated model gives a flight-energy requirement of:

$$E_{\mathrm{flight}} = 352.85\ \mathrm{Wh}$$

and a night-survival contribution of

$$E_{\mathrm{night}} = 46.61\ \mathrm{Wh}$$

Considering an operational reserve equal to $f_{\mathrm{reserve}} = 0.20$, the total recharge energy in the self-survival case becomes

$$E_{\mathrm{req,self}} = \left(E_{\mathrm{flight}} + E_{\mathrm{night}}\right)(1 + f_{\mathrm{reserve}})$$

and therefore

$$E_{\mathrm{req,self}} = (352.85 + 46.61) \cdot 1.20 \approx 479.34\ \mathrm{Wh}$$

The target recharge time is then linked to the same reference configuration used in the previous analyses, preserving consistency with the mass–energy model adopted throughout Chapter 6. The required photovoltaic area is obtained from

$$A_{\mathrm{solar,req}} = \frac{E_{\mathrm{req}}}{N_{\mathrm{sol,target}} e_{\mathrm{solar,sol}} \eta_{\mathrm{charge}} \beta}$$

Three representative recharge targets are considered:

- $N_{\mathrm{sol,target}} = 1$ sol, corresponding to restoration of the energy required by the baseline sortie within one Martian day;
- $N_{\mathrm{sol,target}} = 0.5$ sol and 0.25 sol, representing higher-operational-availability cases with progressively shorter turnaround times between consecutive missions.

The same formulation allows the self-survival and sheltered-survival architectures to be compared:

- in the self-survival case, the recharge energy includes both flight and night-survival contributions:

$$E_{\mathrm{req,self}} = \left(E_{\mathrm{flight}} + E_{\mathrm{night}}\right)(1 + f_{\mathrm{reserve}})$$

- in the sheltered-survival case, part of the night-survival contribution is transferred to the surface-support infrastructure:

$$E_{\mathrm{req,sheltered}} = \left(E_{\mathrm{flight}} + \alpha E_{\mathrm{night}}\right)(1 + f_{\mathrm{reserve}})$$

where α is the fraction of night-survival energy that remains allocated to the aerial vehicle. The value $\alpha = 1$ corresponds to the self-survival architecture, whereas $\alpha = 0$ represents the ideal limiting case in which the night-survival load is entirely transferred to the shelter. An intermediate value, such as $\alpha = 0.5$, represents a partially sheltered configuration in which the surface station reduces, but does not completely eliminate, the onboard nighttime energy requirement.

As an initial reference, the photovoltaic area adopted for the MSH, equal to $0.62\ \mathrm{m}^2$, can be scaled linearly with vehicle mass: since the MSH reference mass is approximately $17.656\ \mathrm{kg}$, the corresponding area for the 30 kg platform can be estimated as

$$A_{\mathrm{solar,scaled}} = A_{\mathrm{solar,MSH}} \frac{m_{\mathrm{gross}}}{m_{\mathrm{MSH}}}$$

which gives

$$A_{\mathrm{solar,scaled}} = 0.62 \frac{30}{17.656} \approx 1.05\ \mathrm{m}^2$$

Applying this scaled area to the reference configuration and assuming, as a first approximation, $\beta = 1$ and $\eta_{\mathrm{charge}} = 0.85$, the recharge time for the self-survival case becomes

$$N_{\mathrm{sol,recharge,self}} = \frac{E_{\mathrm{req,self}}}{A_{\mathrm{solar,scaled}} e_{\mathrm{solar,sol}} \eta_{\mathrm{charge}} \beta}$$

and therefore

$$N_{\mathrm{sol,recharge,self}} = \frac{479.34}{1.05 \cdot 540 \cdot 0.85 \cdot 1} \approx 0.99\ \mathrm{sol}$$

This result underlines that, under ideal solar-availability conditions, a photovoltaic area scaled linearly from the MSH reference would approximately restore the energy required by the 30 kg self-survival platform within one Martian sol. However, the ideal assumption $\beta = 1$ cannot be considered representative of prolonged surface operations, indeed previous Martian missions powered by solar arrays have shown that dust accumulation may progressively reduce photovoltaic output. Lorenz et al. [9] analysed dust accumulation and removal from photovoltaic arrays used by several Martian landers and rovers, identifying a typical output loss of approximately 0.2% per sol, although observed rates may vary between approximately 0.05% and 2% per sol depending on the mission and local conditions. In the present model, the evolution of the solar-availability factor is represented through the exponential relation:

$$I(t) = I(0) e^{-dt}$$

where $I(t)$ is the array output after t sols, $I(0)$ is the initial output and d is the degradation rate associated with dust accumulation. The corresponding availability factor can be written as

$$\beta(t) = \frac{I(t)}{I(0)}.$$

After 100 sols, assuming

$$d = 0.002\ \mathrm{sol}^{-1}$$

the value becomes

$$\beta(100) = e^{-0.002 \cdot 100} = e^{-0.2} \approx 0.82$$

Accordingly, the value $\beta = 0.82$ is adopted in the following analysis as a moderately degraded preliminary condition, representative of a photovoltaic array that has operated for approximately 100 sols without complete restoration of its initial performance. This value is more conservative than the ideal case $\beta = 1$, while not representing the most severe degradation conditions that may occur after longer exposures or in the absence of natural cleaning events.

Natural dust-removal events cannot be assumed to provide a reliable recovery mechanism: missions such as Spirit and Opportunity benefited from occasional cleaning events caused by atmospheric activity, whereas InSight experienced a more continuous degradation with almost no significant dust removal [9]. For this reason, the adoption of $\beta < 1$ avoids overestimating the energy that can be produced by the photovoltaic array during extended operations. The photovoltaic areas required to complete recharge within the selected target times are reported in Table 6.6.4.

Target recharge time $N_{\mathrm{sol},target}$ [sol]	**Self-survival (α = 1) [m^2]**	**Partial sheltered-survival (α = 0.5) [m^2]**	**Sheltered-survival (α =0) [m^2]**
1.00	1.27	1.20	1.12
0.50	2.55	2.40	2.25
0.25	5.09	4.80	4.50

Table 6.6.4 — Required deployed photovoltaic-array area for different recharge-time targets, assuming $\boldsymbol{\beta = 0.82}$

The results reported in Table 6.6.4 show that the required photovoltaic area is governed primarily by the target recharge time rather than by the allocation of the night-survival load. This behaviour follows directly from the adopted formulation, since $A_{\mathrm{solar,req}}$ scales inversely with $N_{\mathrm{sol,target}}$. Reducing the recharge time from one sol to 0.5 sol approximately doubles the required area, while reducing it to 0.25 sol increases the required area to approximately four times the one-sol value.

For a one-sol recharge target, the required area remains relatively limited, decreasing from approximately $1.27\ \mathrm{m}^2$ in the self-survival case to $1.12\ \mathrm{m}^2$ in the ideal sheltered-survival case, so the difference between the two architectures is therefore moderate. By contrast, when the required turnaround time becomes more demanding, the photovoltaic area increases significantly, since for a recharge target of 0.5 sol, the required area lies between approximately 2.25 and $2.55\ \mathrm{m}^2$, whereas a 0.25-sol target requires approximately 4.50–$5.09\ \mathrm{m}^2$. These areas would be increasingly difficult to integrate directly on the rotorcraft because of mass, packaging, structural and rotor-clearance constraints, so that makes the use of an external surface-based recharge system more relevant for mission scenarios requiring short turnaround times and repeated sorties.

The present analysis does not demonstrate that a sheltered base station is necessarily the optimal solution, instead it identifies the operating conditions under which an external recharge architecture may become significant: not primarily for a single daily sortie with relaxed recharge requirements, but for repeated operations requiring faster turnaround and larger photovoltaic collection areas. The possible implementation of this external recharge capability within the final recommended mission architecture is discussed in Chapter 7.

7. Conclusions and Future Work

7.1 Recommended Preliminary Hexacopter Configuration

The results of the baseline sizing and the parametric analyses were combined to define a recommended preliminary configuration: the selected values should be interpreted as a coherent design point identified within the feasible region explored in Chapter 6.

Design parameter	**Recommended value**	**Basis for selection**
Vehicle architecture	Electric hexacopter	Selected for pure VTOL capability, simplicity and suitability for local operations
Gross mass	30 kg	Chosen as a robust design point; heavier configurations provide limited performance improvement at constant battery fraction
Payload mass	3 kg	Maintains positive energy margin and 12% battery fraction; higher values approach or exceed mission closure limit
Number of rotors	6	Compromise between rotor diameter, redundancy and system complexity
Disk loading	8 N/m^2	Retained as a balanced point within the feasible range; lower values increase rotor size, higher values increase power demand
Rotor diameter	1.72 m	Derived from gross mass, six rotors and DL value
Battery mass fraction	12%	Provides a more robust energy margin than the minimum baseline case
Battery mass	3.6 kg	Derived from 12 % of 30 kg gross mass
Battery specific energy	230 Wh/kg	Conservative pack-level value supported by the literature and sufficient for baseline feasibility
Tip Mach number	0.65	Baseline rotor operating value retained to limit compressibility effects
Rotor solidity	0.20	Baseline rotor-design assumption retained in the final configuration
Figure of Merit	0.60	Representative preliminary hover-efficiency value
Mean blade drag coefficient	0.04	Conservative low-Reynolds-number assumption
Operating concept	Local one-way sorties	Consistent with the reference mission profile
Support architecture	Sheltered support station	Proposed to improve recharge, protection and repeated-sortie capability

Table 7.1 — Recommended preliminary hexacopter configuration derived from the baseline sizing and parametric analyses

The selected values in Table 7.1 provide a balanced compromise among vehicle mass, rotor dimensions, onboard energy storage and mission capability, so the resulting vehicle should therefore be regarded as a 30 kg-class electric hexacopter intended for local scientific and reconnaissance sorties in support of a broader Martian surface mission. The following section discusses the rationale behind the main configuration choices and introduces the proposed sheltered-support architecture for repeated operations

7.2 Design Rationale and Configuration Trade-off

The configuration reported in Table 7.1 was selected by combining the results obtained from the baseline sizing with the trends identified through the parametric analyses, with the aim of defining a coherent preliminary design rather than maximising a single performance parameter. The selected configuration therefore represents a compromise among payload capability, rotor dimensions, power demand, battery mass and operational robustness, while remaining consistent with the assumptions and limits of the model developed in the previous chapters.

7.2.1 Airborne configuration trade-off

The hexacopter architecture was retained because it provides a reasonable balance between rotor size and system complexity. A configuration with four rotors would require a larger diameter for each rotor in order to achieve the same total disk area, with a consequent increase in the overall vehicle footprint and greater difficulties in structural integration and packaging. An eight-rotor configuration, on the other hand, would reduce the individual rotor diameter, but it would also increase the number of motors, arms, electronic controllers and associated subsystems, thereby introducing a higher level of mechanical and control complexity.

For the vehicle scale considered in this study, the six-rotor arrangement therefore represents a balanced solution, since it allows the total rotor area to be distributed over a sufficient number of rotors without excessively increasing the number of components.

A gross mass of approximately 30 kg was selected as the reference value for the final configuration: this value is higher than the minimum mass obtained from the baseline iteration, but it provides additional margin for the payload, the battery allocation and the auxiliary subsystems, while still remaining within a scale that is compatible with the local mission considered in the thesis. The gross-mass analysis also showed that increasing the vehicle mass beyond this level does not lead to a proportional improvement in range or endurance, because the additional stored energy is progressively offset by the higher thrust and power required during flight. For this reason, a substantially heavier configuration was not considered advantageous, since it would increase rotor size, power demand and structural complexity without providing a comparable operational benefit.

The selected payload mass is 3 kg, which provides a meaningful scientific capability while preserving a positive mass–energy balance; the payload sensitivity analysis showed that increasing the payload progressively reduces the fraction of the total mass that can be allocated to the battery and, consequently, it decreases the available energy margin. For the 30 kg reference platform, payload values approaching 3.5 kg move the configuration close to the mission-closure limit under the assumptions adopted in the model. The 3 kg payload was therefore retained as a suitable compromise between scientific relevance and energetic feasibility, since it allows the vehicle to carry a non-negligible instrument package without excessively penalising the available battery mass.

A nominal disk loading of $8\ \mathrm{N/m^2}$ was maintained for the final design, and it lies within the intermediate region of the investigated design space and provides a reasonable balance between rotor size and

energy demand, while remaining consistent with the baseline assumptions adopted throughout the thesis.
The same conservative approach was applied to the battery system, for which a pack-level specific energy of $230\ \mathrm{Wh/kg}$ was selected, a value that is consistent with the literature used in the preliminary sizing model and that avoids making the feasibility of the reference configuration dependent on battery technologies that may not yet be available at system level. The battery-technology analysis showed that higher values, such as 250, 300 or $350\ \mathrm{Wh/kg}$, could provide measurable improvements in range, hover duration or battery mass, but these cases were treated as possible future developments rather than as necessary assumptions for the closure of the baseline configuration.
The selected airborne configuration therefore represents a consistent and conservative design point within the investigated feasibility region, without relying on optimistic aerodynamic or battery assumptions.

7.2.2 Proposed sheltered-support architecture

The airborne vehicle alone does not fully define the operational concept considered in this study, since repeated Martian sorties also require the management of night survival, recharge and environmental protection during the periods in which the multicopter remains on the surface. The analysis performed in Section 6.6 showed that transferring the night-survival load from the aerial vehicle to an external shelter produces only a moderate direct benefit when the effect is evaluated on a single sortie.

For the 30 kg reference configuration, the ideal removal of the onboard night-survival contribution corresponds to a battery-mass reduction of approximately $0.38\ \mathrm{kg}$, and if the same battery mass is maintained the recovered energy could alternatively provide approximately 0.96 min of additional hover time or 0.79 km of additional cruise range. These results show that the introduction of a shelter would not be justified solely by the reduction of the onboard night-survival energy, since the direct improvement in vehicle performance remains limited.
The value of the shelter becomes more significant when it is considered as part of a complete support architecture for repeated local operations: on this basis, this study proposes a sheltered surface station equipped with deployable or retractable photovoltaic arrays, in which the multicopter would be hosted during recharge and non-operational periods after completing its sortie. The structure would provide thermal and mechanical protection to the vehicle, while the external photovoltaic surfaces would supply the energy required for future missions and would allow the use of collection areas larger than those that could be integrated directly on the airborne platform.
The photovoltaic arrays would be deployed during favourable illumination periods and retracted or protected during the night, during inactive phases or under adverse environmental conditions, a solution that could reduce prolonged exposure to dust deposition and environmental degradation, while avoiding the mass, volume and rotor-clearance constraints associated with the integration of large solar surfaces directly on the multicopter.

The recharge-area analysis supports this architectural interpretatio: as shown in table 6.6.4, for a recharge time of one sol, the required photovoltaic area decreases only from approximately $1.27\ \mathrm{m}^2$ in the self-survival case to $1.12\ \mathrm{m}^2$ in the ideal sheltered-survival case. The result becomes more relevant when shorter turnaround times are imposed, since a recharge period of 0.5 sol requires approximately $2.25 – 2.55\ \mathrm{m}^2$, while a target of 0.25 sol requires approximately $4.50 – 5.09\ \mathrm{m}^2$.

Photovoltaic surfaces of this magnitude would be increasingly difficult to integrate directly on the multicopter because of mass, structural, packaging and rotor-clearance constraints, whereas a fixed surface station could accommodate them more easily and without directly affecting the flight configuration. The proposed shelter is therefore considered an active element of the mission architecture rather than a simple protective enclosure, since its functions would include thermal protection, photovoltaic recharge, dust shielding and safe parking of the vehicle between consecutive sorties.

Figure 7.2.1 — Preliminary concept of a sheltered support station with retractable photovoltaic arrays for the proposed Martian hexacopter. Created with AI.

This approach could improve the continuity and repeatability of local exploration missions without increasing the mass and geometric complexity of the airborne platform, and at the same time it would introduce additional system-level requirements related to deployment and retraction mechanisms, docking interfaces, electrical power transfer, dust-tolerant joints, thermal control and long-term reliability, all of which lie outside the scope of the present preliminary model and would require dedicated future analyses.

The final concept can therefore be described as an integrated system composed of a 30 kg-class hexacopter designed for local flight operations and a sheltered surface station intended to support recharge, protection and repeated use. The aerial vehicle remains capable of completing the reference sortie on the basis of the assumptions adopted in the model, while the external infrastructure improves the operational continuity and long-term sustainability of the overall mission architecture.

7.3 Key Design Drivers for Future Martian VTOL Platforms

The analyses carried out in this thesis show that the preliminary design of a Martian VTOL vehicle is governed by several strongly coupled parameters, whose effects cannot be evaluated independently. Although the reference configuration developed in the previous sections refers to a specific 30 kg-class hexacopter, the trends identified through the mass–energy model provide more general indications for the development of future Martian aerial platforms.

The first major design driver is the total rotor disk area, which directly affects the induced power required to sustain the vehicle in the rarefied Martian atmosphere. Low disk-loading values are generally favourable from an energetic standpoint, since they reduce the velocity induced through the rotor disk and therefore lower the power required during hovering and vertical flight. However, this advantage is obtained at the cost of larger rotor diameters, increased vehicle footprint and more demanding structural and packaging requirements. Disk loading should therefore not be selected by minimising power alone, but through a trade-off that also includes rotor integration, deployment constraints, ground clearance and compatibility with the surface infrastructure.

A second fundamental driver is the coupling between vehicle mass and onboard energy storage: increasing battery mass provides additional energy capacity, but it also increases the total vehicle weight and consequently the thrust, power and rotor area required for flight. The same mechanism applies to payload growth: every additional kilogram allocated to scientific equipment reduces the fraction of the total mass that can be assigned to the battery and progressively moves the design toward the mission-closure boundary. Future Martian VTOL platforms should therefore be sized through an iterative mass–energy process, rather than by assigning propulsion, payload and battery masses independently.

Battery specific energy remains one of the parameters with the greatest influence on overall mission capability, indeed improvements at pack level can be used either to reduce the mass of the energy-storage system or, at constant battery mass, to increase range, hovering time and operational margin. Nevertheless, the feasibility of a reference design should not depend entirely on optimistic future battery projections, particularly because low-temperature operation, thermal management, degradation and battery-management hardware may reduce the effective performance available under Martian conditions. For this reason, technological improvements in energy storage should be treated as a means of expanding the operational envelope of an already feasible configuration, rather than as the only condition that makes the vehicle possible.

The aerodynamic design of the rotor system also remains a critical development area, since Martian rotors operate simultaneously at low Reynolds numbers and non-negligible local Mach numbers, so reducing disk loading alone is not sufficient to guarantee high efficiency. Rotor solidity, blade-section drag, tip speed and airfoil geometry must be selected together, because an increase in rotational speed may facilitate thrust generation but it also raises profile losses and reduces the margin with respect to compressibility effects. The global coefficients adopted in the present model are suitable for preliminary sizing, but future designs will require dedicated low-Reynolds-number airfoil data, blade-element analyses and high-fidelity rotor simulations.

The mission profile itself should also be considered a primary design variable, since hovering provides one of the main operational advantages of a multicopter, but it is also among the most power-intensive phases of the mission. Similarly, increasing the cruise distance may strongly affect total energy even when the cruise power remains below the hover power, because the transfer phase can occupy a significant fraction of the sortie duration. Future platforms should therefore be designed around a clearly defined operational role, since a vehicle optimised for short-range reconnaissance and prolonged station-keeping will differ substantially from one intended for regional transport or long-distance exploration.

The results also indicate that recharge time, night survival, dust exposure and thermal protection can become system-level constraints that are difficult to manage exclusively onboard without increasing vehicle mass and complexity, so the design boundary should not be limited to the airborne vehicle, but a surface-support architecture may provide an effective way to separate flight-critical functions from non-flight functions, allowing the aerial platform to remain focused on mobility while the ground infrastructure provides energy generation, thermal protection and operational support. The relevance of such an architecture increases particularly for repeated sorties, short turnaround requirements and long-duration missions, in which the cumulative effects of recharge limitations and environmental exposure become more important than the performance of a single flight.

Overall, future Martian VTOL platforms should be developed through an integrated approach in which rotor sizing, mass allocation, battery technology, mission profile and surface support are treated as parts of the same design problem. The main challenge is not simply to generate sufficient thrust in the Martian atmosphere, but to identify a configuration in which aerodynamic efficiency, energy availability, payload capability and operational continuity remain mutually compatible over the complete mission cycle. These elements constitute the principal design drivers emerging from the present study and define the areas in which additional technological development and higher-fidelity analysis would provide the greatest benefit.

7.4 Limitations of the Study

The results presented in this thesis should be interpreted within the limits of the preliminary modelling framework adopted, whose purpose was to identify physically plausible configurations and the main trade-offs governing a Martian multicopter rather than to define a fully detailed or flight-ready vehicle. For this reason, several aspects of the problem were represented through simplified analytical relations, global coefficients and nominal operating conditions, in a form considered appropriate for a first feasibility assessment.

From an aerodynamic point of view, the model is based on momentum-theory relations and aggregate estimates of induced and profile power, while the rotor blades were not designed in detail and the analysis does not include blade-element modelling, three-dimensional flow effects, aeroelastic deformation, rotor–rotor interference or wake interaction. The influence of low Reynolds numbers and local compressibility was represented through global parameters such as mean profile drag coefficient, solidity and tip Mach number, although the actual aerodynamic behaviour would also depend on the selected airfoil geometry, radial blade distribution and operating condition.
A similar level of simplification was adopted for forward flight, where the resistance of the vehicle was represented through an equivalent drag area that accounts in aggregate form for the contributions of the fuselage, support arms, landing gear, hubs and other non-lifting components. Since the final external geometry of the vehicle was not defined, the drag coefficient and frontal area were not derived from a detailed configuration, and the corresponding cruise-power estimates therefore remain sensitive to the actual layout of the platform.

The environmental model was also intentionally limited to a fixed set of nominal conditions associated with the selected reference case, without explicitly including variations in atmospheric density, temperature, wind, turbulence, dust concentration or solar irradiance. These effects could modify rotor performance, control authority, thermal loads and available recharge energy, especially for operations extending over different seasons or times of day, while additional phenomena such as ground effect, dust lifting and interaction with uneven terrain were excluded from the present analysis.

At system level, the mass model does not represent a complete subsystem design, since structural, propulsion, avionics and auxiliary masses were estimated through reference fractions and scaling assumptions rather than through detailed sizing. No dedicated mass calculation was performed for motors, controllers, rotor hubs, support arms, landing gear, wiring, thermal insulation or deployment mechanisms, and the final mass breakdown should therefore be regarded as a feasibility estimate rather than as a verified engineering mass budget.

The battery model follows the same preliminary approach, using pack-level specific energy, a usable-energy fraction and an operational reserve to estimate the required battery mass, without explicitly modelling voltage variation, discharge-rate effects, low-temperature performance, cell ageing, thermal-control energy or degradation over repeated cycles. The night-survival contribution was obtained through a scaling relation derived from the Mars Science Helicopter conceptual-design framework and should therefore be interpreted as a system-level estimate rather than as the result of a detailed transient thermal analysis.

The mission profile was represented as a sequence of discrete operating phases characterised by representative power levels and durations, which made it possible to preserve a clear link between mission structure and energy demand but did not capture transient manoeuvres, attitude changes, gust rejection, navigation corrections, landing-site assessment or contingency operations. The calculated range and hovering capability consequently represent nominal values under the assumed operating conditions rather than guaranteed mission performance.

With regard to the sheltered-support architecture, the analysis was limited mainly to energy allocation and photovoltaic-area requirements, while the mass, volume and structural design of the shelter were not included in the 30 kg airborne gross mass. Deployment and retraction mechanisms, docking interfaces, power-transfer systems, dust-tolerant joints, thermal control and long-term station reliability were not sized in detail, so the proposed support station should be considered a conceptual extension of the mission architecture rather than a fully developed subsystem.

In conclusion, the study does not include a formal multidisciplinary optimisation, uncertainty propagation or probabilistic robustness analysis, and the recommended configuration should therefore be interpreted as a coherent design point within the investigated parameter ranges rather than as a unique global optimum. A higher-fidelity treatment of aerodynamic, structural, thermal, control and energy aspects may modify the exact numerical values of the selected parameters, although the main couplings and design trends identified in the thesis are expected to remain relevant.

7.5 Future Developments

The preliminary framework developed in this thesis provides a coherent basis for the assessment of Martian VTOL concepts, not only because it leads to a physically plausible reference configuration, but also because it establishes a design logic in which rotor sizing, mission energy, battery mass and operational constraints are treated as parts of the same coupled problem. Future work should therefore aim to increase the fidelity of the individual models without losing this integrated perspective, since the usefulness of the approach lies precisely in its ability to connect aerodynamic performance, mass allocation and mission capability within a common sizing process.

A natural development of this work would be the refinement of the aerodynamic representation of the rotor system, replacing the global coefficients used in the preliminary analysis with blade-level data derived from low-Reynolds-number airfoil testing, blade-element methods and higher-fidelity numerical simulations. Such an extension would make it possible to evaluate more accurately the effects of blade geometry, radial loading, rotor–rotor interaction, wake behaviour and local compressibility, thereby improving the estimates of thrust, profile losses and power demand across the complete operating envelope rather than only at a few representative conditions.

As the aerodynamic model becomes more detailed, the vehicle mass model should also evolve from the current system-level representation toward a component-based engineering description. Propulsion units, rotor hubs, support arms, landing gear, avionics, electrical distribution, wiring, thermal insulation and structural elements should be sized according to their actual mechanical, electrical and thermal requirements, so that the proposed 30 kg-class configuration can be checked against a complete and traceable mass budget. This step would also clarify whether the selected rotor diameter, vehicle footprint and overall architecture remain compatible with launch packaging, deployment, landing stability and surface operations.

A similar increase in fidelity would be required for the energy system, whose behaviour under Martian conditions cannot be represented fully by pack-level specific energy alone. Future analyses should include low-temperature capacity loss, discharge-rate limitations, thermal-control demand, cell ageing, end-of-life degradation and repeated cycling, while advanced battery technologies should be evaluated at pack level rather than only on the basis of cell performance. Their actual benefit will depend on the additional mass required for containment, insulation, heating, battery management and safety, and may therefore be smaller than suggested by nominal specific-energy values. Replacing the current night-survival scaling law with a transient thermal model based on vehicle geometry, insulation and environmental conditions would further improve the credibility of the total energy budget.

The operational model could also be extended beyond the present phase-based representation by introducing acceleration and deceleration, attitude changes, navigation corrections, gust rejection, landing-site assessment and contingency manoeuvres. Including atmospheric variability in terms of density, temperature, wind and dust loading would allow the design to be assessed over a broader range of seasons, local times and operating sites, transforming the present nominal case into a more robust mission-level evaluation. In this way, the feasibility of the vehicle would no longer be judged only under a single set of reference conditions, but against a realistic operational envelope.
Within this broader mission perspective, the sheltered-support architecture proposed in the thesis deserves a dedicated development effort because its potential value extends beyond the reduction of night-survival energy. A complete assessment should define the thermal enclosure, photovoltaic deployment and retraction mechanisms, docking interface, electrical connection, dust-mitigation strategy and long-term reliability of the surface station, while also accounting for its mass, volume and energy cost at mission level. Such an analysis would make it possible to determine whether transferring recharge, environmental protection and part of the thermal-management burden from the aerial vehicle to the surface infrastructure produces a net advantage, particularly for repeated sorties and long-duration exploration campaigns.

Once these refinements are introduced, the complete problem could be reformulated within a multidisciplinary design-optimisation framework in which gross mass, payload, rotor diameter, disk loading, tip speed, battery allocation and mission requirements are varied simultaneously under aerodynamic, structural, thermal and operational constraints. This would allow the analysis to move beyond the identification of a single plausible reference point and toward the definition of a family of mission-specific configurations, each suited to a different balance between payload capability, range, hovering time, recharge frequency and system complexity.

The transition from analytical feasibility to engineering credibility would finally require a progressive validation programme combining numerical studies, subsystem testing and experiments under representative Martian conditions. Rotor tests in low-density facilities, thermal-vacuum campaigns, hardware-in-the-loop simulations and autonomous-control demonstrations would be necessary to verify whether the performance predicted by the present model can be reproduced by real hardware and maintained in the presence of environmental variability, degradation and off-nominal events.
Seen in this perspective, the configuration proposed in the thesis should not be regarded as the endpoint of the design process, but as a physically consistent starting point for further development. The results indicate that a local Martian multicopter with meaningful payload capability is compatible with the current technological framework, provided that rotor area, battery mass and mission requirements are balanced carefully and that non-flight functions are managed at system level. Future Martian aerial vehicles are therefore likely to evolve not as isolated flying machines, but as integrated elements of a wider exploration architecture in which mobility, energy infrastructure and surface support are designed together.

The principal contribution of this work lies in identifying the couplings that must be controlled for Martian VTOL flight to become operationally useful. By clarifying how aerodynamic efficiency, mass allocation, energy storage, mission profile and support infrastructure interact, the study defines a structured path from preliminary sizing toward more mature aerial platforms and provides a foundation for the development of the next generation of Martian exploration systems.

Bibliography

[1] M. D. Guynn, M. A. Croom, S. C. Smith, R. W. Parks, and P. A. Gelhausen.
Evolution of a Mars Airplane Concept for the ARES Mars Scout Mission.
2nd AIAA "Unmanned Unlimited" Systems, Technologies, and Operations Conference,
San Diego, California, 2003.
Available: https://doi.org/10.2514/6.2003-6578

[2] W. Johnson, S. Withrow-Maser, L. Young, C. Malpica, W. J. F. Koning,
W. Kuang, M. Fehler, A. Tuano, A. Chan, A. Datta, C. Chi, R. Lumba,
D. Escobar, J. Balaram, T. Tzanetos, and H. F. Grip.
Mars Science Helicopter Conceptual Design.
NASA Technical Memorandum NASA/TM—2020–220485, March 2020.

[3] V. Youhanna, L. Felicetti, and D. Ignatyev.
Preliminary Design Exploration of Prospective Multirotor Aerobots for Mars.
Proceedings paper, 2024.

[4] V. Youhanna, L. Felicetti, and D. Ignatyev.
Systematic methodology for the preliminary design of future rotary VTOL Martian aerobots.
Acta Astronautica, vol. 231, pp. 246–267, 2025.
Available: https://doi.org/10.1016/j.actaastro.2025.01.059

[5] M. Radotich, S. Withrow-Maser, Z. deSouza, S. Gelhar, and H. Gallagher.
A Study of Past, Present, and Future Mars Rotorcraft.
Vertical Flight Society's 9th Biennial Autonomous VTOL Technical Meeting,
Virtual, January 26–28, 2021.

[6] H. Song and C. Underwood.
A Mars VTOL Aerobot: Preliminary Design, Dynamics and Control.
IEEE Aerospace Conference, 2007.

[7] H. Bézard, T. Désert, J.-M. Moschetta, and T. Jardin.
Aerodynamic design of a Martian micro air vehicle.
8th European Conference for Aeronautics and Space Sciences, EUCASS, 2019.
Available: https://doi.org/10.13009/EUCASS2019-217

[8] W. J. F. Koning, W. Johnson, and B. G. Allan.
Generation of Mars Helicopter Rotor Model for Comprehensive Analyses.
AHS Specialists' Conference on Aeromechanics Design for Transformative Vertical Flight,
San Francisco, California, 2018.

[9] R. D. Lorenz, G. M. Martínez, A. Spiga, A. Vicente-Retortillo, C. E. Newman,
N. Murdoch, F. Forget, E. Millour, and T. Pierron.
Lander and rover histories of dust accumulation on and removal from solar arrays on Mars.
Planetary and Space Science, vol. 207, article 105337, 2021.

Available: https://doi.org/10.1016/j.pss.2021.105337

[10] J. Delaune, J. Izraelevitz, S. Sirlin, D. Sternberg, L. Giersch, L. P. Tosi,
E. Skliyanskiy, L. Young, M. Mischna, S. Withrow-Maser, J. Mueller,
J. Bowman, M. S. Wallace, H. F. Grip, L. Matthies, W. Johnson,
M. Keennon, B. Pipenberg, H. Patel, C. Lim, A. Schutte, M. Veismann,
H. Cummings, S. Conley, J. Bapst, T. Tzanetos, R. Brockers, A. Jain,
D. Bayard, A. Chmielewski, O. Toupet, J. Burdick, M. Gharib, and J. Balaram.
Mid-Air Helicopter Delivery at Mars Using a Jetpack.
IEEE Aerospace Conference, 2022.

[11] L. A. Young, P. Lee, E. Aiken, G. Briggs, S. Withrow-Maser,
G. M. Pisanich, and H. Cummings.
The Future of Rotorcraft and other Aerial Vehicles for Mars Exploration.
Vertical Flight Society's 77th Annual Forum & Technology Display, Virtual, 2021.

[12] M. Giuranna, S. Tellmann, F. Montmessin, D. Belyaev, L. Trompet,
M. Pätzold, P. Wolkenberg, M. A. Lopez-Valverde, O. Korablev, and F. Forget.
Vertical Structure of the Martian Atmosphere: The View from Mars Express.
Space Science Reviews, vol. 221, article 36, 2025.
Available: https://doi.org/10.1007/s11214-025-01155-9

[13] R. Viggiano, Y. Lin, and D. Dornbusch.
Solid-state Architecture Batteries for Enhanced Rechargeability and Safety (SABERS):
Beyond Li-Ion: Technology to Enable Sustainable Electric Aviation.
NASA imaginAviation, 2023.

[14] Advanced Research Projects Agency-Energy.
PROPEL-1K: Pioneering Railroad, Oceanic and Plane Electrification with 1K Energy
Storage Systems. Project Descriptions.
ARPA-E, 2025.

[15] J. Liu.
Progress and Status of Battery500 Consortium Phase II.
DOE Vehicle Technologies Office Annual Merit Review, Project ID bat317, Pacific
Northwest National Laboratory, 2022.

[16] W. West, M. Smart, and J. Herman.
Battery System Design, Testing, and Operation for the Mars Perseverance Rover and
Ingenuity Helicopter.
NASA Jet Propulsion Laboratory, California Institute of Technology, 2021.

[17] Y. Jie, S. Wang, S. Weng, Y. Liu, M. Yang, C. Tang, X. Li, Z. Zhang, Y. Zhang,
Y. Chen, F. Huang, Y. Xu, W. Li, Y. Guo, Z. He, X. Ren, Y. Lu, K. Yang, S. Cao,
H. Lin, R. Cao, P. Yan, T. Cheng, X. Wang, S. Jiao, and D. Xu.
Towards long-life 500 Wh kg−1 lithium metal pouch cells via compact ion-pair

aggregate electrolytes.
Nature Energy, 2024.
Available: https://doi.org/10.1038/s41560-024-01565-z

[18] S. Withrow-Maser, W. Johnson, L. Young, H. Cummings, A. Chan, T. Tzanetos, J. Balaram, and J. Bapst.
An Advanced Mars Helicopter Design.
AIAA ASCEND, 2020.

[19] J. Balaram, T. Canham, C. Duncan, M. Golombek, H. F. Grip, W. Johnson, J. Maki, A. Quon, R. Stern, and D. Zhu.
Mars Helicopter Technology Demonstrator.
AIAA Atmospheric Flight Mechanics Conference, Kissimmee, Florida, 2018.
Available: https://doi.org/10.2514/6.2018-0023

[20] W. Ayele and V. Maldonado.
Conceptual Design of a Robotic Ground-Aerial Vehicle with an Aeroelastic Wing Model for Mars Planetary Exploration.
Aerospace, vol. 10, no. 5, article 404, 2023.
Available: https://doi.org/10.3390/aerospace10050404

[21] R. D. Lorenz.
Flight Power Scaling of Airplanes, Airships, and Helicopters: Application to Planetary Exploration.
Journal of Aircraft, vol. 38, no. 2, pp. 208–214, 2001.

[22] S. Withrow-Maser, W. Johnson, L. Young, W. J. F. Koning, W. Kuang, C. Malpica, J. Balaram, and T. Tzanetos.
Mars Science Helicopter: Conceptual Design of the Next Generation of Mars Rotorcraft.
AIAA ASCEND, 2020.

[23] D. P. Raymer.
Aircraft Design: A Conceptual Approach.
6th ed. Reston, Virginia: American Institute of Aeronautics and Astronautics, 2018.

[24] R. D. Lorenz.
Planetary Exploration with Ingenuity and Dragonfly: Rotary-Wing Flight on Mars and Titan.
Reston, Virginia: American Institute of Aeronautics and Astronautics, 2022.
Available: https://doi.org/10.2514/4.106378

[25] NASA.
Mars: Facts.
NASA Science.

Available: https://science.nasa.gov/mars/facts/
Accessed: May 29, 2026.

[26] European Space Agency.
Comparing the Atmospheres of Mars and Earth.
ESA, 2018.
Available:
https://www.esa.int/ESA_Multimedia/Images/2018/04/Comparing_the_atmospheres_of_Mars_and_Earth
Accessed: May 29, 2026.

[27] NASA.
Perseverance Explores the Jezero Crater Delta.
NASA Science, 2022.
Available: https://science.nasa.gov/resource/perseverance-explores-the-jezero-crater-delta/
Accessed: May 29, 2026.

[28] N. Mangold, S. Gupta, O. Gasnault, D. Dromart, G. D. Tarnas, S. F. Sholes,
B. Horgan, C. Quantin-Nataf, A. J. Brown, S. Le Mouélic, et al.
Perseverance rover reveals an ancient delta-lake system and flood deposits at
Jezero crater, Mars.
Science, vol. 374, no. 6568, pp. 711–717, 2021.
Available: https://doi.org/10.1126/science.abl4051

[29] NASA Jet Propulsion Laboratory.
Mars Helicopter Ingenuity.
NASA/JPL.
Available: https://mars.nasa.gov/technology/helicopter/
Accessed: May 29, 2026.

[30] J. G. Leishman.
Principles of Helicopter Aerodynamics.
2nd ed. Cambridge: Cambridge University Press, 2006.

[31] W. Johnson.
Rotorcraft Aeromechanics.
Cambridge: Cambridge University Press, 2013.

[32] T. J. Mueller and J. D. DeLaurier.
Aerodynamics of Small Vehicles.
Annual Review of Fluid Mechanics, vol. 35, pp. 89–111, 2003.
Available: https://doi.org/10.1146/annurev.fluid.35.101101.161102

[33] T. J. Mueller, ed.
Fixed and Flapping Wing Aerodynamics for Micro Air Vehicle Applications.
Progress in Astronautics and Aeronautics, vol. 195.

Reston, Virginia: American Institute of Aeronautics and Astronautics, 2001.

[34] J. Appelbaum and D. J. Flood.
Solar Radiation on Mars.
Solar Energy, vol. 45, no. 6, pp. 353–363, 1990.
Available: https://doi.org/10.1016/0038-092X(90)90156-7

[35] B. Scrosati and J. Garche.
Lithium batteries: Status, prospects and future.
Journal of Power Sources, vol. 195, no. 9, pp. 2419–2430, 2010.
Available: https://doi.org/10.1016/j.jpowsour.2009.11.048

[36] J. B. Goodenough and K.-S. Park.
The Li-ion rechargeable battery: A perspective.
Journal of the American Chemical Society, vol. 135, no. 4, pp. 1167–1176, 2013.
Available: https://doi.org/10.1021/ja3091438

[37] K. A. Farley, K. H. Williford, K. M. Stack, R. Bhartia, A. Chen,
M. de la Torre, K. Hand, Y. Goreva, C. D. K. Herd, R. Hueso, et al.
Mars 2020 Mission Overview.
Space Science Reviews, vol. 216, article 142, 2020.
Available: https://doi.org/10.1007/s11214-020-00762-y

[38] J. P. Grotzinger, J. Crisp, A. R. Vasavada, R. C. Anderson, C. J. Baker,
R. Barry, D. F. Blake, P. Conrad, K. S. Edgett, B. Ferdowski, et al.
Mars Science Laboratory Mission and Science Investigation.
Space Science Reviews, vol. 170, pp. 5–56, 2012.
Available: https://doi.org/10.1007/s11214-012-9892-2

[39] M. P. Golombek, R. A. Cook, T. Economou, W. M. Folkner,
A. F. C. Haldemann, P. H. Kallemeyn, J. M. Knudsen, R. M. Manning,
H. J. Moore, T. J. Parker, et al.
Overview of the Mars Pathfinder Mission and Assessment of Landing Site Predictions.
Science, vol. 278, no. 5344, pp. 1743–1748, 1997.
Available: https://doi.org/10.1126/science.278.5344.1743

[40] NASA Jet Propulsion Laboratory.
Ingenuity Mars Helicopter on the Martian Surface (Artist's Concept).
JPL, 2020.
Available: https://www.jpl.nasa.gov/images/pia23720-ingenuity-mars-helicopter-on-the-martian-surface-artists-concept/
Accessed: May 29, 2026.

[41] U.S. Geological Survey.
Jezero Crater, Mars.

USGS, 2020.
Available: https://www.usgs.gov/media/images/jezero-crater-mars-1
Accessed: May 29, 2026.

[42] H. Babu.
Study of Inlet Perturbations on Excitation of a Laminar Separation Bubble.
Proceedings paper, 2012.
Available: https://repository.up.ac.za/server/api/core/bitstreams/b262819a-7c14-468c-9f08-9849a7339c8f/content
Accessed: May 29, 2026.

[43] UST – Unmanned System & Tech.
Flotta.
Available: https://www.ust-italia.com/flotta/
Accessed: May 29, 2026.
[44] Toscana Drone.
DJI VTOL: il nuovo ala fissa per l'agricoltura.
Available: https://www.toscanadrone.com/it/blog/38-dji-vtol-il-nuovo-ala-fissa-per-l-agricoltura.html
Accessed: May 29, 2026.

[45] PR Newswire.
Korea Innovation Foundation Selects 2 Innovative Technology Companies, Narma and SPS, for Global Technology Commercialization Support Program North America.
Available: https://www.prnewswire.com/news-releases/korea-innovation-foundation-selects-2-innovative-technology-companies-narma-and-sps-for-global-technology-commercialization-support-programnorth-america-302300753.html
Accessed: May 29, 2026.

[46] M. Bertani.
Preliminary design of a fixed-wing VTOL UAV for Martian flight.
Master's thesis, Politecnico di Milano, School of Industrial and Information Engineering, 2023.
Available:
https://www.politesi.polimi.it/handle/10589/1/browse?type=title&sort_by=ASC&order=1&rpp=60&etal=-1&offset=49131&starts_with=Q
Accessed: May 29, 2026.

[47] W. Johnson.
Rotorcraft Aeromechanics.
Cambridge University Press, Cambridge, United Kingdom, 2013.
DOI: https://doi.org/10.1017/CBO9781139235655.
Available: https://www.cambridge.org/core/books/rotorcraft-aeromechanics/6DE729BB2AFED9F94E59823086568C1E.
Accessed: July 9, 2026.

[48] J. G. Leishman.

Introduction to Aerospace Flight Vehicles, Chapter: Helicopters.
Embry-Riddle Aeronautical University Pressbooks, 2023.
Available: https://eaglepubs.erau.edu/introductiontoaerospaceflightvehicles/chapter/helicopters/.
Accessed: July 9, 2026.

[49] W. Johnson.
Influence of Lift Offset on Rotorcraft Performance.
NASA Technical Paper NASA/TP-2009-215404, Ames Research Center, Moffett Field, California, 2009.
Available: https://ntrs.nasa.gov/citations/20100026468.
Accessed: July 9, 2026.

[50] J. M. van Aken, J. W. Lim, and C. Tung.
Estimating Blade Section Airloads from Rotor Blade Pressure Measurements.
American Helicopter Society / NASA rotorcraft publication, 2003.
Available: https://rotorcraft.arc.nasa.gov/Publications/files/vanAken_AHS03.pdf.
Accessed: July 9, 2026.